AD721920

HUGONIOT EQUATION OF STATE MEASUREMENTS FOR ELEVEN MATERIALS TO FIVE MEGABARS

by
W.M. Isbell
F.H. Shipman
A.H. Jones

Materials & Structures Laboratory
Manufacturing Development, General Motors Corporation
General Motors Technical Center, Warren, Michigan 48090

This document has been approved for public release and sale; its distribution is unlimited.

Copy No. 10

MSL-68-13

HUGONIOT EQUATION OF STATE MEASUREMENTS FOR ELEVEN MATERIALS TO FIVE MEGABARS

by

W.M. Isbell

F.H. Shipman

A.H. Jones

Materials & Structures Laboratory

Manufacturing Development, General Motors Corporation

General Motors Technical Center, Warren, Michigan 48090

1968, December

Prepared for

DEPARTMENT OF THE ARMY

U.S. ARMY BALLISTIC RESEARCH LABORATORIES

ABERDEEN PROVING GROUND, MARYLAND 21005

UNDER CONTRACT DA-18-001-AMC-1128 (X)

DASA File No. 15.025

MSL-68-13

ABSTRACT

An experimental technique is utilized in which a light-gas gun is used to launch flat impactor plates to high velocities (∿ 8 km/sec) at specimens suspended at the muzzle of the gun. Impact-induced shock waves at pressures to ∿ 5 megabars are recorded and are used to determine the shock state in the specimen. The ability to launch unshocked, stress-free flat plates over a wide and continuous velocity range, coupled with the ability to launch impactor plates of the same material as the target, results in hugoniot measurements of relatively high precision. Measurements were made on Fansteel-77 (a tungsten alloy), aluminum (2024-T4), copper (OFHC, 99.99%), nickel (99.95%), stainless steel (type 304), titanium (99.99%), magnesium (AZ31B), beryllium (S-200 and I-400), uranium (depleted), Plexiglas, and quartz phenolic. The results are compared with those of other researchers.

Deviation from linear shock velocity - particle velocity was found in aluminum beginning at ∿ 1.0 megabars, probably attributable to melting in the shock front.

TABLE OF CONTENTS

TABLE OF CONTENTS (Continued)

LIST OF ILLUSTRATIONS

LIST OF ILLUSTRATIONS (Continued)

LIST OF ILLUSTRATIONS (Continued)

LIST OF ILLUSTRATIONS (Continued)

LIST OF ILLUSTRATIONS IN APPENDIX

LIST OF TABLES

LIST OF TABLES (Continued)

LIST OF TABLES IN APPENDIXES

SECTION I

INTRODUCTION

This report describes the experimental procedures and presents the results of the work performed under contract DA-18-001-AMC-1126(X). The work was sponsored by the U. S. Army Ballistic Research Laboratories, Aberdeen Proving Ground, Aberdeen, Maryland, during the period June 1966 to June 1968. Very high pressure measurements were made to determine the hugoniot equations of state of several metals, a composite and a plastic. Results of these measurements are compared with measurements made by Al'tshuler, McQueen, Skidmore and others. This work extends the scope of a General Motors sponsored research project reported earlier(1) which described the use of a light-gas gun to obtain pressures substantially above those reported by other researchers in this country.

The materials tested are copper (OFHC, 99.99%), nickel (99.95%), titanium (99.95%), aluminum (2024-T4), stainless steel (type 304), magnesium (AZ31B), beryllium (S-200), beryllium (I-400), Fansteel-77 (90% W, 6% Ni, 4% Cu), uranium (depleted), quartz phenolic, and Plexiglas (Rohn and Haas II UVA). Table 1 lists the measured pressure range for each material.

Section II of this report presents a detailed description of the experimental techniques employed for the determination of the hugoniot equations of state. Data analysis is briefly described in Section III, with the details presented in Appendix A. Appendix A also describes and lists the data analysis computer program SHOVEL used to reduce the experiment data. Included in Appendix B is a summary of the results of an error analysis.

Experimental results and comparison with other experiments are presented in Section IV. Section V contains a summary of the experimental results and conclusions.

TABLE 1

SUMMARY OF MATERIALS TESTED AND PRESSURE RANGES EXAMINED

MATERIAL	PRESSURE RANGE (Mb)
Fansteel-77	0.3 - 5.0
Copper (OFHC, 99.99%)	1.0 - 4.5
Aluminum (2024-T4)	0.5 - 2.2
Nickel (99.95%)	0.8 - 4.7
Stainless Steel (Type 304)	0.8 - 4.2
Titanium (99.95%)	0.4 - 2.7
Beryllium (I-400)	0.5
Beryllium (S-200)	0.3 - 1.6
Quartz Phenolic	1.3
Magnesium (AZ31B)	0.2 - 1.4
Plexiglas (Rohn and Haas, II UVA)	0.7 - 1.0
Uranium (depleted)	0.8 - 4.6

SECTION II

EQUATION OF STATE MEASUREMENT

In the past two decades, high explosives have been used to initiate compressive waves with amplitudes from tens of kilobars to several megabars in many materials. High explosive plane wave generators placed either in direct contact with the material or in contact with a "standard" material upon which the specimens were placed, were used to measure hugoniot states to approximately 600 kilobars. Considerably higher pressures were obtained from explosive systems in which the high explosive was used to accelerate a thin flier plate across a gap and then impact the specimen surface. In this manner, pressures to approximately 2 megabars were generated in materials of high density by McQueen and Marsh[2] of Los Alamos Scientific Laboratory (LASL). Hart and Skidmore[3] increased the pressure range of these measurements to over 5 megabars, using a radially converging explosive system which accelerated plates to high velocities at some expense in precision; the converging shock wave system adding complexity to the analysis. Al'tshuler, et al,[4] extended the range of measurements to above 10 megabars, accelerating his flier plates in an undisclosed fashion. Work in the United States has not progressed above the 2 megabars reported by McQueen until this study, which provides an extension of lower pressure data to over 5 megabars.

For this study an "accelerated reservoir" light-gas gun was used to accelerate flier plates to velocities extending above 8 kilometers per second. This method of experimentation offers significant advantages over the explosive techniques previously used. Unshocked, stress-free impactors of similar or dissimilar material to the specimen can be impacted over a wide and continuous pressure range. Of significance is the simplicity of the calculation of the shock state in the specimen, using either symmetric impact assumptions or the measured hugoniot of the gun-launched impactor. For experiments in which the shock is created in a standard by either direct contact with explosives or on being struck by an explosively accelerated plate, the hugoniot point is less readily calculable. In this case, it is necessary to assume a form of the equation of state for the standard in order to get the hugoniot point for the specimen.

THEORETICAL CONSIDERATIONS

The application of the principles of conservation of mass, momentum, and energy across a discontinuity have led to the well-known Rankine-Hugoniot equations. The equations were derived originally for fluids, but may be applied to solids when the pressure P, is understood to represent the one-dimensional stress normal to the wave front. These equations may be used to represent the discontinuous change of pressure P, density ρ, specific volume V, and internal energy E, across a shock front as they are related to the shock wave velocity U_s, and the particle velocity behind the shock front u_p, (Figure 1).

$$P - P_o = \rho_o U_s u_p \qquad (1)$$

$$\rho_o U_s = \rho (U_s - u_p) \qquad (2)$$

$$E - E_o = 1/2\ (P + P_o)\ (V_o - V) \qquad (3)$$

Thus a measurement of the shock wave velocity and the particle velocity associated with the shock wave provides sufficient information to calculate the change in the thermodynamic state of the specimen (assuming that steady state conditions prevail behind the shock front).

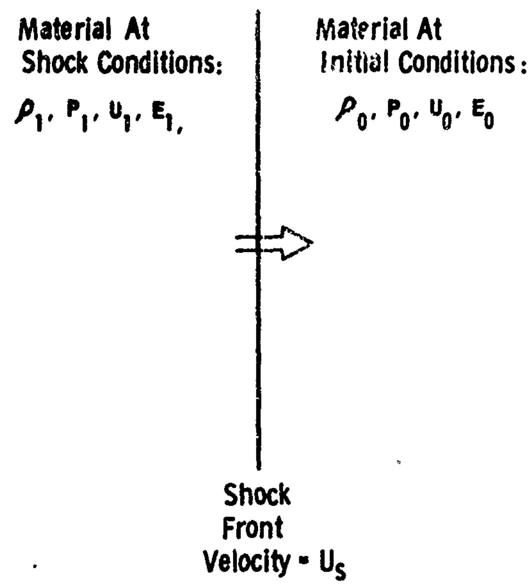

Figure 1 Schematic of Shock Wave Parameters

Although measurement of shock velocity is relatively straightforward, the measurement of particle velocity is more difficult experimentally. For this study, two techniques were used to calculate the particle velocity associated with a measured shock velocity. The first method applies by symmetry. For an impact of a specimen launched at velocity v onto a specimen of the same material a shock wave is induced with particle velocity equal to one-half the impact velocity, or

$$u_p = 1/2\ v \qquad (4)$$

To rigorously apply this condition, it is necessary that the impactor and specimen be in the same thermodynamic state, i.e., the impactor has not been shock heated nor subjected to irreversible changes due to shock loading during acceleration. These conditions have been satisfied for this study.

Since the impact velocity is measured with high precision (customarily ∿ 0.05%), the particle velocity also can be calculated with similar precision. A series of tests are conducted over a range of different impact velocities, the highest pressure being obtained at the highest impact velocity (about 8 km/sec). Each test furnishes a point on the locus of final compressed states known as the hugoniot. Figure 2 shows, in the pressure-particle velocity plane, a graphical description of the conditions of symmetrical impact.

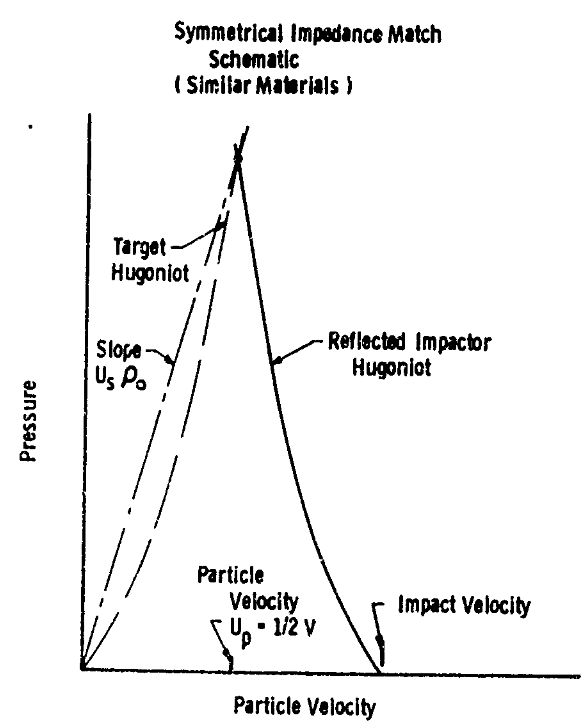

Figure 2 Schematic of Symmetrical Impact Analysis

To obtain pressures higher than those created by symmetrical impact at the maximum launch velocity, it is possible to impact the specimen with a material of higher shock impedance (defined as the product of the initial density and the shock velocity) and to calculate the resultant particle velocity and pressure by an adaptation of the impedance matching technique developed by Walsh et al.[5] With this technique, a measurement of the velocity of the impactor material, the hugoniot of which has been previously measured, is sufficient, when combined with a measurement of the shock velocity in the specimen material, to determine a point on the hugoniot of the specimen. Figure 3 shows an impactor of known hugoniot striking a specimen with velocity v. A single shock wave of velocity U_s is induced in the specimen. The intersection of the line $\rho_o U_s$ and the hugoniot of the impactor, centered at velocity v, determines the shock pressure and the particle velocity in the specimen.

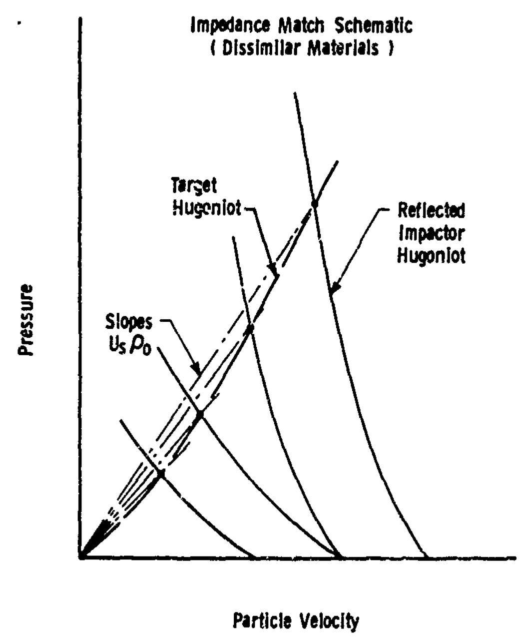

Figure 3 Schematic of Dissimilar Materials Impact Analysis

EXPERIMENTAL TECHNIQUES

The experimental determination of hugoniot equations of state using the impedance match technique is based on the measurement of the shock velocity in the specimen and of the velocity of the impactor. With the techniques described below, these two measurements can be made with precisions of approximately 0.5 and 0.05 percent respectively, resulting in hugoniots of good accuracy considering the limited number of tests conducted on several of the materials.

The light-gas gun range and basic instrumentation have been described in several other papers[1,6,7,8] and are again included here for completeness of this report.

Launching Techniques

The gun used to accelerate the impactor is an accelerated-reservoir light-gas gun with a launch tube bore diameter of either 29 mm or 64 mm. This type of gun maintains a reasonably constant pressure on the base of the projectile during the launch, allowing a relatively gentle acceleration of the impactor materials.

Figure 4 shows the layout of the range. The gun consists of the following major components:

1. Powder chamber
2. Pump tube, 89 mm internal diameter by 12 m long
3. Accelerated-reservoir high-pressure coupling
4. Launch tube, either 29 mm internal diameter by 8 m long or 64 mm diameter by 8 m long
5. Instrumented target chamber and flight range.

Figure 4 Layout of ARLG Gun Range

When the gun is loaded for firing, gunpowder is placed in the powder chamber and the pump tube is filled with hydrogen. The hydrogen is compressed by a plastic nosed piston which has been accelerated by the burnt gunpowder. In turn, the projectile is accelerated by the release of the compressed hydrogen through a high pressure burst diaphragm.

Prior to firing, the flight range and instrument chamber are evacuated and then flushed with helium to approximately 10^{-2} Torr to eliminate any spurious effects due to gas build-up and ionization between projectile and target. The sealing lips on the rear of the plastic sabot are pressed tightly against the sides of the launch tube by the high pressure gas and effectively eliminate blow-by of the hydrogen gas.

Careful attention to the condition of the launch tube is necessary for successful firing in the high velocity ranges. Bore linearity of better than 0.2 mm over the full 8 m length of the launch tube is maintained. Internal diameter is maintained constant to within 0.01 mm. Launch tubes are cleaned and honed after each firing and are removed every 15 to 20 firings for reconditioning.

Figures 5 and 6 show the instrumentation chamber designed for the high pressure studies. This chamber is connected to the barrel of the gun through an O-ring seal to allow free axial movement of the launch tube. The target chamber and target are shock-mounted to prevent premature motion before projectile impact. To facilitate this, several stages of mechanical isolation have been arranged in the barrel, I-beam support structure and the concrete foundation.

The impact chamber is a steel cylinder of 61 cm O.D. and 1.5 m length. Physical access and instrument ports are precisely machined in a horizontal plane and in planes 45° above the horizontal. Two stations of six ports each are accurately spaced 30.5 cm apart.

Operationally, the ports are closed against O-ring vacuum seals with Plexiglas or magnesium windows for optical and x-ray access or with steel cover plates.

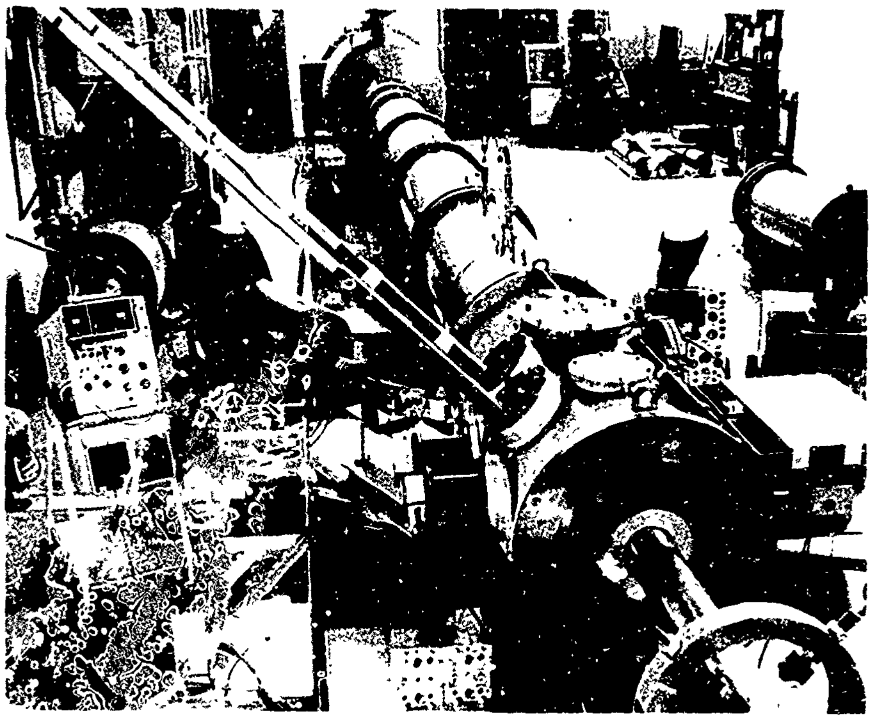

Figure 5 Target Chamber Set-up with Continous Writing Streak Camera in Position

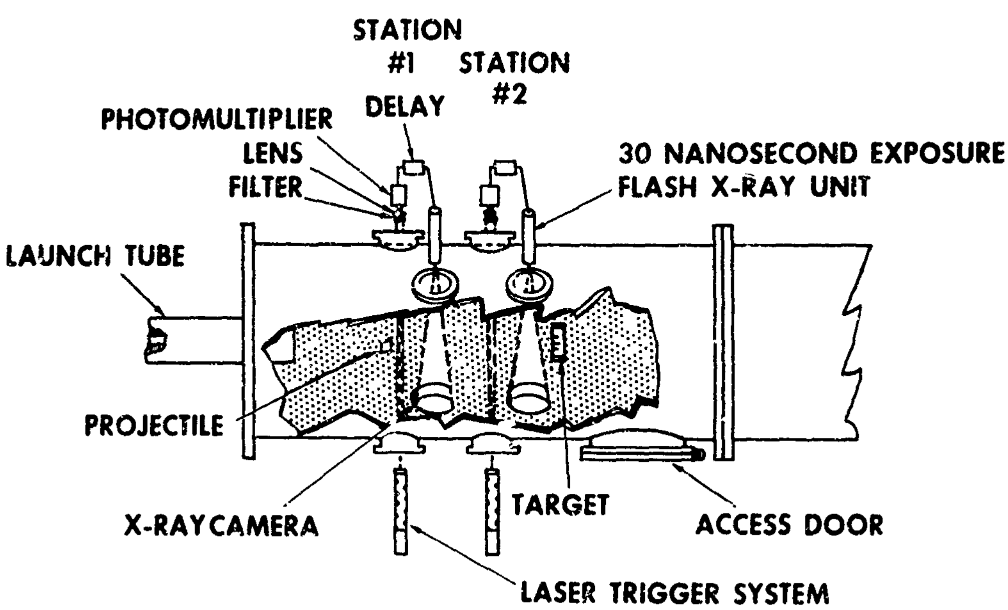

Figure 6 Top View of Target Chamber

INSTRUMENTATION

The impactor velocity measuring system consists of a laser triggering system and two short duration flash x-rays.[8] With this system, impactor velocities are measured accurate to 0.05%. The triggering system consists of a neon-helium gas laser aimed at a photo-detector across the impact chamber orthogonal to and intersecting the line of flight of the projectile. A photomultiplier monitors the laser light output through a set of masks and a narrow band optical filter. When light interruption occurs due to projectile passage, a sharp change of voltage level is converted into a signal of sufficient amplitude to trigger a Field Emission Corporation 30 nanosecond dual flash x-ray unit. The x-ray flash exposes a Polaroid film plate on the opposite side of the chamber by means of a fluorescing intensifier screen. The trigger and x-ray flash system is then duplicated to record the passage of the projectile in the second field of view 30.5 cm further down range.

The spacing between the two x-ray field centerlines is indicated by fiducial wires which are measured by an optical comparator to within 0.2 mm. Measurements of the impactor face position relative to the window fiducials allow calculation of actual projectile position and travel over the time interval measured between flash exposures. Figure 7 is an example of the shadowgraphs of the two x-ray stations showing the projectile in free flight before impact.

A second method is also employed to measure impactor velocity. The time interval between the first x-ray flash and the impact of the projectile on the target is recorded electronically. The impactor and target positions are measured from the x-ray shadowgraphs and a velocity is calculated. Variations in measurements between the two techniques are usually less than 0.05%.

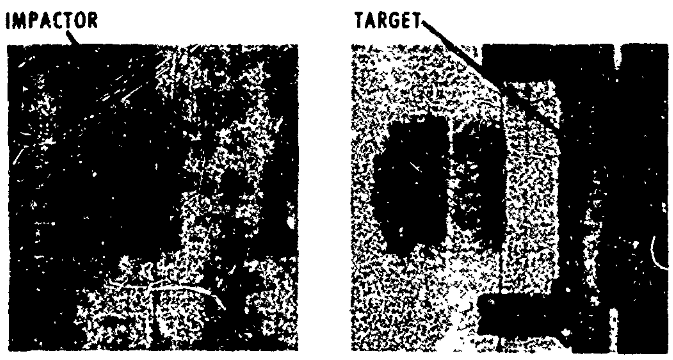

Figure 7 X-ray Shadowgraphs of Projectile Before Impact

The target is located approximately 60 cm from the launch tube muzzle and is included in the #2 x-ray field of view. Measurements of the shock wave transit time in the target are made using four coaxial self-shorting pins as sensors. The shorting of a pin results in a sharply rising current to ground which produces a signal across the time-interval-meter input termination resistors. The circuit is so designed that each pin signal can be seen on three output lines and is free of any reflections or ringing for several hundred nanoseconds. The individual circuits are "tuned" by the use of trimmer capacitors so that the rise time of each signal is 1.0 ± 0.1 nsec to 12 volts. Thus it is possible for the combined mechanical-electronic signal system to make use of the ± 1/2 nsec resolution of the time recording instruments.

The shock wave transit time-interval-meters are Eldorado Model 793 counters. These counters have a specified time resolution of ± 1/2 nsec and may be read digitally to the nearest nanosecond. They require an input signal of 1 volt with a rise time approximately 1 nsec. Although instrument stability is specified to be one part in 10^4 for long term and five parts in 10^6 for short term, in actual practice, the instruments are calibrated prior to each shot over a period of about 10 minutes. The shot is then fired within five minutes of completion of the calibration procedure.

The planarity of the shock wave induced in the target is dependent on the impactor flatness at impact. The impactor surface is machine lapped and then hand polished flat to 0.5×10^{-3} mm. Tests performed with impactors of Fansteel-77 and OFHC copper indicate the surface curvature after launch to be less than the 5 nanosecond time resolution of the optical recording system at a launch velocity of 7 km/sec.

The impactor tilt relative to the target specimen front surface is sensitive to launch tube linearity and sabot alignment as well as to target alignment. The capability to adjust the target position and perpendicularity relative to the launch tube centerline by an optical technique brings the average tilt at impact to approximately 0.005 radians (approximately 15 nanoseconds of tilt at an impact velocity of 7 km/sec).

Because of the comparatively gentle acceleration of the projectile to its terminal velocity, the impactor plate is not shock heated. In addition, free flight in an evacuated range precludes aerodynamic heating. This accounts for the flatness of the impactor after launch and significantly reduces the complexity of the experiment. The estimated temperatures rise during launch of the order of 1°C.

TARGET DESIGN AND CONSTRUCTION

The 29 mm diameter of the launch tube places restrictions on the diameter of the impactor plate and on the size of the specimen which are severe enough to require a thorough study of the optimization of target dimensions. In general, it is desirable to operate over as long a time base as possible for transit time measurements. However, the launch tube diameter controls the allowable specimen thickness. For larger specimens rarefactions from both the unconfined edges and free rear surface of the impactor plate could overtake the head of the shock wave before measurements have been taken. To determine the maximum specimen thickness which would still maintain an unrarefacted area on the rear surface of the specimen on which sensors could be placed to record wave arrival, the following analysis was used.

A typical estimate of the angle of intrusion of plastic rarefaction waves from the specimen edges, α_1, is to assume that $\tan \alpha_1 \approx 1$ (see Figure 8), and to ignore the elastic rarefaction wave system. Although for many materials this assumption is justified, for some materials this criterion is inadequate; in particular, materials with a low Poisson's ratio should be calculated more carefully.

The elastic wave velocity, C_e, is given by

$$C_e = C_p \sqrt{\frac{3(1-\nu)}{1+\nu}} = C_p K \qquad (5)$$

where ν is Poisson's ratio and C_p is the plastic wave velocity, which for strong shocks is a function of u_p, the particle velocity. Existing experimental results indicate that ν is a weak

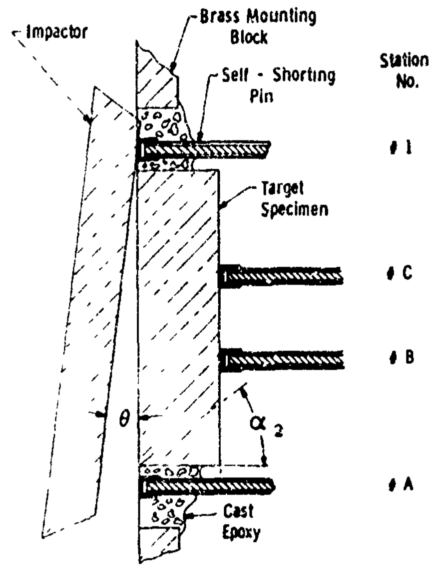

Figure 8 Schematic of Target and Impactor

function of the shock strength.[6,9,10] To a good approximation, the elastic rarefaction angle, α_2, is

$$\tan \alpha_2 = \left[K^2 \tan^2 \alpha_1 + (K^2-1) \left(\frac{U_s - u_p}{U_s} \right)^2 \right]^{1/2} \qquad (6)$$

Figure 9 is a plot of α_2 versus Poisson's ratio for the metals listed in Table 2. The calculation assumes a value of tan $\alpha_1 = 0.7$, taken from the work of Al'tshuler[9], who notes that for compressions greater than ∿ 1.3, tan α_1 becomes essentially constant at 0.70 ± .03 and $\frac{U_s - u_p}{U_s}$ is taken as unity - its maximum value. Included in Figure 9 is a comparison of values of tan α_2 measured in this laboratory[10] for copper, aluminum, titanium and beryllium. As these measurements fall below the calculated line of the minimum allowable design angle, it is felt that equation (6) provides a reasonably conservative design critera. In practice, the design angle is chosen several degrees larger than the values listed.

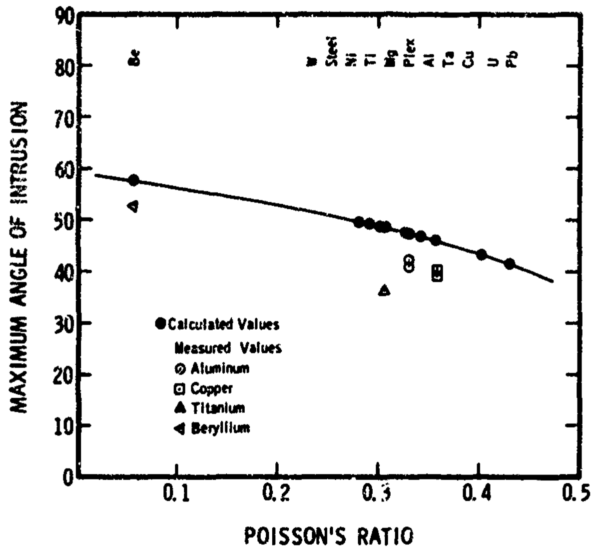

Figure 9 Intrusion Angle of Elastic Edge Rarefaction vs Poisson's Ratio

Impactor thicknesses were chosen to avoid rarefactions originating at the impactor free rear surface from overtaking the shock wave until shock transit time measurements were complete. A single impactor thickness was calculated which was adequate for all materials and was used in all tests.

The target specimen was a machined and ground disc with the impact and rear surfaces machine lapped and hand polished to a surface finish of 1 microinch rms or better. The lapping procedure employed produced surface flatness within $\sim 10^{-3}$ mm. Parallelism was maintained to $\sim 10^{-3}$ radians. The thicknesses of all specimens were measured to an accuracy of $\pm 0.5 \times 10^{-3}$ mm.

The target specimen thicknesses at the pin stations were measured with a Zeiss light-section microscope employed as a comparator. The use of the light-section microscope avoids the problem of an indicator marring the specimen surface since no physical contact is made with the surface. Rather, the vertical position of a thin beam of light projected on the specimen is compared with the position of the beam projected on a laboratory grade gage block and the specimen thickness is calculated.

The basic features of the target design employed in this work are illustrated in Figure 10. Two coaxial shorting pins were passed by the edge of the specimen disk with their cap faces exactly in the plane of the specimen impact surface. These pins were used to initiate the timing for the shock wave transit time measurement and to measure impactor tilt in terms of the time interval difference between their respective closures.

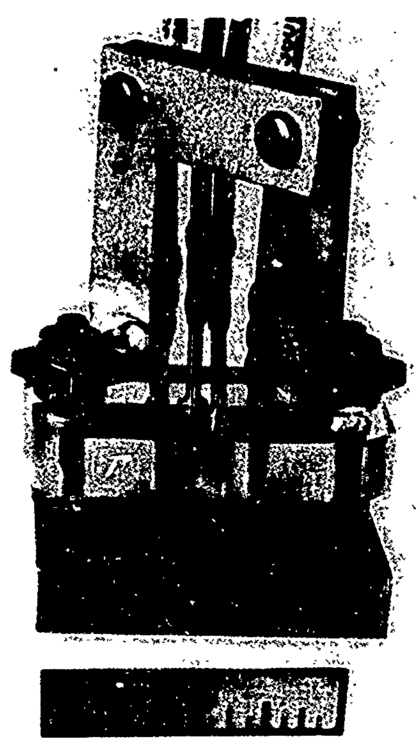

Figure 10 Photograph of Target

TABLE 2

CALCULATED MINIMUM DESIGN ANGLES
OR MAXIMUM EDGE RAREFACTION ANGLES
CALCULATED FROM EQUATION (6)

Material	Poisson's Ratio	Minimum Design Angle, α_2
Aluminum	.332	47°
Beryllium	.055	58°
Copper	.356	45°
Tantalum	.342	46°
Tungsten	.280	50°
Uranium	.402	43°
Titanium	.304	48°
Lead	.430	41°
Magnesium	.306	49°
Nickel	.300	48°
Steel (Mild)	.290	49°
Plexiglas	.327	47°

Two rear surface pins (or one, depending upon the target diameter) were mounted in line with the tilt pins to record the shock wave arrival at the rear surface. All four pins were mounted in a guide fixture which assured the proper geometrical spacing. The tilt pins were fixed in position in a dimensionally stable epoxy, while the rear surface pins were spring loaded in place in the pin guide. The pin retainer and cable bracket lent rigidity to the assembly to prevent accidental damage to the pin shafts.

The four-pin targets, in conjunction with the four Eldorado one-nanosecond time interval meters, produced four values of the shock wave transit time. From these four values a sin~1~ shock wave velocity in the specimen was calculated and, by a system of cross-checking, an indication of the precision of the measurement was available.

The degree of non-planarity of impact between target and impactor is calculated by comparing shock transit times recorded by the counters started by each of the two front surface pins. The time difference between the shorting of the front surface pins, Δt_t (which, when combined with the impact velocity, yields the tilt angle, θ) is calculated from $\Delta t_t = t_{1-C} - t_{A-C} = t_{1-B} - t_{A-B}$, where t_{1-C} is the time recorded on the counter started by pin #1 and stopped by pin C (Figure 10a).

For the highest velocity tests (7-8 km/sec), it was necessary to lighten the projectile by reducing the diameter and the thickness of the impactor plate. The target designed for these highest pressure shots had a slightly smaller diameter and thickness and was provided with only one coaxial shorting pin on the rear surface.

The coaxial self-shorting pins* employed in this work as sensors consisted of a one millimeter diameter tube of brass surrounding a teflon sleeve and a copper inner conductor. The pins were connected to RG174 50Ω cable by soldered joints and were made self-shorting by the placement of a brass cap over the sensing end, which left a small gap (on the order of 0.050 ± .002 mm) between its inner face and the flat end of the inner conductor. When a large amplitude stress wave reaches the cap face, the cap is set into motion and the gap is closed at the

* Model CA-1039, Edgerton, Germeshausen and Grier, Santa Barbara, California.

free surface velocity of the cap material. The pin gaps were measured by x-ray shadowgraphy, of which Figure 11 is an example, and the measurements were employed in the shock velocity calculations for corrections to pin closure times.

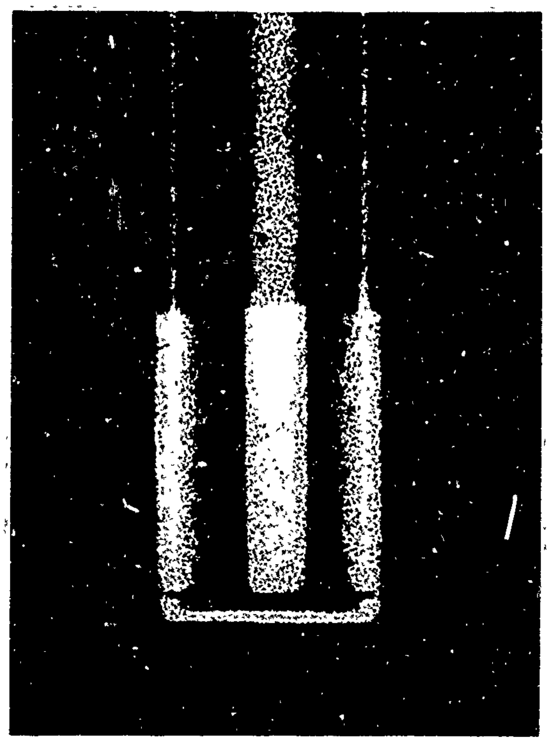

Figure 11 X-ray of Coaxial Shorting Pin

SECTION III

DATA ANALYSIS

The analysis of the experimental data obtained in the research program is based upon the impedance match solution for the determination of particle velocity, pressure, energy and volume of the shock state in the specimen. The requisite information in the analysis is the shock wave velocity, the impact velocity, and the hugoniot of the impactor. A general description of the method of data analysis is given here, with the detailed equations presented in Appendix A.

SHOCK WAVE VELOCITY

The measurements relevant to shock wave velocity are the target thickness and the shock wave transit time interval. In order to calculate the shock wave transit time, it is necessary to make refinements upon the recorded time interval.

Two sources of refinement to the measurement are:

(i) Inclusion of the effects of shock wave tilt resulting from non-planar projectile impace on the target.

(ii) Correction for the differences of closing times of coaxial pins with different gaps, which involves:

(a) Calculation of the interaction of the impactor with the two front surface pins

(b) Calculation of the interaction of the specimen material with the two rear surface pins.

To calculate the closing velocity of the cap for the direct impact of the projectile material on the front surface pins, an impedance match solution is applied, using the impact velocity, the hugoniot of the impactor and the hugoniot of the cap material (brass).

The pin gap correction for the interaction of the rear surface pins and the specimen is based on the impedance match solution of the shock wave in the target being transmitted into the pin material. The hugoniot of the specimen must first be estimated to provide the necessary constants. The shock transit time is first calculated with no pin gap corrections and a preliminary hugoniot point is determined for the specimen. This hugoniot point is then used to calculate pin interactions and, through a series of iterations (usually two) the preliminary hugoniot point is modified until satisfactory convergence is reached (differences < 0.01%).

IMPACT VELOCITY

Measurement of impact velocity has been discussed earlier under "Instrumentation". The flash x-ray system used furnishes high precision velocity determination providing the projectile maintains a constant velocity during the time of measurement. A check on this premise is provided by the seconding system which measures velocity over a longer baseline. No evidence of projectile acceleration or deceleration during its free flight has been observed.

HUGONIOT OF THE IMPACTOR

Measurement of impactor hugoniots for tests in which specimens are impacted with dissimiliar materials are discussed in the following section "Experimental Results".

SECTION IV
EXPERIMENTAL RESULTS

The experimental work effort was first concentrated on the measurement of the hugoniots of the three materials to be used as impactor plates for dissimilar material impacts. The materials were chosen to (i) cover a range of shock impedances, (ii) be easily obtainable and consistent in their material properties from batch to batch, and (iii) to coincide with standards chosen by other laboratories. The materials investigated were Fansteel-77 (a tungsten alloy), OFHC copper, and 2024-T4 aluminum. The ratio of shock impedances of the copper and Fansteel-77 with respect to the aluminum is approximately 1:2:4. These three materials were more thoroughly investigated than the remaining materials so that errors in the impedance match solution for materials impacted by these standards would be minimized.

A typical test series for the determination of the hugoniot of a specimen material, for instance nickel, began with a series of shots using nickel for both impactor and target over the full velocity range of the gun. To obtain pressures higher than those created by like-like impact at the highest velocity, the series continued with impacts using a material of higher impedance than the specimen; in the case of nickel, Fansteel-77 was used. Impact velocities were adjusted to space the shots over the pressure range to be investigated.

In the following section, the experimental data are presented in tabulated and graphical form. Fits to the shock velocity vs particle velocity data have been made by the method of least squares and are listed for each material. The tabulations include measured and calculated parameters and an indication of the "weighting factor" used in the least square fits. In general, test results were weighted according to whether the target had single or double pins, the double pin targets generally having a higher weighing factor due to the redundant measurements of shock wave velocity.

The tabulated data also include the impactor material and the impact velocity. Additional figures are included to illustrate comparison with other researchers.

FANSTEEL-77

Fansteel-77, a tungsten alloy composed nominally of 90% tungsten, 6% nickel, and 4% copper was employed as the standard for the highest pressure tests. Fansteel-77 was chosen over pure tungsten because the metallurgical structure reduces the brittleness of the material (which can cause plate fracture during launch) while maintaining high strength and density.

In the initial work the quality control of the Fansteel-77 stock material presented several problems. The material is produced by powder metallurgical techniques which include pressing and sintering of a billet of the material. The porosity of the surface of the billet was found to be somewhat dependent upon the compacting pressure prior to sintering. The core of the billet, however, was found upon metallographic examination to exhibit essentially no porosity, and sample to sample variations in density were less than 0.5% when the outside 1 mm was removed from a 50 mm diameter bar. The chemical and physical properties of Fansteel-77 are presented in Table 3.

TABLE 3

CHEMICAL AND PHYSICAL PROPERTIES

OF FANSTEEL-77

Chemical Properties

Element	Wt %
W	90 ±.1
Cu	3.8 ±.6
Ni	6.1 ±.2

Physical Properties

Yield Strength (0.2% elong.)		85,000 psi (min)
Ultimate Tensile Strength		98,000 psi (min)
Density		17.01 ± .01 gm/cm^3
Poisson's Ratio:		0.286
Acoustic Velocities*:	Longitudinal, C_1 =	5.049 km/sec
	Shear , C_s =	2.765 km/sec
	Bulk , C_o =	3.912 km/sec

* Ultrasonic tests were performed by J. Havens and R. Lingle of this laboratory.

The test series on Fansteel-77 resulted in a hugoniot over the pressure range .35 Mb to 5.0 Mb. Symmetric impacts were used on all tests so that particle velocity may be assumed to be one-half the impact velocity. Both second and third order fits were made to the data; however, the linear relationship $U_s = C + Su_p$ describes the data with the root mean square (RMS) deviation not significantly larger than the higher order fits. The relationship is given by:

$$U_s = 4.008 + 1.262\ u_p \text{ km/sec}$$

RMS deviation of U_s was ± 0.021 km per second for the seventeen data points. The results are presented in Table 4.

The data points taken are displayed in the U_s vs u_p plane in Figure 12. In one shot the velocity was not measured directly with the x-ray system and instead was calculated from the gun firing parameters. Estimates made in this manner are quoted with standard errors in velocity of ± 2%.

In Figures 13, 14 and 15 are displayed the data for Fansteel-77 compared with the data obtained by researchers of the Ballistics Research Laboratory of the United States Army, Aberdeen Proving Grounds* and the data of Hart and Skidmore[3] for a tungsten alloy similar to Fansteel-77.

The Ballistics Research Laboratories data are in excellent agreement with the results obtained here. The hugoniot measured by Hart and Skidmore has the quadratic form:

$$U_s = 2.95 + 2.47\ u_p - 0.342\ u_p^2 \text{ (km/sec)}$$

* Mr. George Hauver, private communication.

TABLE 4

HUGONIOT DATA FOR FANSTEEL-77

$V_o = 0.0588\ cm^3/gm$
$\rho_o = 17.01 \pm .01\ gm/cm^3$

Shot	Impactor Material	Impact Velocity (km/sec)	Shock Velocity (km/sec)	Particle Velocity (km/sec)	Pressure (Mb)	Relative Volume	Volume (cm^3/gm)	Density (gm/cm^3)	Weighting Factor
S-23	FS	0.906	4.599	0.453	0.354	.9015	.0530	18.87	3
C-922+	FS	1.478*	4.978	0.740 ±.019	0.627 ±.016	.8514 ±.0039	.0501	19.98	1
C-1161°	FS	1.952	5.194	0.976	0.862	.8121	.0477	20.95	3
C-939+	FS	2.152	5.336	1.076	0.977	.7984	.0469	21.31	1
C-1218	FS	2.689	5.661	1.344	1.294	.7626	.0448	22.31	3
C-921+	FS	2.689	5.756	1.344	1.316	.7665	.0451	22.19	3
C-933+	FS	2.774	5.786	1.387	1.365	.7603	.0447	22.37	2
S-21	FS	2.849	5.855	1.425	1.419	.7566	.0445	22.48	3
C-1155°	FS	3.413	6.163	1.706	1.788	.7232	.0425	23.52	3
C-914+	FS	3.548	6.221	1.774	1.877	.7148	.0420	23.80	1
C-940+	FS	3.618	6.365	1.809	1.959	.7158	.0421	23.76	3
S-18	FS	3.648	6.412	1.824	1.989	.7155	.0421	23.77	
C-931+	FS	3.994	6.490	1.997	2.205	.6923	.0407	21.57	
C-923+	FS	4.657	6.939	2.329	2.749	.6644	.0391	25.60	1
C-1220	FS	4.809	7.082	2.405	2.897	.6604	.0388	25.76	3
C-1232	FS	6.646	8.239	3.323	4.529	.6077	.0357	27.99	1
C-962+	FS	6.936	8.390	3.468	4.949	.5867	.0345	29.00	1

* Impact velocity determined from measured gun firing parameters
\+ Tests performed under General Motors sponsored program
° Tests performed under contract NAS2-3427

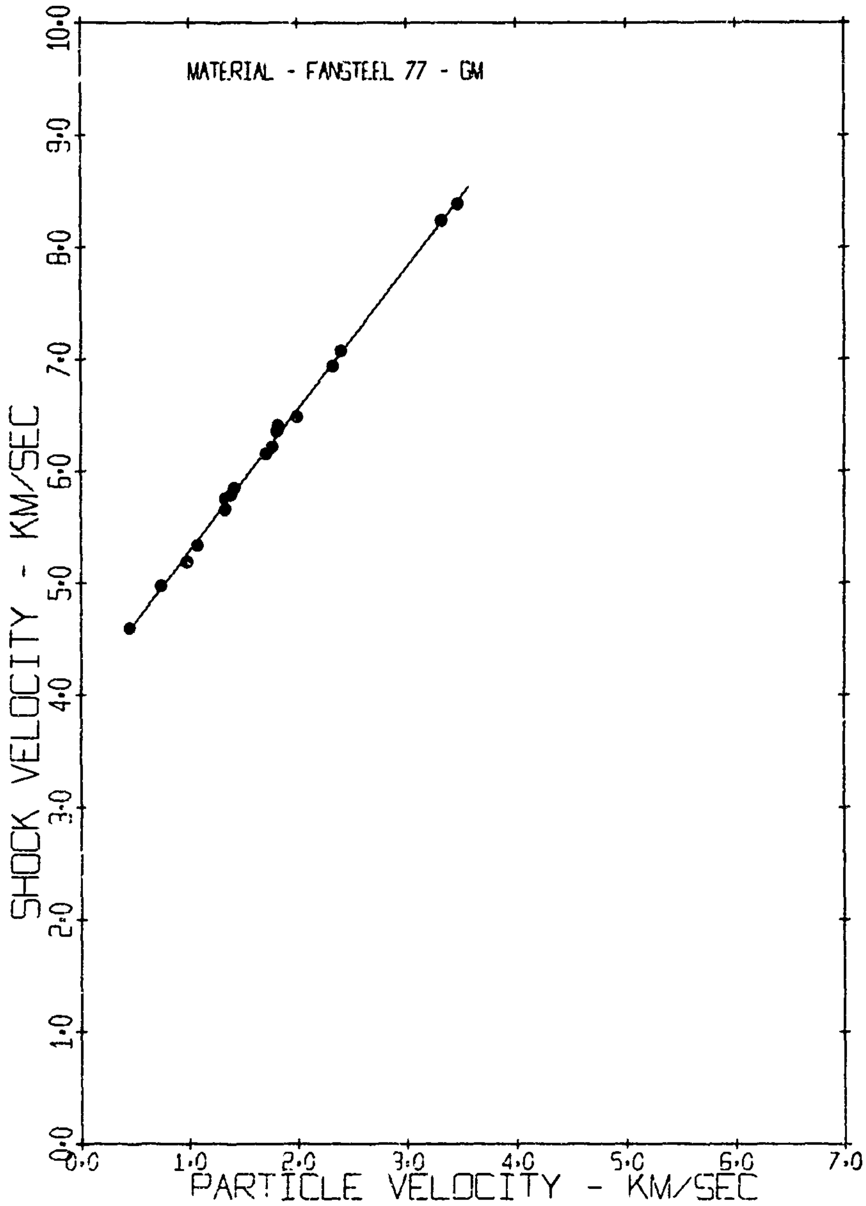

Figure 12 Shock Velocity vs Particle Velocity for Fansteel-77

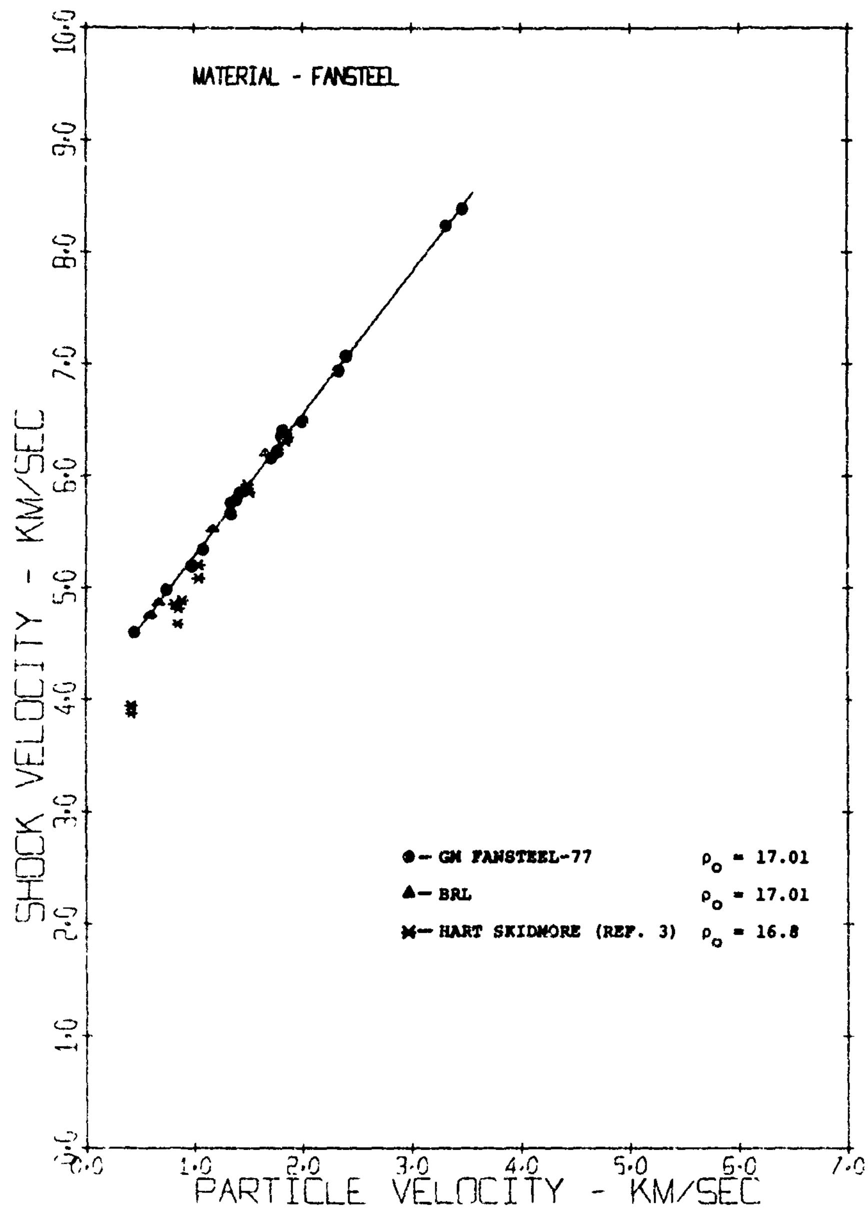

Figure 13 Shock Velocity vs Particle Velocity for Fansteel-77

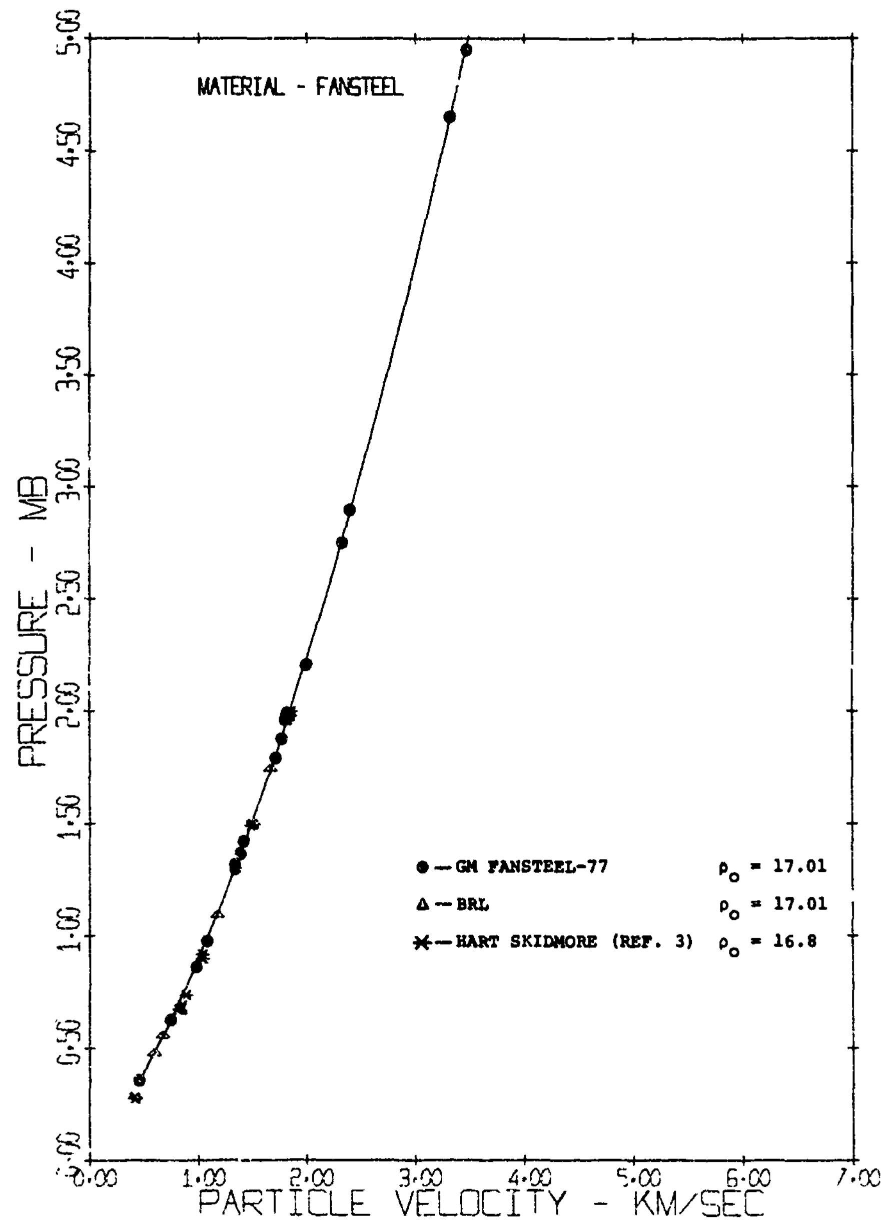

Figure 14 Pressure vs Particle Velocity for Fansteel-77

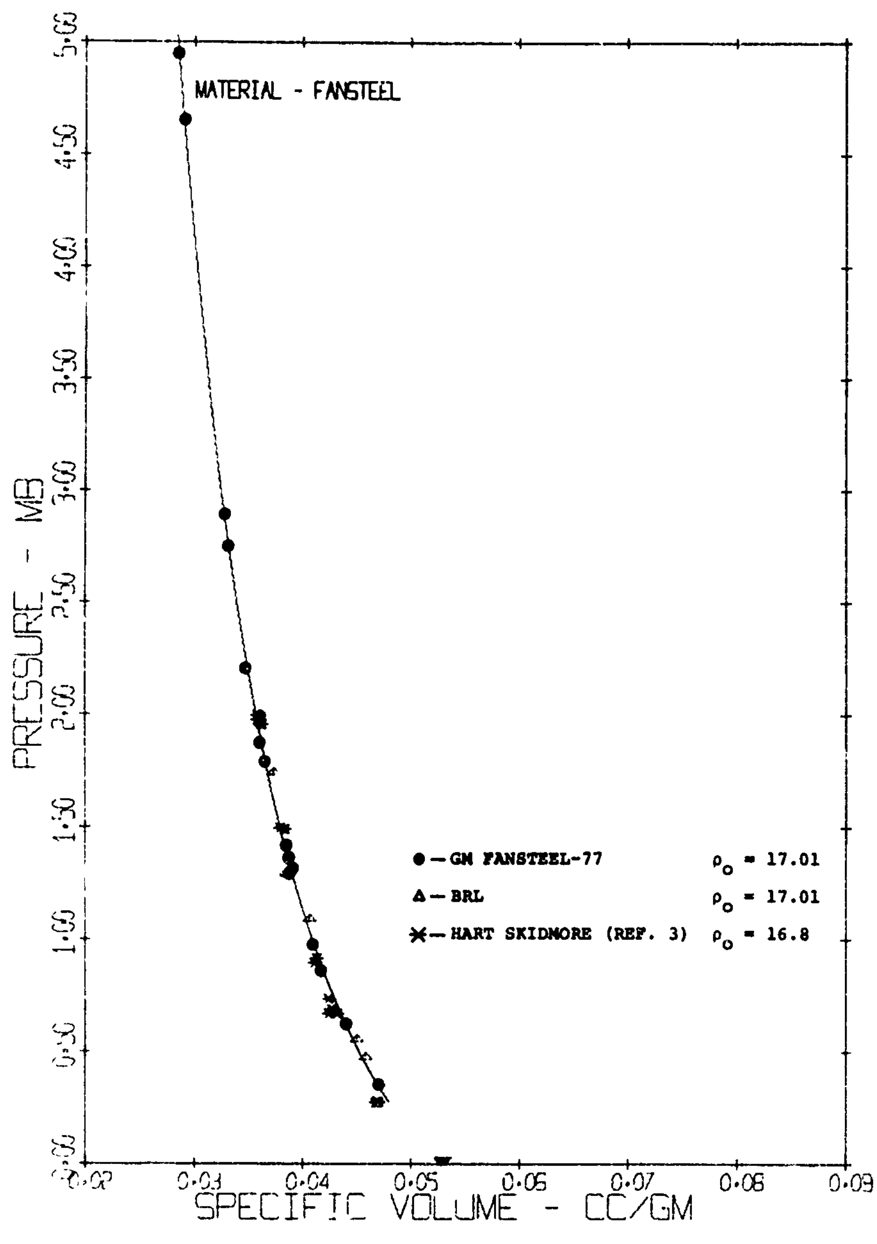

Figure 15 Pressure vs Specific Volume for Fansteel-77

and falls below the present data at lower values of u_p. This behavior is not readily explainable since the intercept of the linear fit to the present work, C_o = 4.008 km/sec., is in agreement with the bulk sound velocity measured ultrasonically, C_o = 3.912 km/sec.

It is interesting to note that the hugoniots for pure tungsten (as measured by LASL) and for Fansteel-77 are quite similar, the LASL linear fit for tungsten being given by:

$$U_s = 4.029 + 1.237\ u_p \text{ km/sec}$$

although the density of the tungsten is 13% higher than that of Fansteel-77.

OFHC COPPER

OFHC copper of 99.99% purity is employed as a standard for the intermediate and high pressure ranges in the hugoniot experiments of a number of laboratories. Physical characteristics of the copper are described in Table 5. The results of twelve tests are presented here in Table 6. The linear fit to the data in the U_s - u_p plane is given by:

$$U_s = 3.964 + 1.463\ u_p \text{ km/sec}$$

Root Mean Square Deviation of U_s = ± 0.009 km/sec for 12 data points. The hugoniot equation recently published by LASL(12) is given by:

$$U_s = 3.940 + 1.489\ u_p \text{ km/sec}$$

in close agreement with the present results.

TABLE 5

CHEMICAL & PHYSICAL PROPERTIES

OF OFHC COPPER*

Chemical Composition

Element	Wt %
Iron	0.0005
Sulphur	0.0025
Silver	0.0010
Nickel	0.0006
Antimony	0.0005
Lead	0.0006
Copper	Remainder

Physical Properties

Density 8.930 gm/cm^3

Poisson's Ratio: 0.332

Acoustic Velocities: Longitudinal, C_l = 4.757 km/sec

Shear, C_s = 2.247 km/sec

Bulk, C_o = 3.99 km/sec

* Based on manufacturers specifications.

TABLE 6

HUGONIOT DATA FOR OFHC COPPER

$V_o = 0.1120\ cm^3/gm$
$\rho_o = 8.930\ gm/cm^3$

Shot	Impactor Material	Impact Velocity (km/sec)	Shock Velocity (km/sec)	Particle Velocity (km/sec)	Pressure (Mb)	Relative Volume	Volume (cm^3/gm)	Density (gm/cm^3)	Weighting Factor
1081	Cu	3.426	6.463	1.713	0.989	.7350	.0823	12.15	3
1240	FS	3.875	7.414	2.343	1.551	.6840	.0766	13.06	3
S-98	Al	7.929	7.815	2.631	1.836	.6633	.0743	13.46	1
S-1[illegible]	FS	4.673	8.062	2.808	2.022	.6517	.0730	13.70	3
1082	Cu	6.434	8.669	3.217	2.490	.6289	.0704	14.20	3
S-76	Cu	7.018	9.076	3.509	2.843	.6134	.0687	14.56	3
963	Cu	7.097	9.149	3.549	2.900	.6121	.0685	14.59	1
1090	Cu	7.12[illegible]	9.196	3.561	2.924	.6128	.0686	14.57	1
1249	FS	6.728	9.785	3.988	3.485	.5924	.0663	15.07	1
S-82	Cu	7.937	9.802	3.971	3.476	.5949	.0666	15.01	1
S-[illegible]9	FS	7.405	10.390	4.368	4.053	.5796	.0649	15.41	1
S-161	FS	7.932	10.785	4.674	4.502	.5666	.0635	15.76	1

The data are presented in Figure 16, which now includes a legend to indicate the impactor material used. The use of different impactors provides a good method for cross-checking the hugoniots of the standards as suggested by McQueen[11]. The hugoniot established by Fansteel-77 impacting copper is indistinguishable from the copper on copper tests. This both checks the accuracy with which the Fansteel-77 hugoniot was determined and provides additional confidence in the use of impedance matching techniques as used in this experimental system. A single test was conducted using 2024 aluminum as an impactor. All tests were used in the calculation of the fit given above. The resulting hugoniot displays a very small RMS deviation, ($\sim$ 0.1% in shock velocity).

Figures 17, 18 and 19 compare the present data with the data of Al'tshuler[9,13], Walsh[5] and McQueen[2]. Agreement within $\sim$ 2% in the linear fit was obtained (i.e., the reported shock velocities are within $\sim$ 2% of the values predicted by the present linear fit).

A close examination of the data indicates a small (< 1%) deviation from a linear fit beginning at $u_p \approx 2.4$ km/sec. It is likely that this deviation is associated with melting in the s k front (see the following discussion on 2024-T4 aluminum). This phenomenon will be discussed more fully in a forthcoming report.

2024-T4 ALUMINUM

The hugoniot experiments performed on 2024-T4 aluminum extend over a pressure range of 0.45 to 2.2 Mb. Fourteen tests were conducted, employing the following impactors: Fansteel-77 - 5 tests; OFHC copper - 5 tests; and 2024-T4 aluminum - 4 tests. In addition, Shot No. 98 from the series on copper is included

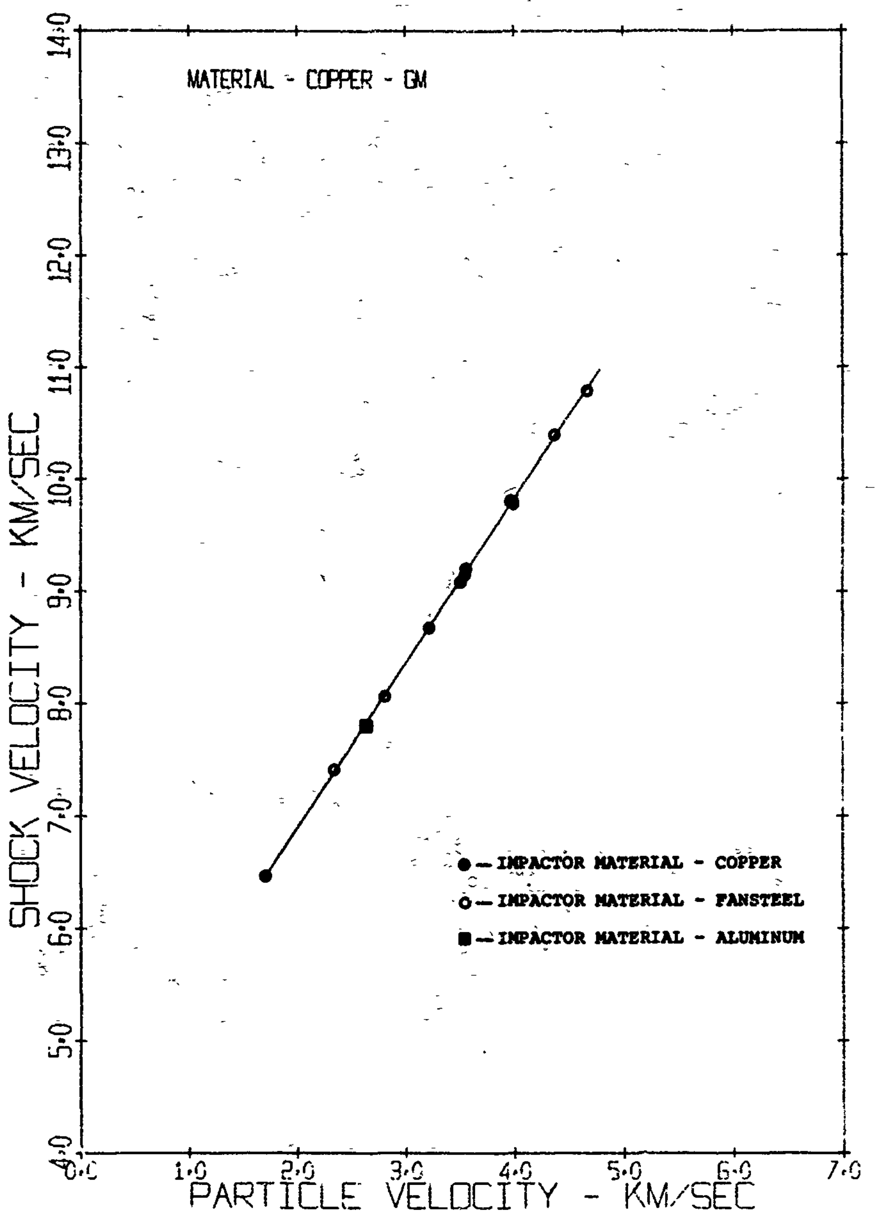

Figure 16 Shock Velocity vs Particle Velocity for Copper

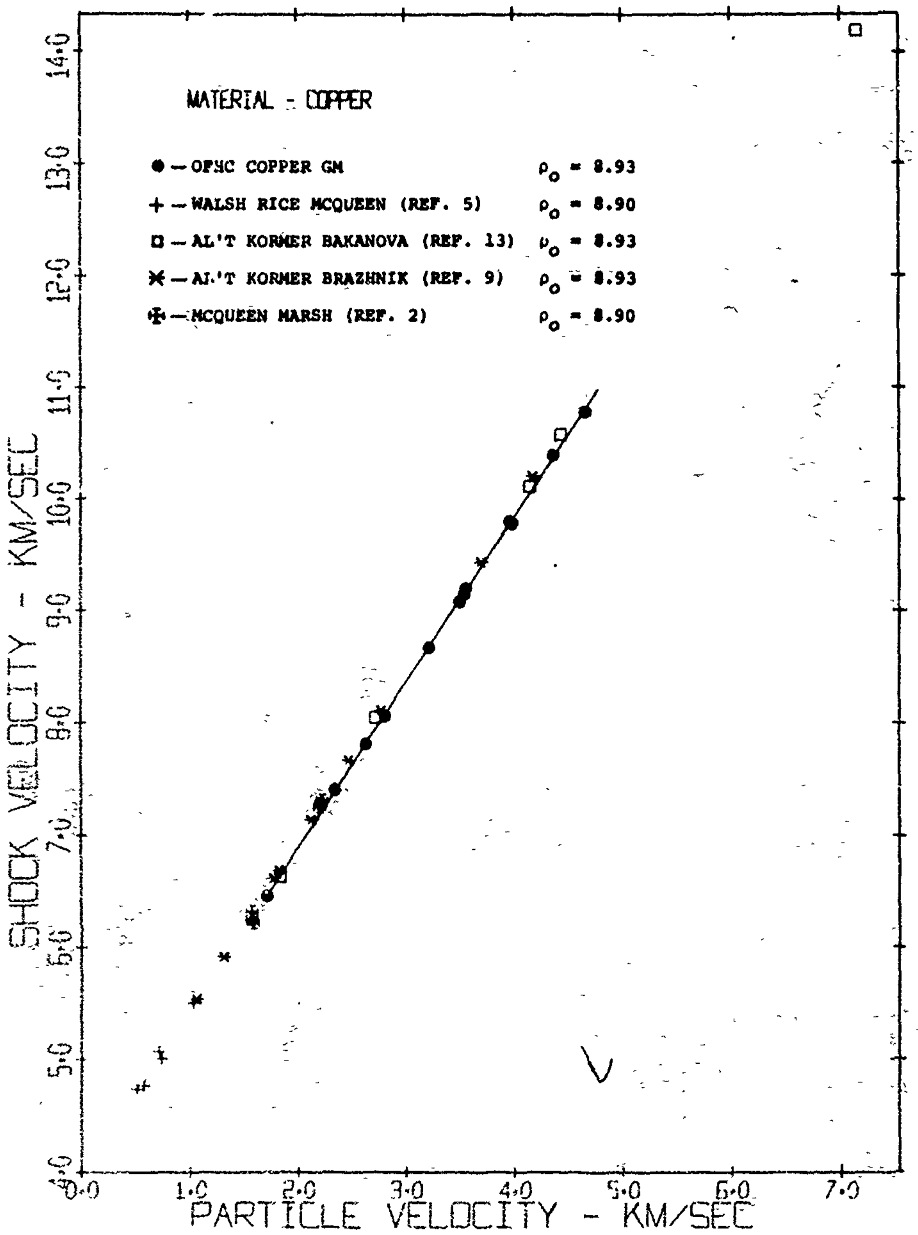

Figure 17 Shock Velocity vs Particle Velocity for Copper

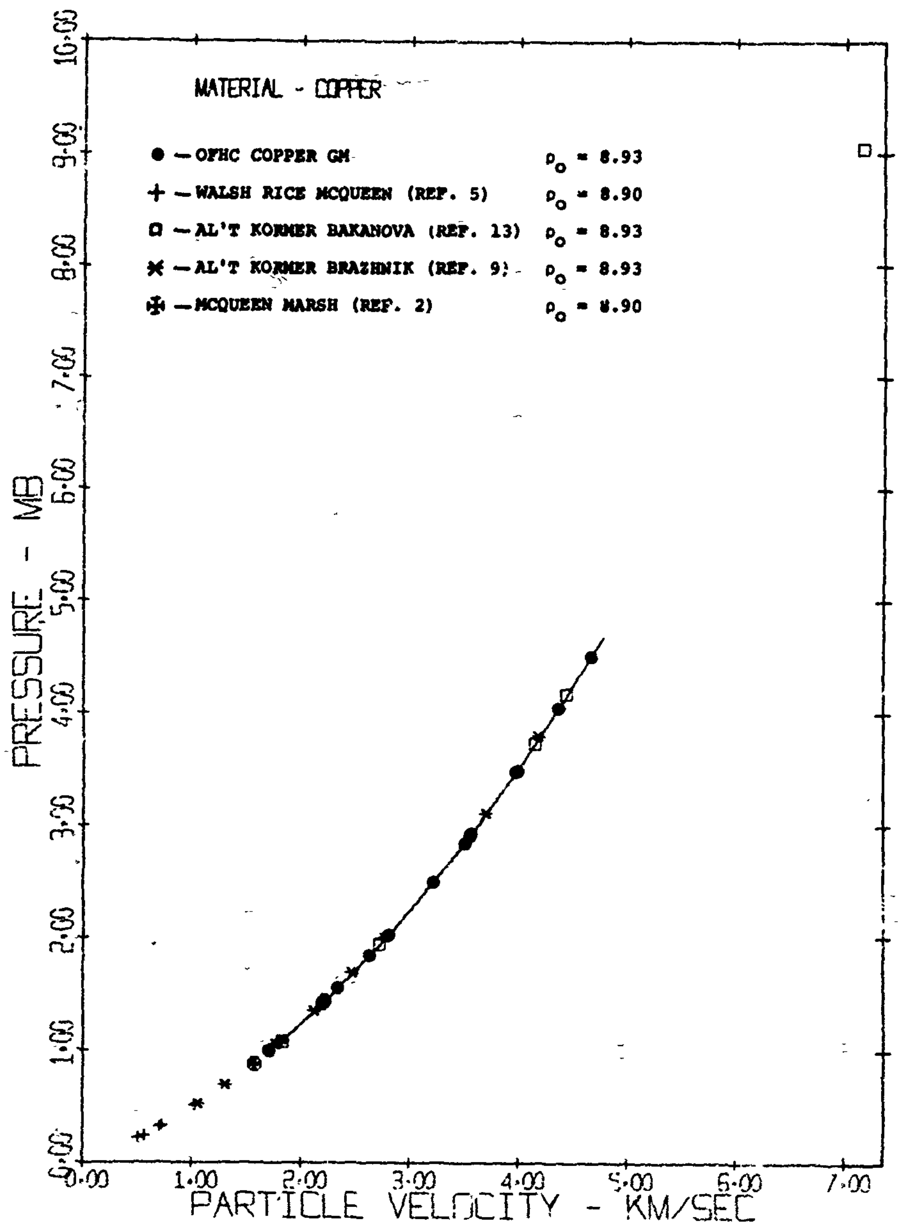

Figure 18 Pressure vs Particle Velocity for Copper

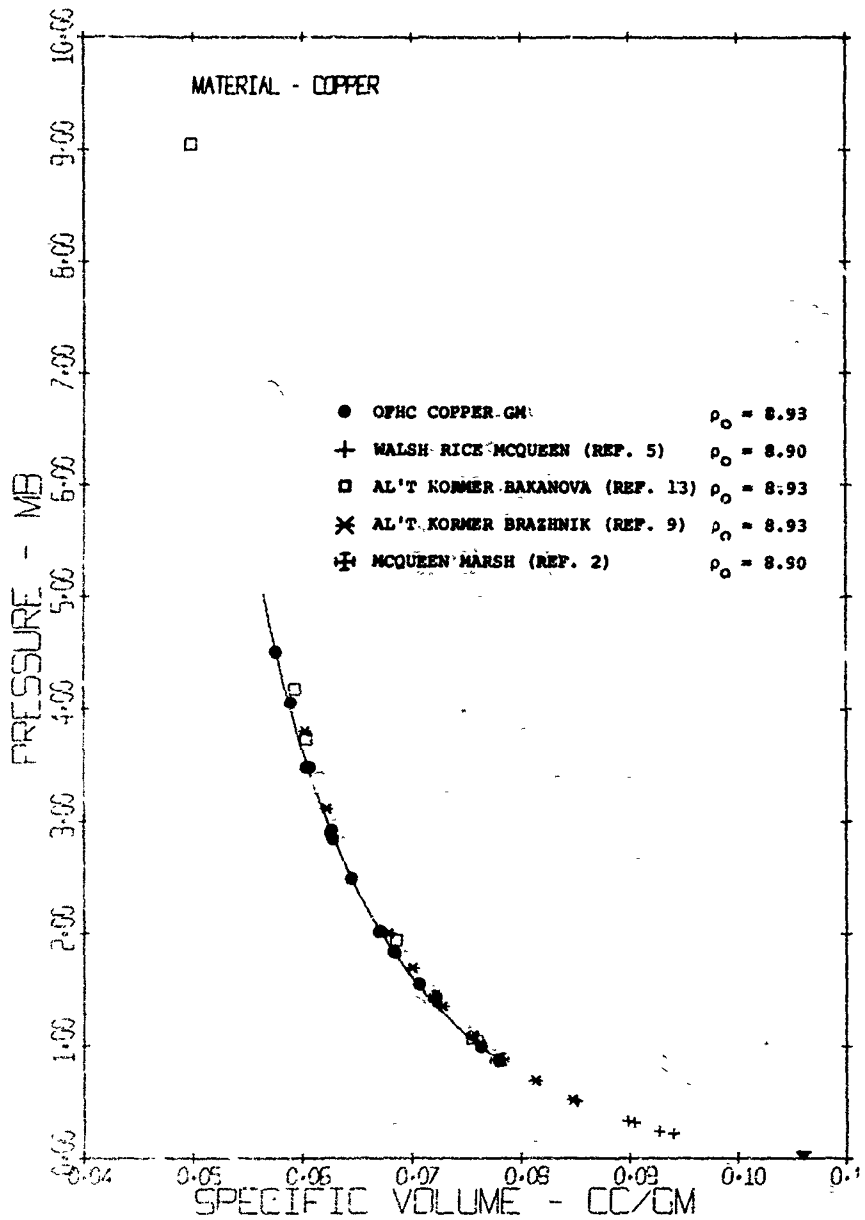

Figure 19 Pressure vs Specific Volume for Copper

as a cross-check by reversing the impactor and specimen materials and impacting an aluminum plate into a copper target. If the hugoniot of the copper is assumed to be known the state in the aluminum may be calculated.

The chemical and physical properties of 2024-T4 aluminum are tabulated in Table 7 and the data are presented in tabular form in Table 8. The measured initial density of the aluminum was $2.783 \pm .001$ gm/cm^3.

Figures 20 and 21 are a plot in the $U_s - u_p$ plane of the experimental results. The linear fit is from LASL, Reference 22. A departure from linear behavior is seen, beginning at $U_p \approx 3.5$ km/sec ($P \approx 1$ megabar), where shock velocity falls below the line representing a linear fit to the data. Although the data shows scatter, it is felt that the trend of the data in this region is beyond experimental error. The linear fit of LASL, $U_s = 5.328 + 1.338\ u_p$, to data below this pressure range, was compared to the present data by calculating deviations of the data from this fit. The deviations are plotted in Figure 22 along with other high pressure data from Russian researchers. Only the ten tests showing least internal scatter and tilt are plotted.

Urlin[15] has proposed a model for melting in the front of a shock wave and predicts an observable effect on the linear $U_s - u_p$ relation. For aluminum the melting is calculated to begin at approximately 1 megabar. The present data follows the trend predicted by Urlin, although whether melting, experimental inaccuracy, or other phenomena is the explanation for the large deviations found between $U_p = 3.5$ to 4.5 km/sec remains to be verified.

The comparison of hugoniot data from other workers[9,13,14,16] is shown in Figures 21, 23 and 24, and displays the area of divergence.

If all the present data points are combined the data may be represented by the equation:

$$U_s = 5.471 + 1.310\ u_p$$

Root Mean Square Deviation = ± .022 km/sec for 11 data points.

TABLE 7
CHEMICAL & PHYSICAL PROPERTIES
OF 2024-T4 ALUMINUM*

Chemical Composition

Element	Wt %
Silicon	0.5
Iron	0.5
Copper	3.8 - 4.9
Manganese	0.3 - 0.9
Magnesium	1.2 - 1.8
Chromium	0.10
Zinc	0.25
Aluminum	Remainder

Physical Properties

Yield Strength		47,000 psi
Ultimate Tensile Strength		68,000 psi
Hardness (Brinell No.)		120
Density (measured)		2.783 gm/cm^3
Poisson's Ratio:		0.332
Acoustic Velocities:	Longitudinal, C_l	= 6.38 km/sec
	Shear, C_s	= 3.20 km/sec
	Bulk, C_o	= 5.20 km/sec

* Based on Alcoa Aluminum Handbook and specimen certification.

TABLE 8

HUGONIOT DATA FOR 2024-T4 ALUMINUM

$V_o = 0.3593\ cm^3/gm$
$\rho_o = 2.783\ gm/cm^3$

Shot	Impactor Material	Impact Velocity (km/sec)	Shock Velocity (km/sec)	Particle Velocity (km/sec)	Pressure (Mb)	Relative Volume	Volume (cm^3/gm)	Density (gm/cm^3)	Weighting Factor
C-1238	FS	2.583	8.099	2.017	0.455	.7510	.2698	3.706	1
S-65	Al	6.161	9.504	3.081	0.815	.6758	.2428	4.118	1
S-74	Cu	4.883	9.793	3.289	0.896	.6642	.2387	4.190	1
S-198°	Al	6.876	9.839	3.439	0.942	.6505	.2337	4.278	1
S-17	FS	4.775	10.047	3.663	1.024	.6354	.2283	4.380	1
S-197°	Al	7.526	10.432	3.763	1.092	.6393	.2297	4.353	1
S-185°	Cu	5.621	10.313	3.789	1.088	.6326	.2273	4.399	1
S-199°	Cu	5.654	10.159	3.828	1.082	.6232	.2239	4.466	1
S-68	Al	8.067	10.594	4.034	1.189	.6192	.2225	4.494	1
C-1246	FS	5.400	10.585	4.127	1.216	.6101	.2192	4.562	1
S-183°	Cu	6.567	10.884	4.438	1.344	.5922	.2128	4.699	1
S-66	Cu	7.833	12.351	5.237	1.800	.5760	.2070	4.832	1
S-98+	Cu	7.929	12.460	5.297	1.837	.5749	.2066	4.841	1
S-69	FS	7.947	13.228	5.962	2.196	.5491	.1973	5.068	1

° Tests performed under GM sponsorship

+ Aluminum impacted into OFHC copper standard

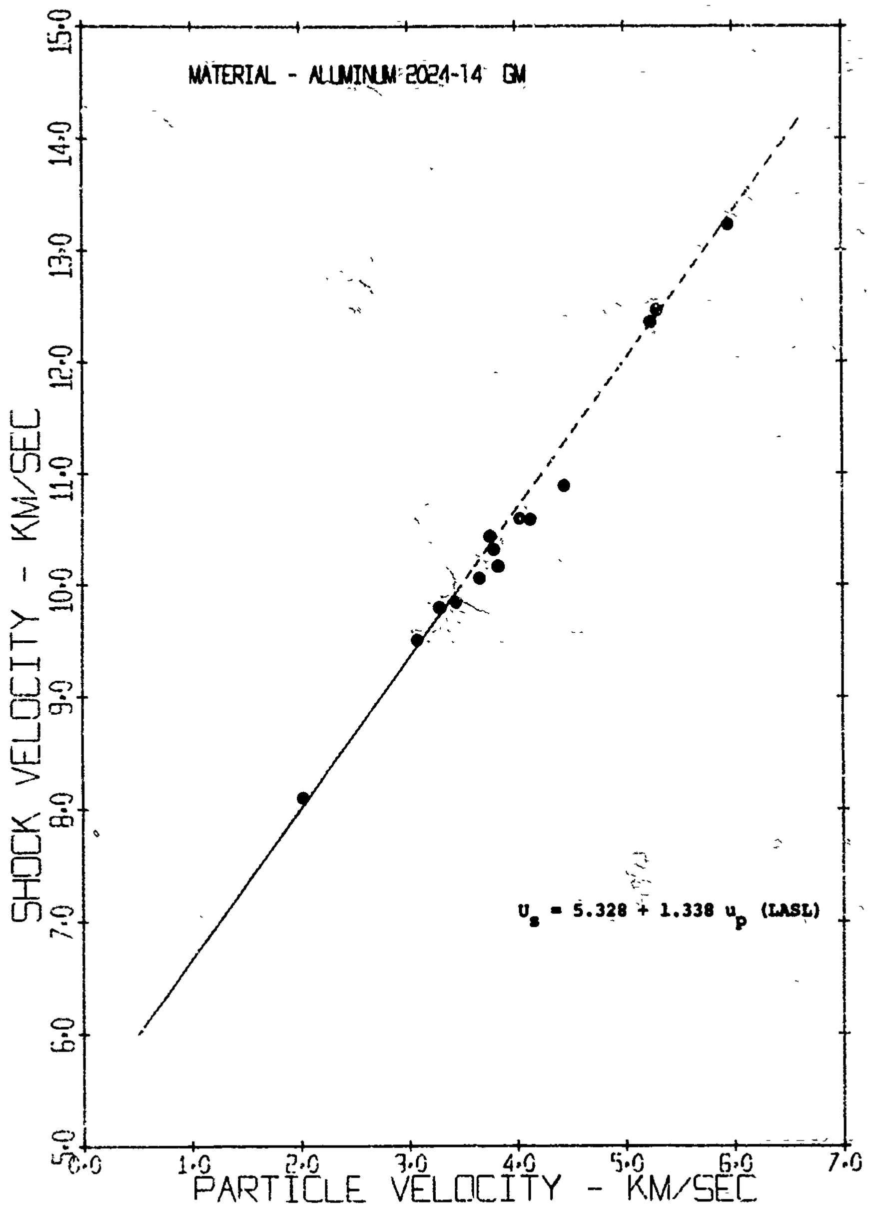

Figure 20 Shock Velocity vs Particle Velocity for 2024-T4 Aluminum

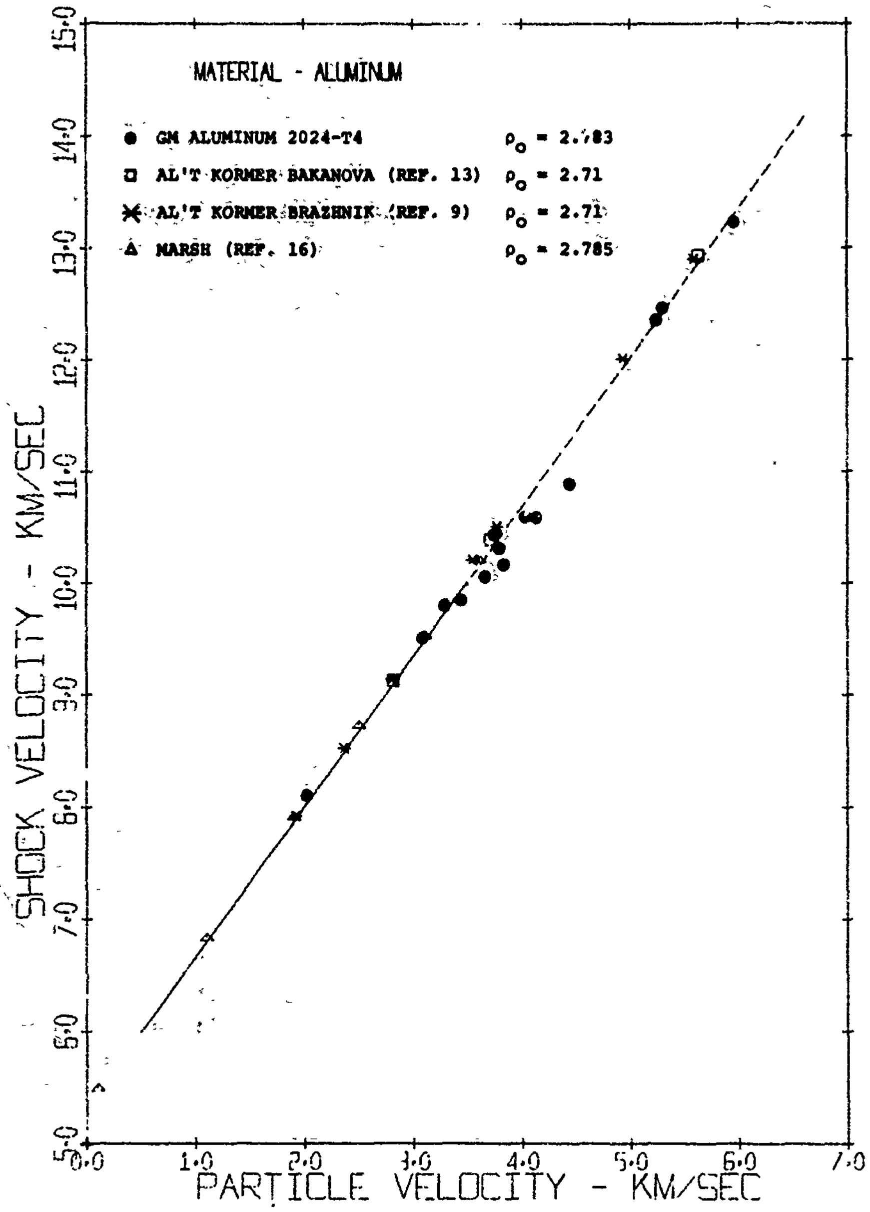

Figure 21 Shock Velocity vs Particle Velocity for Aluminum

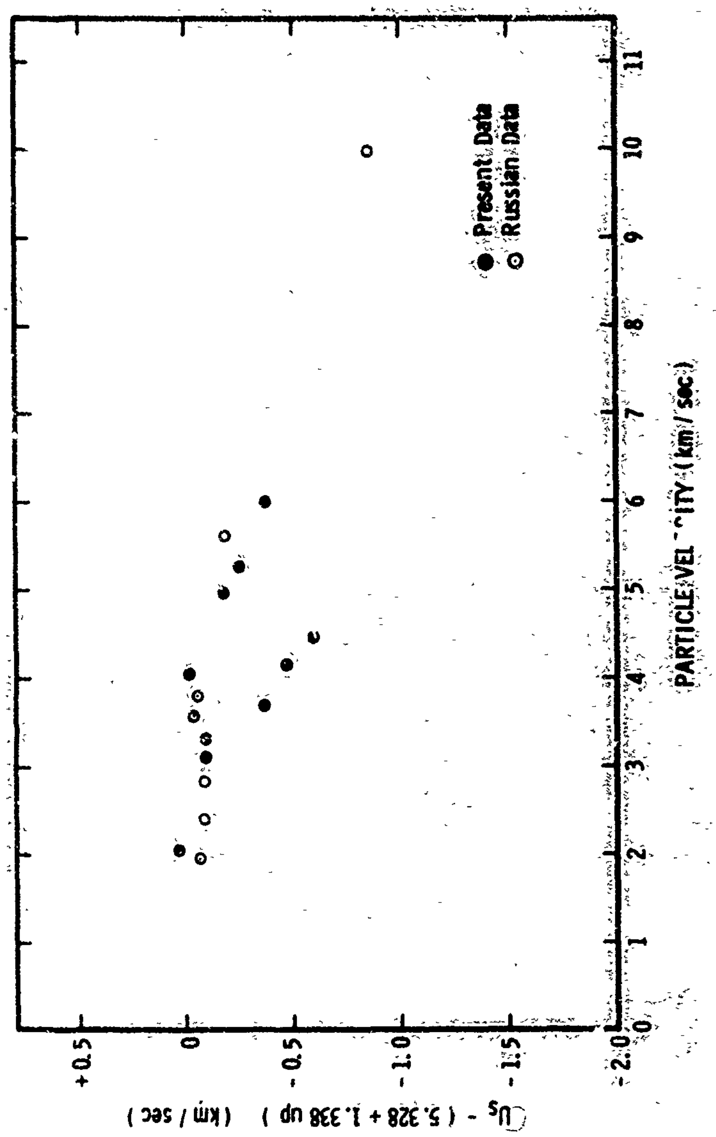

Figure 22 Deviation of Aluminum Data from Linear Fit

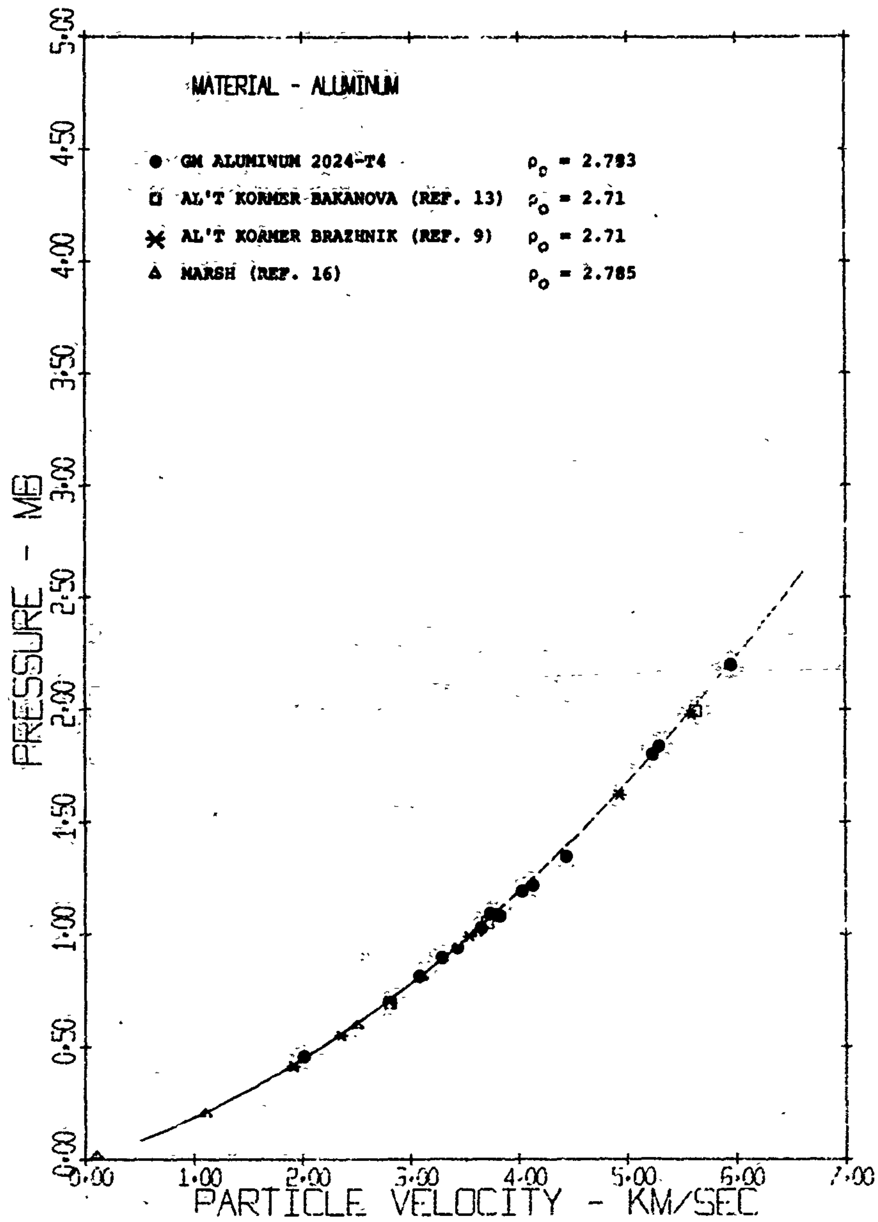

Figure 23 Pressure vs Particle Velocity for Aluminum

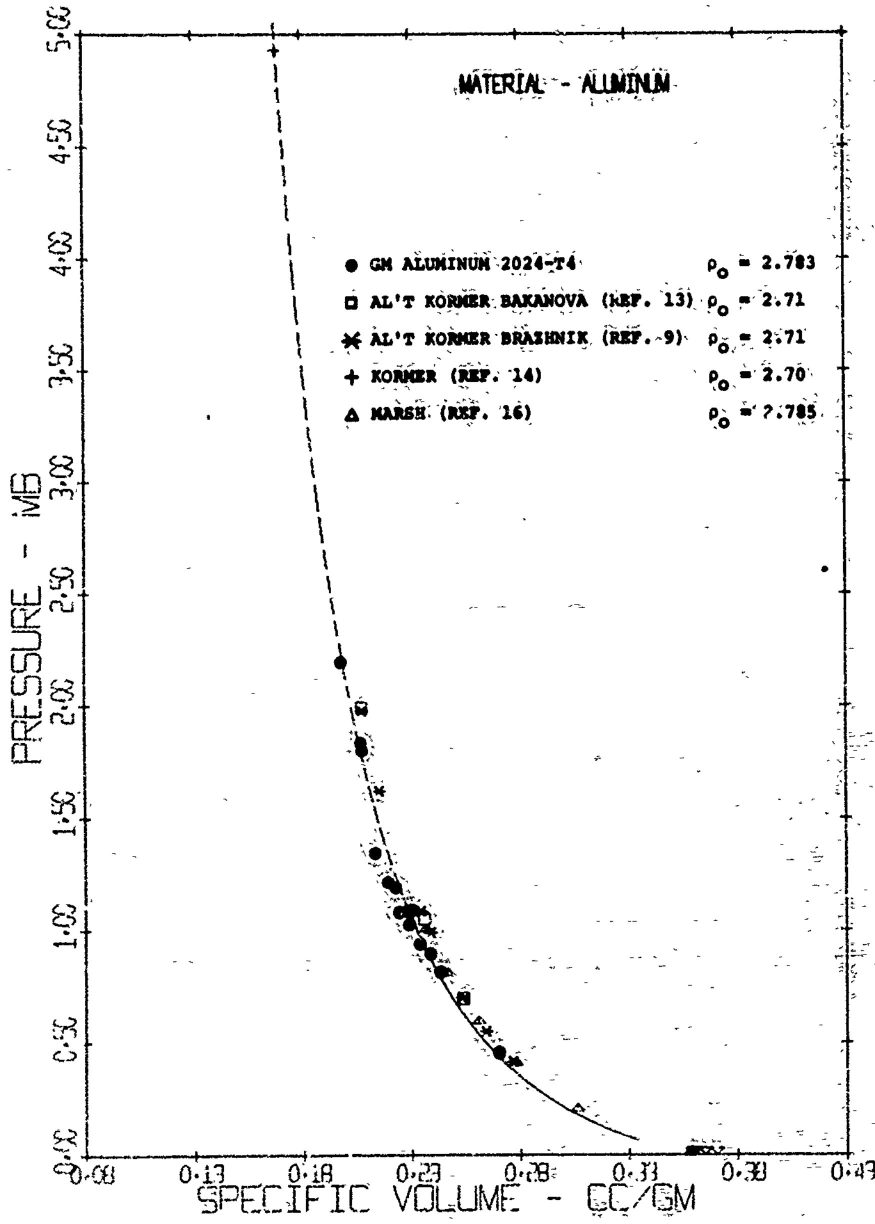

Figure 24. Pressure vs Specific Volume for Aluminum

DEPLETED URANIUM

Five tests were performed for the determination of the hugoniot of depleted uranium over the pressure range 0.9 to 4.6 megabars. The impactors were either OFHC copper or Fansteel-77. No similiar material impact tests were performed. The data is shown in Figures 25, 26 and 27. Excellent agreement was obtained with the high pressure (above 2 megabars) data of Skidmore and Morris[17].

The density of the samples was 18.951 gm/cm^3. The chemical and physical properties are summarized in Table 9, and the hugoniot data are presented in Table 10. It was noted that the freshly lapped surfaces oxidized rapidly, turning from a light tan to a dark blue-brown color. That this oxide layer is very thin may be demonstrated by the fact that several swipes of the surface on a wet lapping plate removes the darkened layer.

The linear fit to the present data is given by the equation:

$$U_s = 2.443 + 1.582\ u_p \text{ km/sec}$$

Root Mean Square Deviation = ± .029 km/sec for 5 data points.

Skidmore's data for 5 data points is included in the figures and is fit by the quadratic equation:

$$U_s = 2.55 + 1.504\ u_p + .0901\ (u_p - 2.50)^2 \text{ km/sec}$$

for $u_p > 2.5$ km/sec.

The linear fit from LASL[12] is $U_s = 2.487 + 1.539\ u_p$.

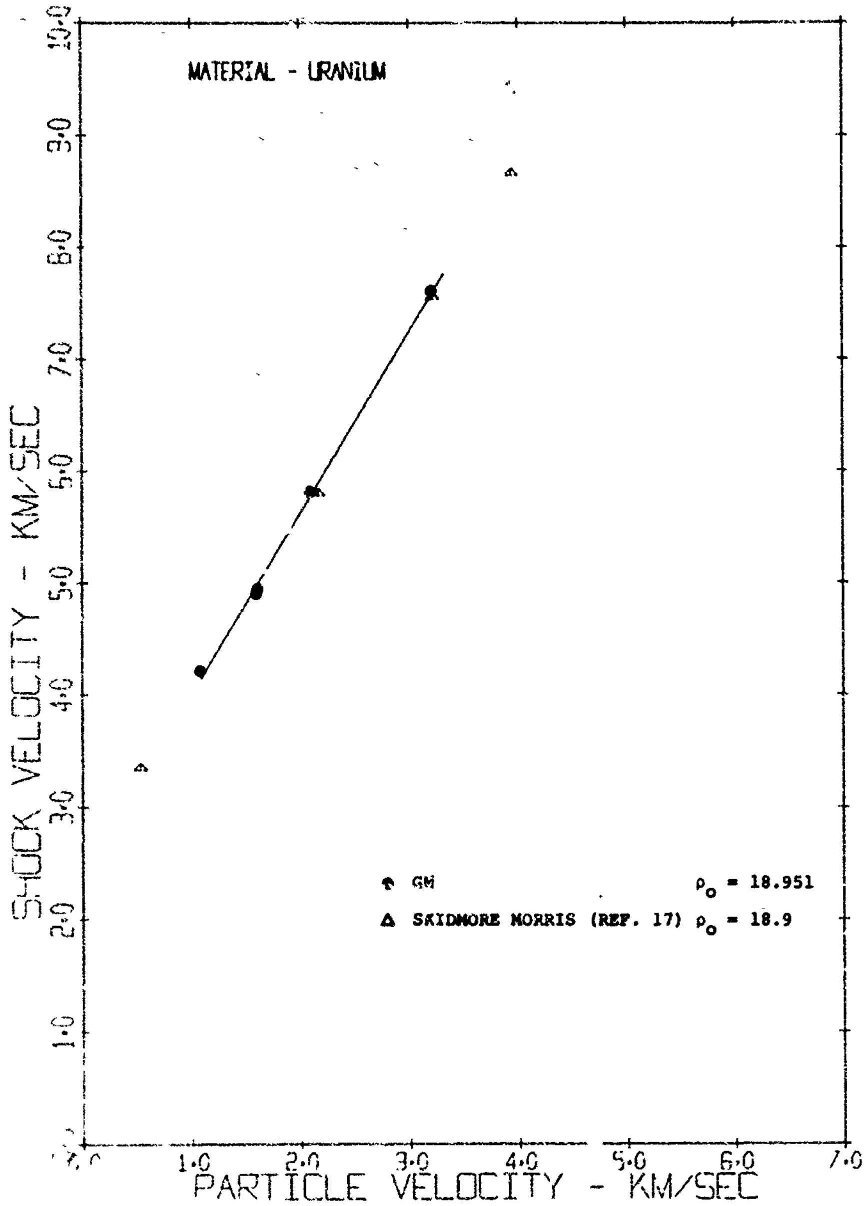

Figure 25 Shock Velocity vs Particle Velocity for Uranium

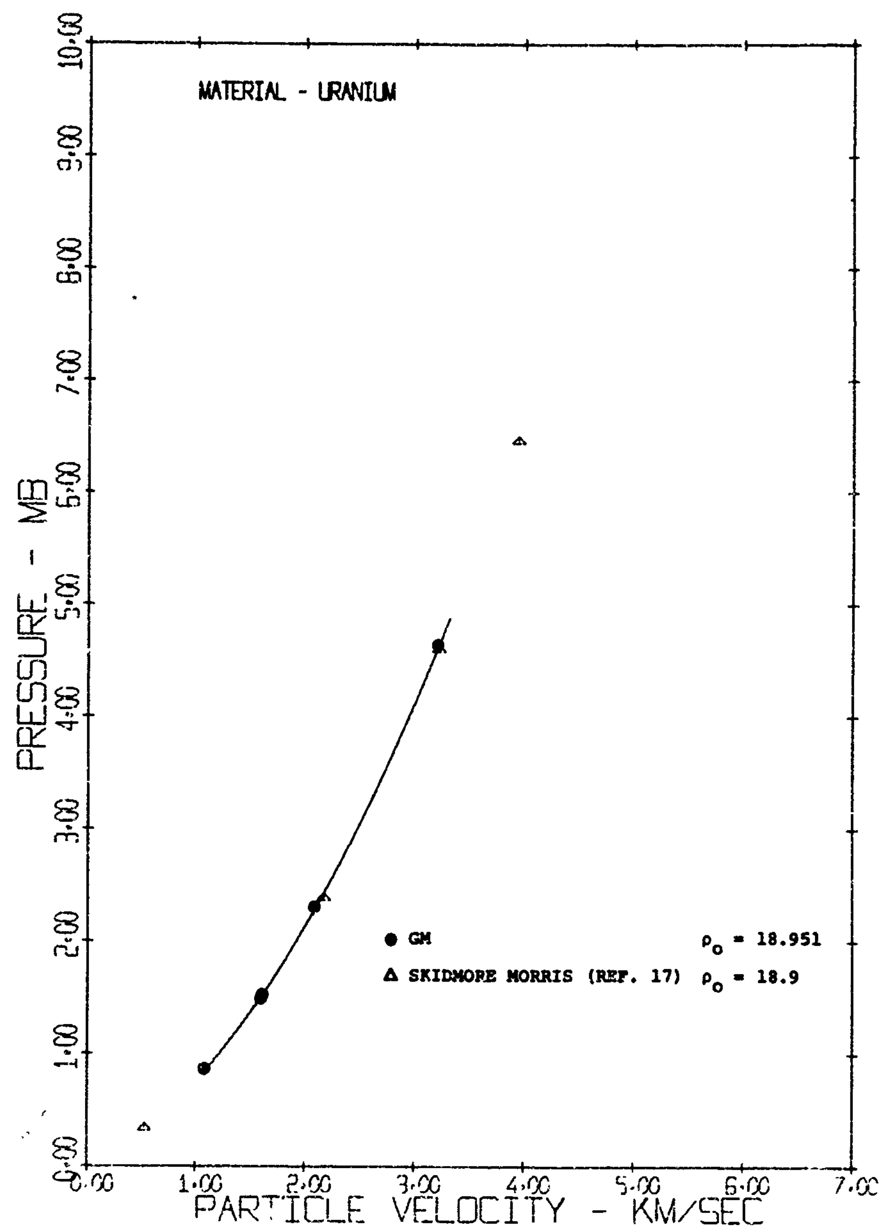

Figure 26 Pressure vs Particle Velocity for Uranium

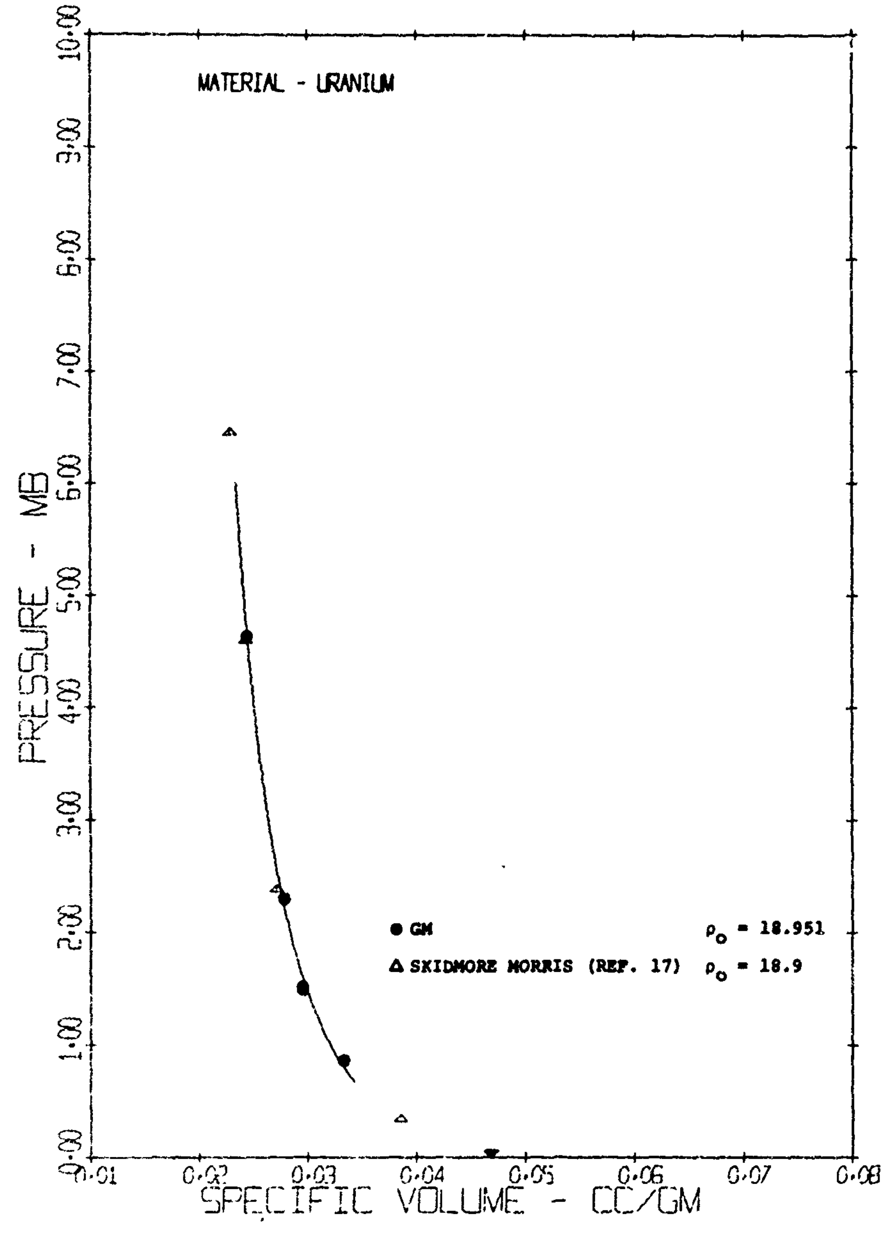

Figure 27 Pressure vs Specific Volume for Uranium

TABLE 9

CHEMICAL AND PHYSICAL PROPERTIES OF DEPLETED URANIUM

Chemical Properties

Element	Wt (ppm)
Aluminum	9
Boron	0.3
Cadmium	0.3
Chromium	3
Copper	8
Iron	10
Magnesium	2
Manganese	15
Molybdenum	2
Nickel	20
Lead	1
Silicon	40
Samarium	1
Uranium wt %	99.8%

Physical Properties:

Yield (0.1% elongation)		47,250 psi
Tensile Strength		124,000 psi
Density (measured		18.951 gm/cm^3
Poisson's Ratio:		0.402
Acoustic Velocities:	Longitudinal	C_1 = 2.97 km/sec
	Shear	C_s = 1.20 km/sec
	Bulk	C_o = 2.63 km/sec

TABLE 10

HUGONIOT DATA FOR DEPLETED URANIUM

$V_o = .0528\ cm^3/gm$
$\rho_o = 18.95\ gm/cm^3$

Shot	Impactor Material	Impact Velocity (km/sec)	Shock Velocity (km/sec)	Particle Velocity (km/sec)	Pressure (Mb)	Relative Volume	Volume (cm^3/gm)	Density (gm/cm^3)	Weighting Factor
1273	FS	2.044	4.206	1.077	0.859	.7439	.0393	25.47	3
S-125	Cu	3.885	4.902	1.602	1.488	.6732	.0355	28.15	3
S-124	Cu	3.918	4.940	1.613	1.510	.6735	.0355	28.14	3
1274	FS	4.134	5.806	2.086	2.295	.6407	.0338	29.58	3
S-128	Cu	7.967	7.596	3.214	4.627	.5769	.0304	32.85	1

NICKEL

Five tests were performed to obtain hugoniot data for nickel. Three of the tests employed nickel impactors and two impactors were of Fansteel-77. The nickel was purchased under specification ASTM-B-160-61 as 99.5% purity. The chemical and mechanical properties of the material are listed in Table 11.

The experimental data are tabulated in Table 12 and displayed in Figures 28, 29, 30 and 31. The least squares linear fit to the data is:

$$U_s = 4.456 + 1.555\ u_p \text{ km/sec}$$

Root Mean Square Deviation = ± 0.012 km/sec for 5 data points.

The data of McQueen and Marsh[2], Walsh[5], and Al'tshuler[18] are also displayed in the figures and show reasonable agreement with the present data. The data of Al'tshuler extends over a wider pressure range (1.1 to 9.2 megabars) than the General Motors data. The Al'tshuler data is best fit by a quadratic curve:

$$U_s = 4.370 + 1.775\ u_p - 0.047\ u_p^2 \text{ km/sec}$$

Sigma U_s = 0.008 km/sec for 4 data points.

TABLE 11

CHEMICAL AND PHYSICAL PROPERTIES OF NICKEL

Chemical Properties

Element	Weight %
Carbon	0.11
Manganese	0.26
Iron	0.09
Sulphur	0.005
Silicon	0.02
Copper	0.02
Nickel	99.47

Physical Properties

Yield Strength at 0.2% Elongation	82,500 psi
Tensile Strength	89,000 psi
Density	8.864 gm/cm^3

Poisson's Ratio: 0.300

Acoustic Velocities: Longitudinal, C_l = 5.76 km/sec
Shear, C_s = 3.08 km/sec
Bulk, C_o = 4.53 km/sec

TABLE 12

HUGONIOT DATA FOR NICKEL

$V_o = 0.1128\ cm^3/gm$
$\rho_o = 8.864\ gm/cm^3$

Shot	Impactor Material	Impact Velocity (km/sec)	Shock Velocity (km/sec)	Particle Velocity (km/sec)	Pressure (Mb)	Relative Volume	Volume (cm^3/gm)	Density (gm/cm^3)	Weighting Factor
S-85	Ni	2.662	6.546	1.331	0.772	.7967	.0899	11.13	3
S-87	Ni	3.839	7.407	1.919	1.260	.7409	.0836	11.96	3
S-86	Ni	7.184	10.070	3.592	3.206	.6433	.0726	13.78	3
S-120	FS	7.934	11.572	4.581	4.699	.6041	.0682	14.67	1
S-95	FS	7.993	11.607	4.616	4.749	.6023	.0680	14.72	1

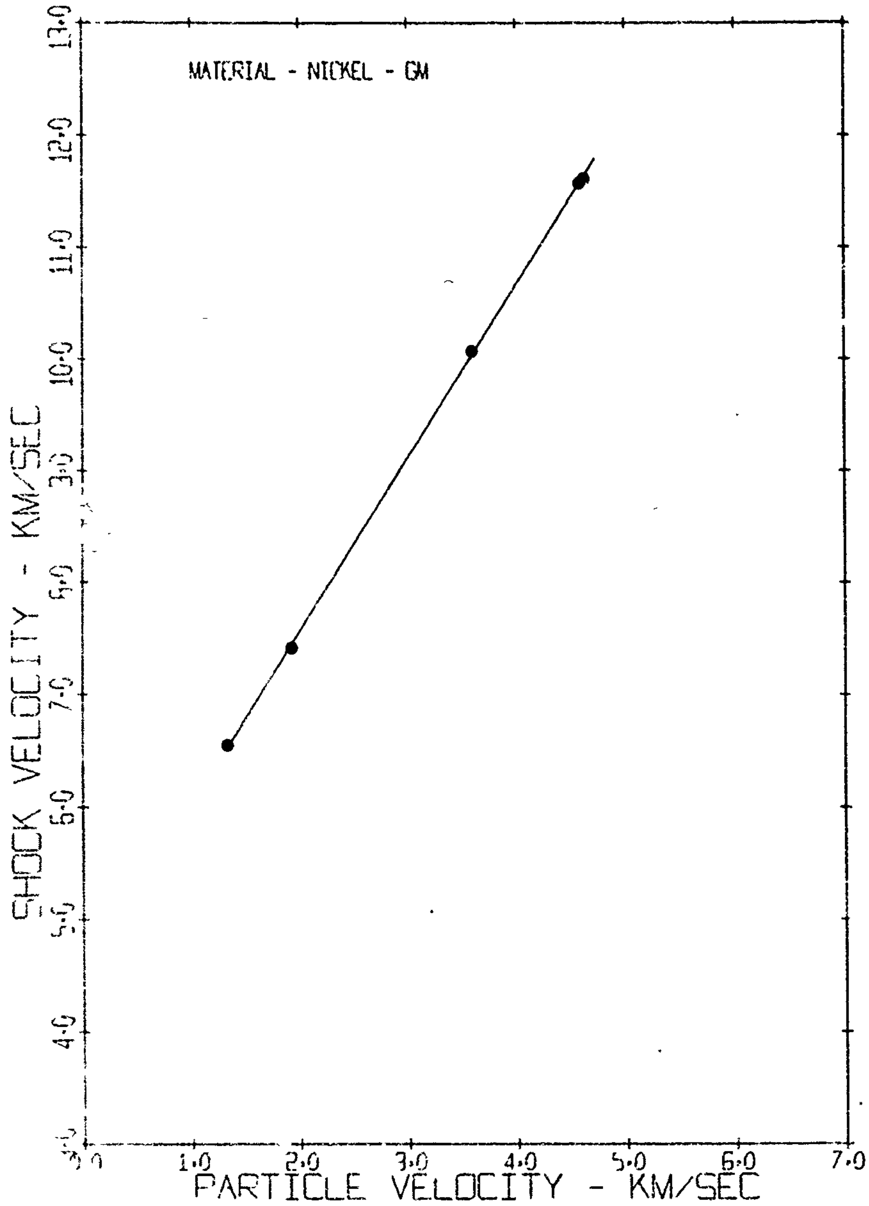

Figure 28 Shock Velocity vs Particle Velocity for Nickel

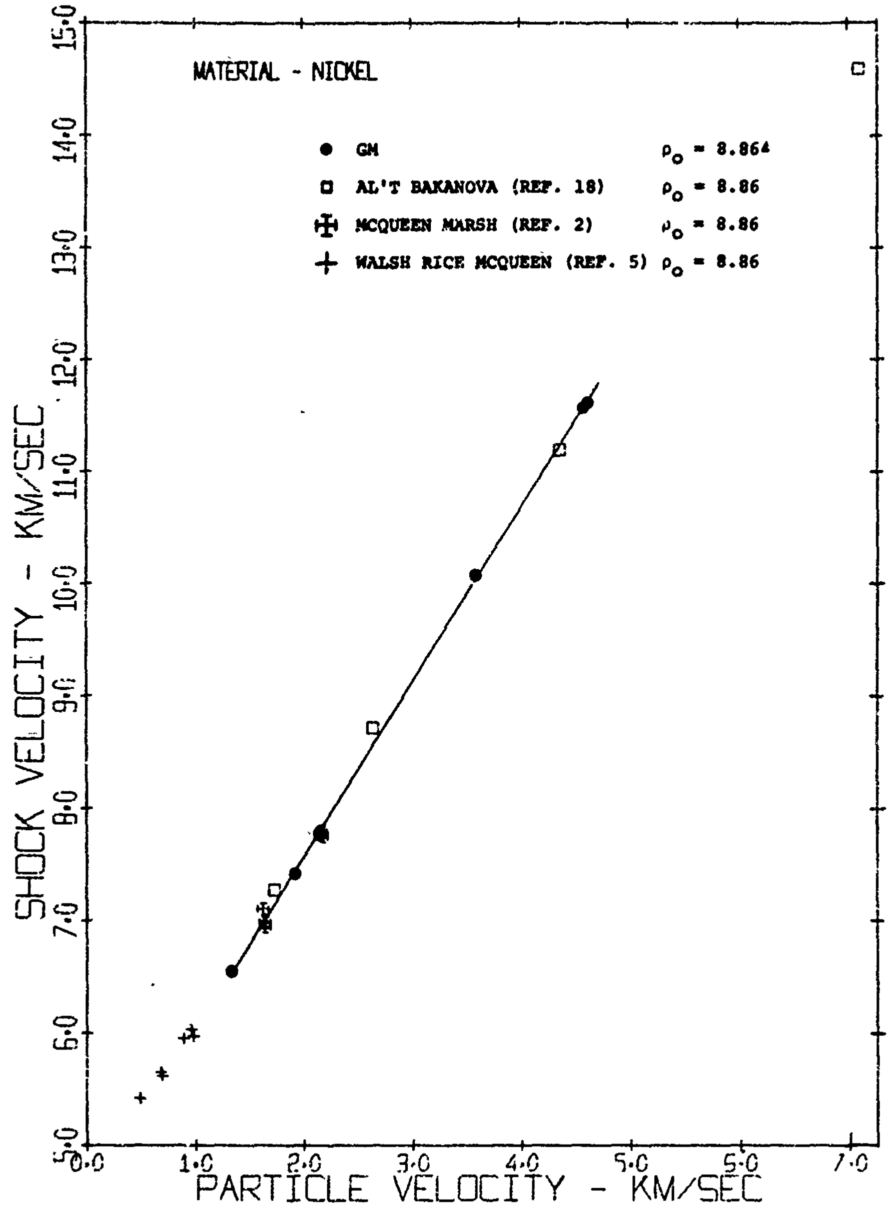

Figure 29 Shock Velocity vs Particle Velocity for Nickel

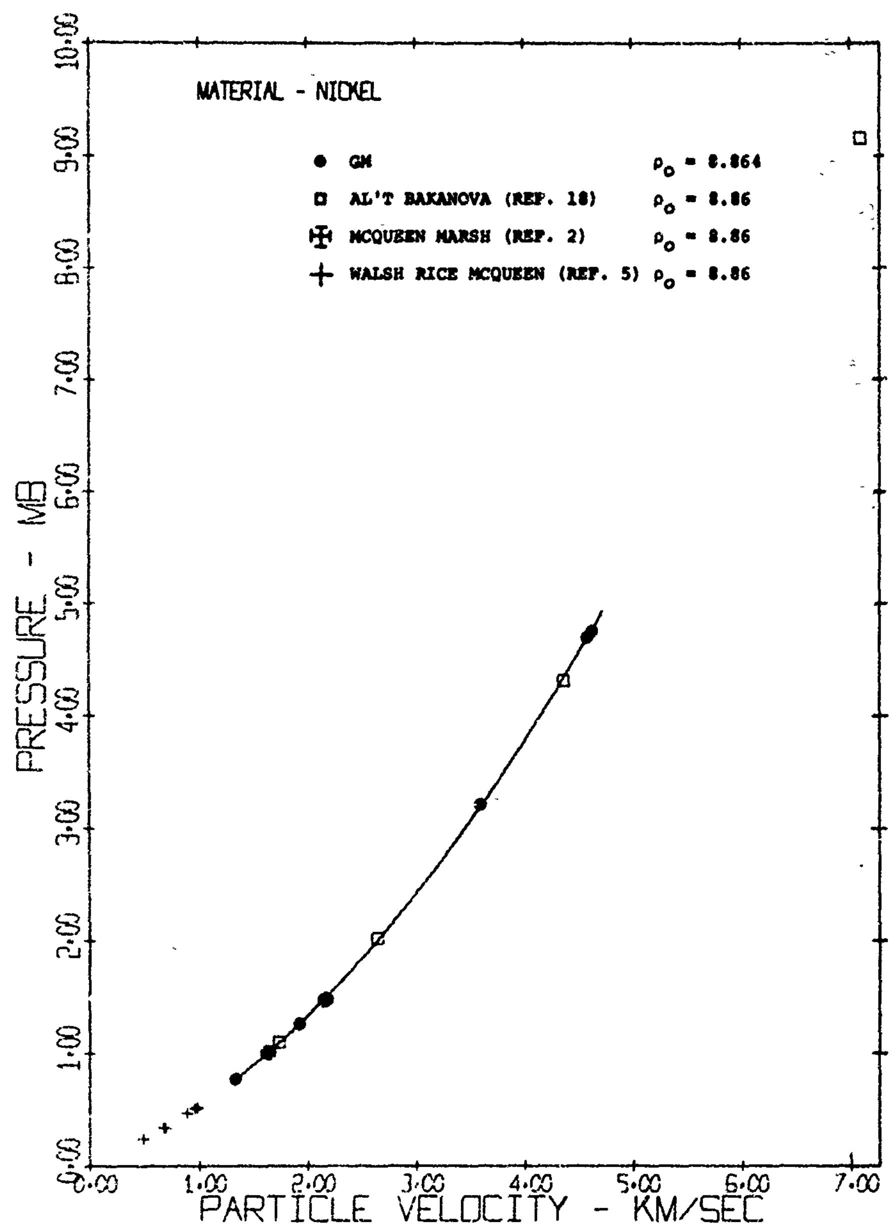

Figure 30 Pressure vs Particle Velocity for Nickel

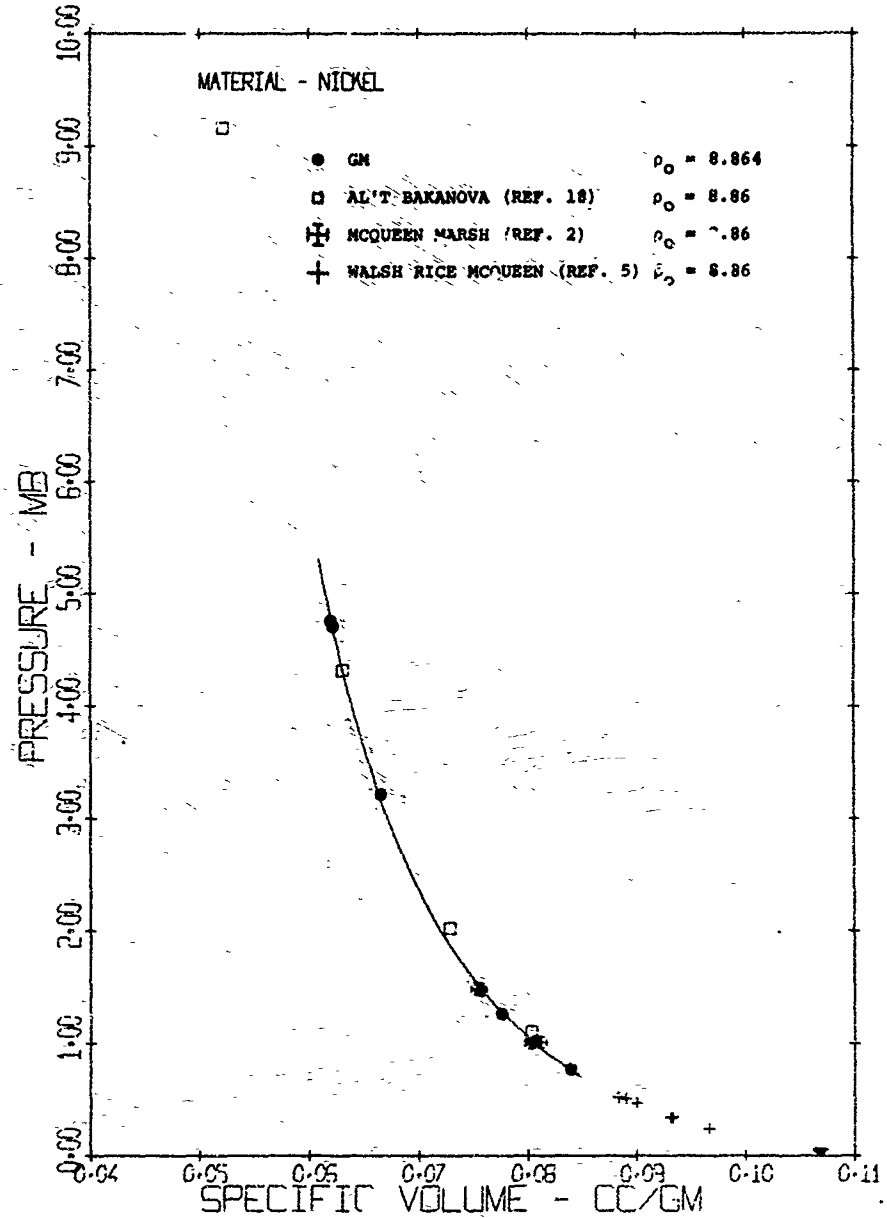

Figure 31   Pressure vs Specific Volume for Nickel

TYPE 304 STAINLESS STEEL

The composition and mechanical properties of Type 304 Stainless Steel are presented in Table 13. The measured density is 7.905 gm/cm^3. The hugoniot data over a pressure range of 0.8 to 4.3 megabars are listed in Table 14 and are presented graphically in Figures 32, 33 and 34. The linear hugoniot fit is given by:

$$U_s = 4.722 + 1.441 \; up \; km/sec$$

Root Mean Square Deviation of U_s = ± 0.023 km/sec for 4 data points.

Also displayed are the data from the U. S. Army Ballistics Research Laboratories[19] for comparison with the present results. Although the pressure ranges tested are barely overlapping, the extrapolation of the present dat to lower pressures is in reasonable agreement with the Ballistics Research Laboratories results.

TABLE 13

CHEMICAL AND PHYSICAL PROPERTIES OF TYPE 304 STAINLESS STEEL

Chemical Composition

Element	Weight %
Carbon	0.065
Manganese	1.62
Phosphorous	0.029
Sulphur	0.028
Silicon	0.49
Nickel	8.80
Chromium	18.73
Molybdenum	0.14
Copper	0.17
Iron	69.86
Other (CO)	0.070

Mechanical Properties

Yield Strength		55,000 psi
Tensile Strength		90,500 psi
Hardness		BHN 192
Density		7.905 gm/cm^3
Poisson's Ratio:		0.290
Acoustic Velocities:	Longitudinal	C_1 = 5.74 km/sec
	Shear	C_s = 3.12 km/sec
	Bulk	C_o = 4.47 km/sec

TABLE 14

HUGONIOT DATA FOR TYPE 304 STAINLESS STEEL

$V_o = 0.1265\ cm^3/gm$
$\rho_o = 7.905\ gm/cm^3$

Shot	Impactor Material	Impact Velocity (km/sec)	Shock Velocity (km/sec)	Particle Velocity (km/sec)	Pressure (Mb)	Relative Volume	Volume (cm^3/gm)	Density (gm/cm^3)	Weighting Factor
S-93	St.St.	2.993	6.877	1.497	0.814	.7823	.0990	10.11	3
S-77	St.St.	5.648	8.760	2.824	1.956	.6776	.0857	11.67	3
S-88	St.St.	7.214	9.980	3.607	2.846	.6386	.0808	12.38	3
S-119	FS	7.883	11.459 ±.128	4.730	4.285 ±.046	.587 ±.004	.074	13.46	1

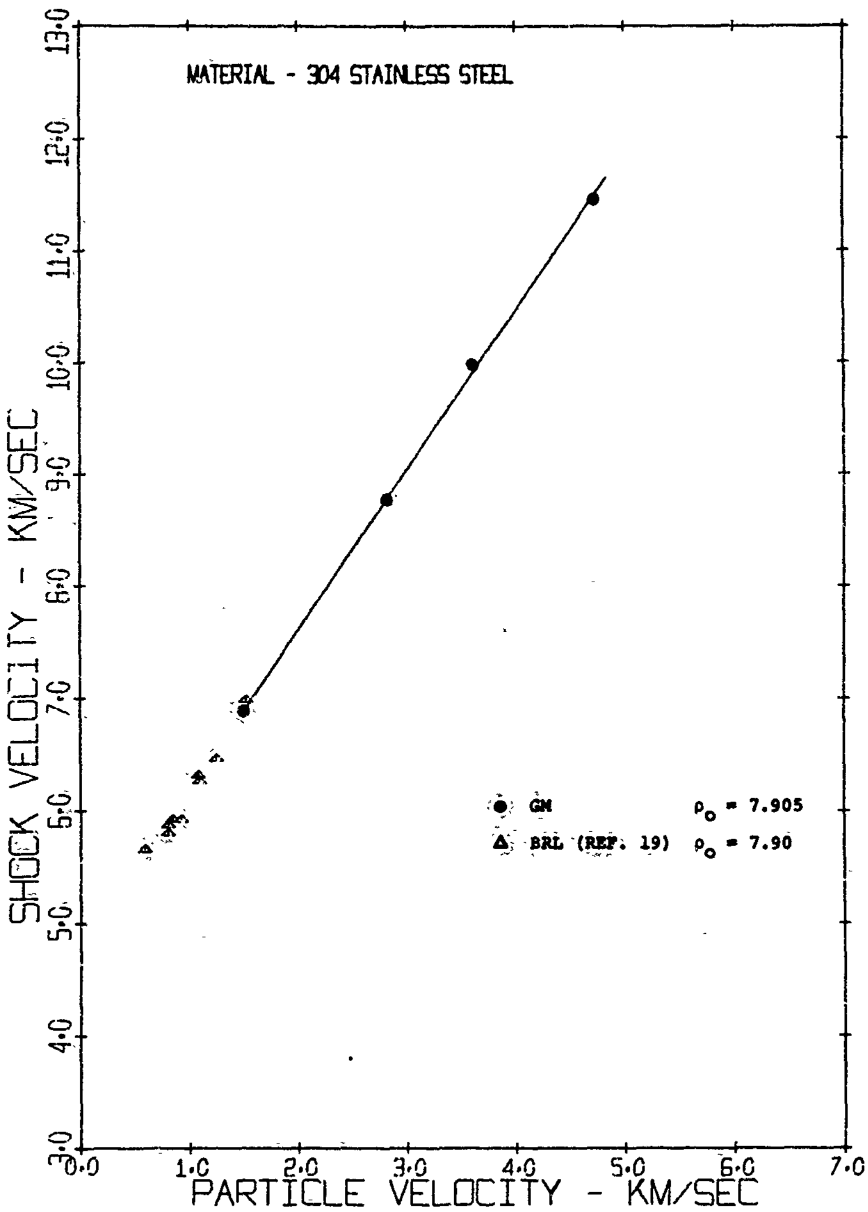

Figure 32 Shock Velocity vs Particle Velocity for 304 Stainless Steel

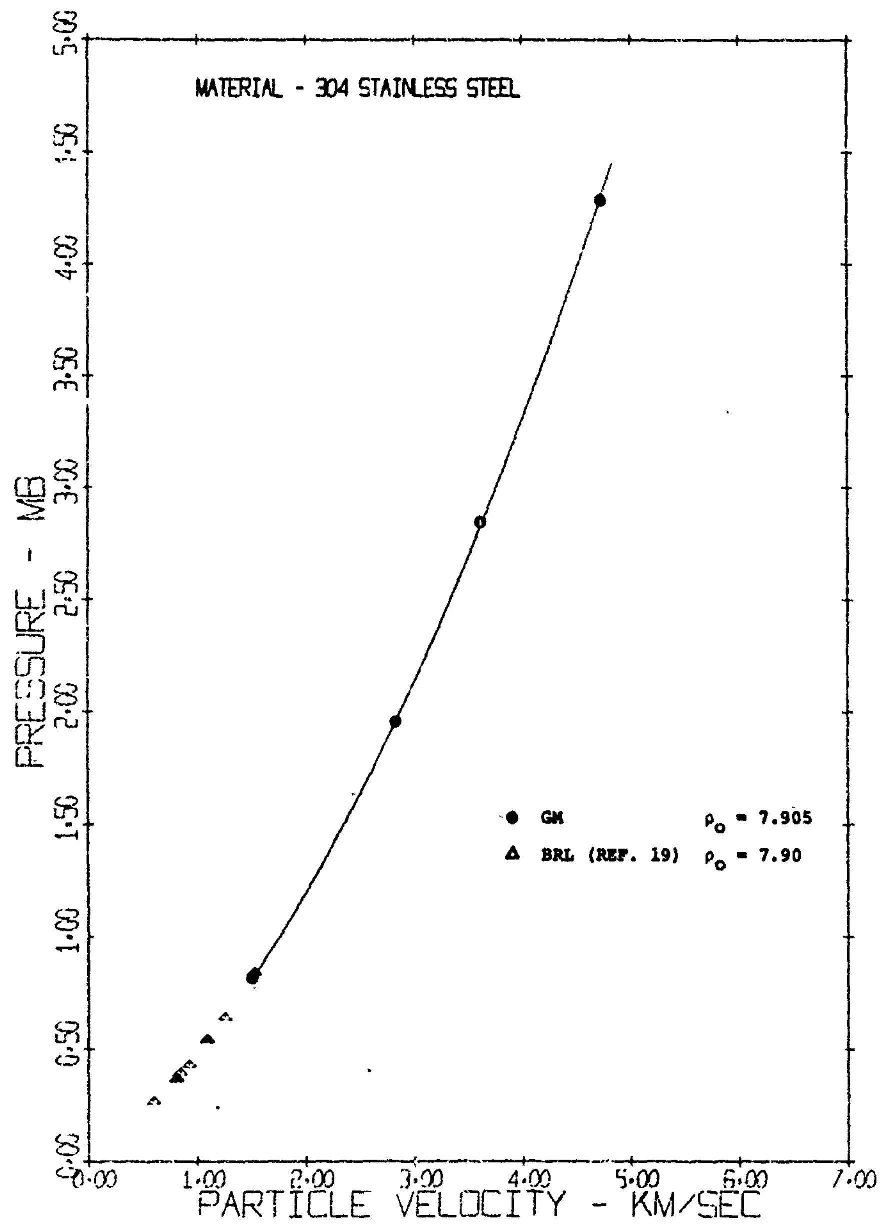

Figure 33 Pressure vs Particle Velocity for 304 Stainless Steel

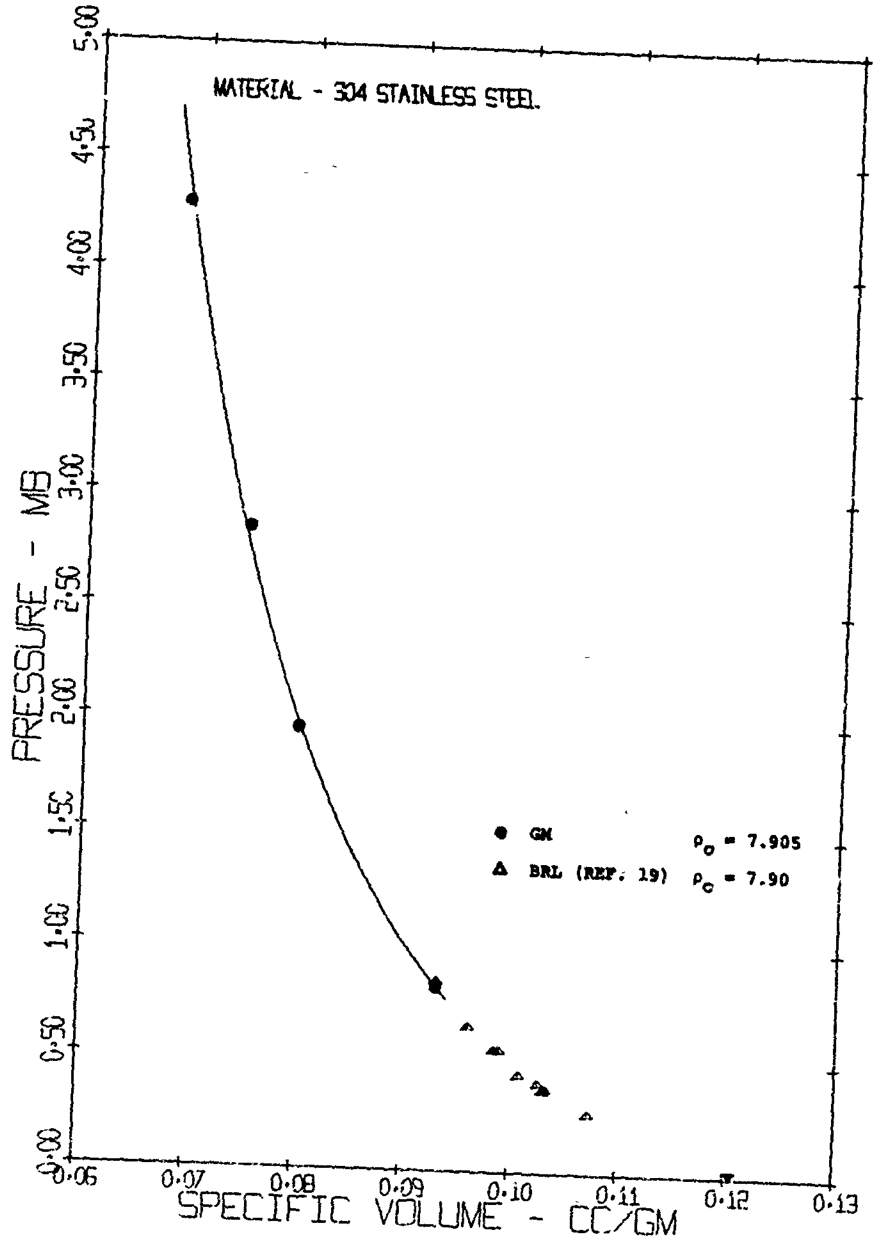

Figure 34 Pressure vs Specific Volume for 304 Stainless Steel

TITANIUM

Three hugoniot tests were performed on titanium over a pressure range of 0.4 to 2.7 Megabars. The chemical and physical properties of the titanium samples are listed in Table 15. The hugoniot data are presented in Table 16 and in Figures 35, 36, 37 and 38. The linear fit to the hugoniot is given by:

$$U_s = 4.692 + 1.126\ u_p \text{ km/sec}$$

Root Mean Square Deviation of U_s = ± 0.014 km/sec for 3 data points.

In the figures are graphical comparisons of the data of Krupnikov[20], Walsh[5], and LASL[12] with the present work.

Krupnikov: $U_s = 4.89 + 1.11\ u_p$ km/sec (0.8 to 2.8 Mb)

Walsh: $U_s = 4.590 + 1.259\ u_p$ km/sec (0.7 to 1.4 Mb)

LASL: $U_s = 4.877 + 1.049\ u_p$ km/sec (0.8 to 1.1 Mb)

A surprisingly large spread in slope and intercept is seen, consolidation of all the data above yields a linear fit:

$$U_s = 4.695 + 1.146\ u_p$$

Root Mean Square Deviation of U_s = ± 0.045 km/sec for 13 data points, deviating but very little from the General Motors data alone.

TABLE 15

CHEMICAL AND PHYSICAL PROPERTIES OF TITANIUM

Chemical Composition

Element	Weight %
Carbon	0.02
Nitrogen	0.010
Iron	0.25
Oxygen	0.115 - 0.123
Titanium	99.60

Mechanical Properties

Yield Strength at 0.2% Elongation	50,000 - 55,500 psi
Tensile Strength	75,600 - 76,300 psi
Density	4.508 gm/cm^3
Poisson's Ratio:	0.304
Acoustic Velocities:	Longitudinal, C_l = 6.118 km/sec
	Shear, C_s = 3.246 km/sec
	Bulk, C_o = 4.83 km/sec

TABLE 16

HUGONIOT DATA FOR TITANIUM

$V_o = 0.2218\ cm^3/gm$
$\rho_o = 4.508\ gm/cm^3$

Shot	Impactor Material	Impact Velocity (km/sec)	Shock Velocity (km/sec)	Particle Velocity (km/sec)	Pressure (Mb)	Relative Volume	Volume (cm^3/gm)	Density (gm/cm^3)	Weighting Factor
S-81	Ti	2.845	6.321	1.422	0.405	.7750	.1719	5.817	1
S-83	Ti	5.242	7.604	2.621	0.899	.6553	.1454	6.879	1
S-92	FS	7.849	10.934	5.534	2.728	.4939	.1096	9.128	1

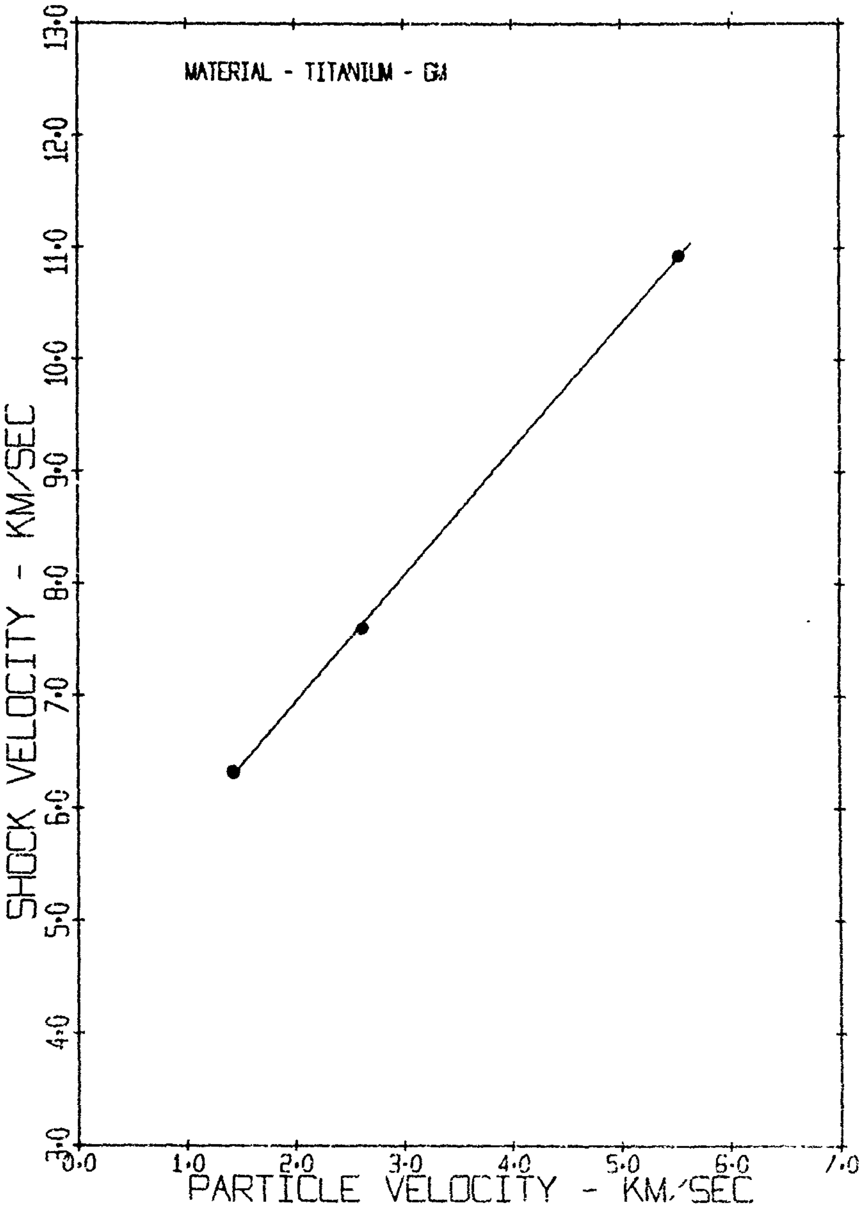

Figure 35 Shock Velocity vs Particle Velocity for Titanium

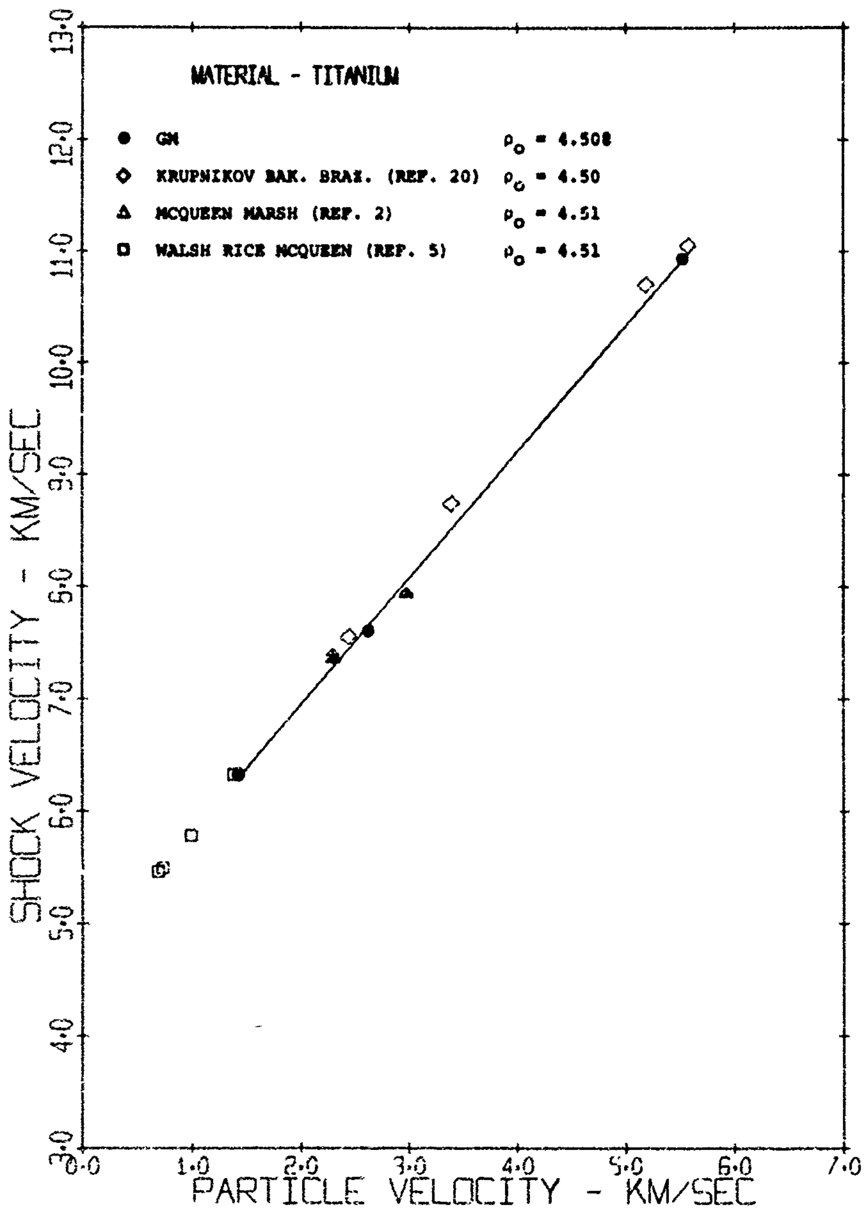

Figure 36 Shock Velocity vs Particle Velocity for Titanium

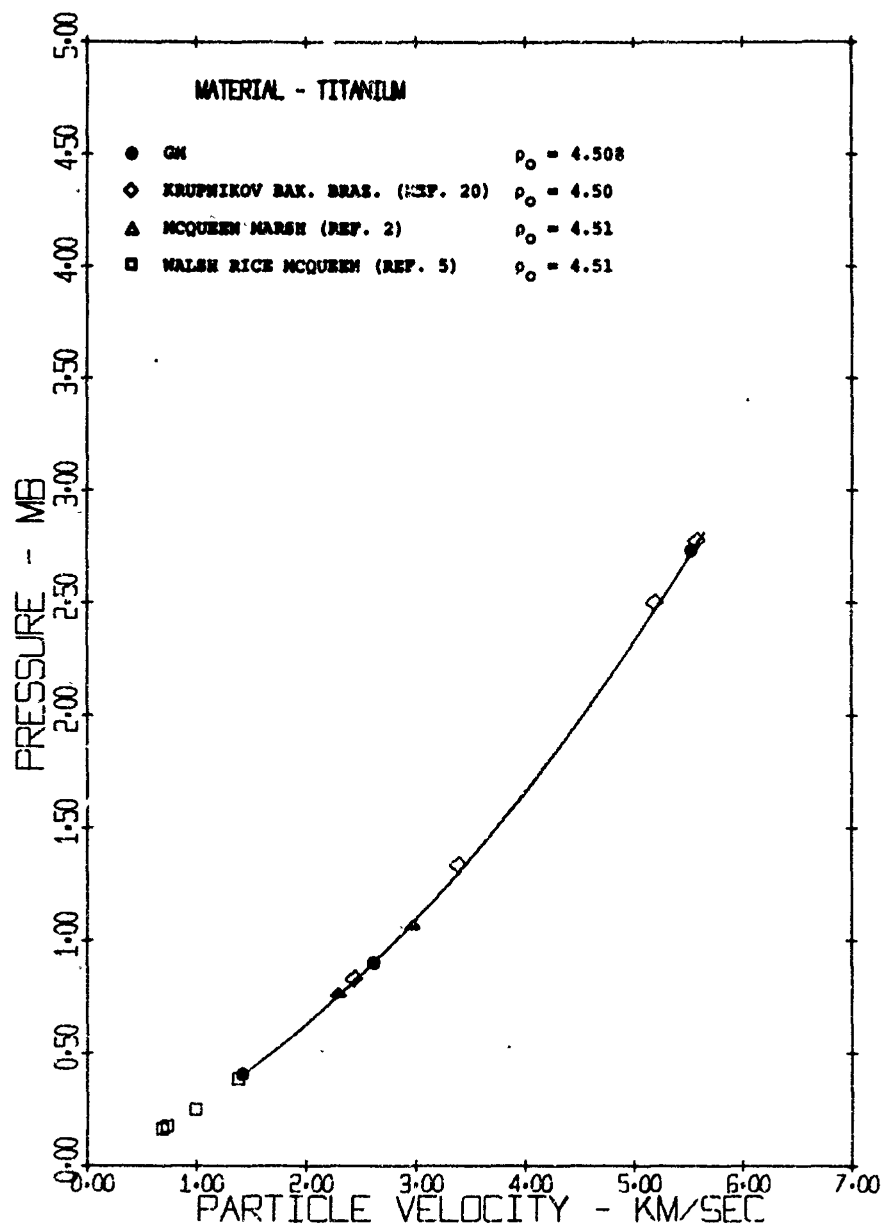

Figure 37 Pressure vs Particle Velocity for Titanium

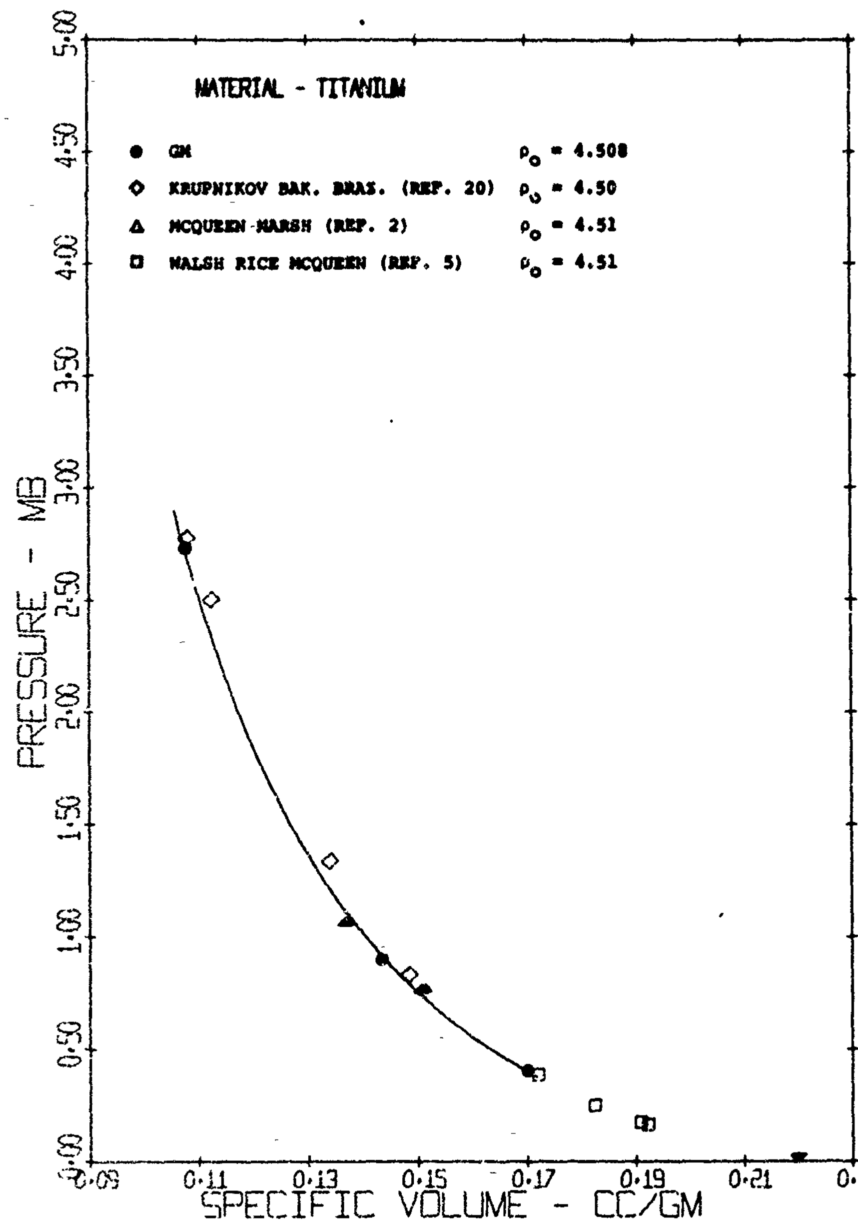

Figure 38 Pressure vs Specific Volume for Titanium

BERYLLIUM

Hugoniot experiments were performed on two types of beryllium, designated as S-200 and I-400, having nominal compositions of 2% and 4% BeO respectively.

The chemical and physical properties of the beryllium specimens as furnished by the supplier, Brush Beryllium Co., are listed in Table 17. The specimen preparation presented somewhat of a problem in that dust and small fragments of the material are considered toxic. All polishing and lapping of samples were performed in closed and vented work areas.

The beryllium presented the most difficult case for accurate hugoniot measurements with a restricted target size because the elastic release wave velocity is relatively high and the target thickness is thus necessarily less than that for other materials. (See Figure 9 for the maximum angle of intrusion of the side rarefactions).

The hugoniot data presented in Table 18 include seven tests on S-200, the material of major interest, and one comparison test on I-400. The impactors for the test series were OFHC copper (3 tests) and Fansteel-77 (5 tests). The data are presented graphically in Figures 39, 40 and 41. A linear fit was made to the data for the S-200 beryllium:

$$U_s = 8.390 + 0.975\ u_p \text{ km/sec}$$

Root Mean Square Deviation of $U_s = \pm\ 0.017$ km/sec for 7 data points.

TABLE 17

CHEMICAL AND PHYSICAL PROPERTIES OF S-200 AND I-400 BERYLLIUMS

Chemical Composition

Material	I-400 Wt. %	S-200 Wt. %
Beryllium Oxide	3.96	2.00
Carbon	0.18	0.126
Iron	0.16	0.163
Aluminum	0.04	0.054
Magnesium	0.02	0.035
Silicon	0.04	0.080
Manganese	0.01	-----
Beryllium	95.77	98.18
Other	0.10	0.04 max

Mechanical Properties

		I-400	S-200
Yield Strength		56,000 psi	37,500 psi
Ultimate Tensile Strength		66,700 psi	57,700 psi
Density		1,881 gm/cm^3	1.857 gm/cm^3
Poisson's Ratio:		0.055	
Acoustic Velocities:	Longitudinal, C_1 =	12.83	12.916
	Shear, C_s =	8.80	8.86
	Bulk, C_o =	7.83	7.87

TABLE 18

HUGONIOT DATA FOR BERYLLIUM

S-200 $V_o = 0.5385\ cm^3/gm$, $\rho_o = 1.851\ gm/cm^3$

I-400 $V_o = 0.5316\ cm^3/gm$, $\rho_o = 1.881\ gm/cm^3$

Shot	Impactor Material	Impact Velocity (km/sec)	Shock Velocity (km/sec)	Particle Velocity (km/sec)	Pressure (Mb)	Relative Volume	Volume (cm^3/gm)	Density (gm/cm^3)	Weighting Factor
1271	FS	2.205	9.965	1.631	0.302	.8363	.4504	2.220	3
S-122	Cu	2.695	10.266	1.903	0.363	.8147	.4387	2.280	3
1272	FS	4.330	11.779	3.459	0.757	.7063	.3804	2.629	3
S-123	Cu	5.596	12.218	3.990	0.905	.6734	.3627	2.758	1
1276	FS	7.734	13.034	4.792	1.160	.6324	.3405	2.937	3
S-126	Cu	7.945	13.970	5.678	1.473	.5936	.3196	3.129	3
1277	FS	7.734	14.324	6.139	1.633	.5714	.3077	3.250	1
1278(I-400)	FS	3.191	10.981	2.549	0.526	.7679	.4082	2.450	0

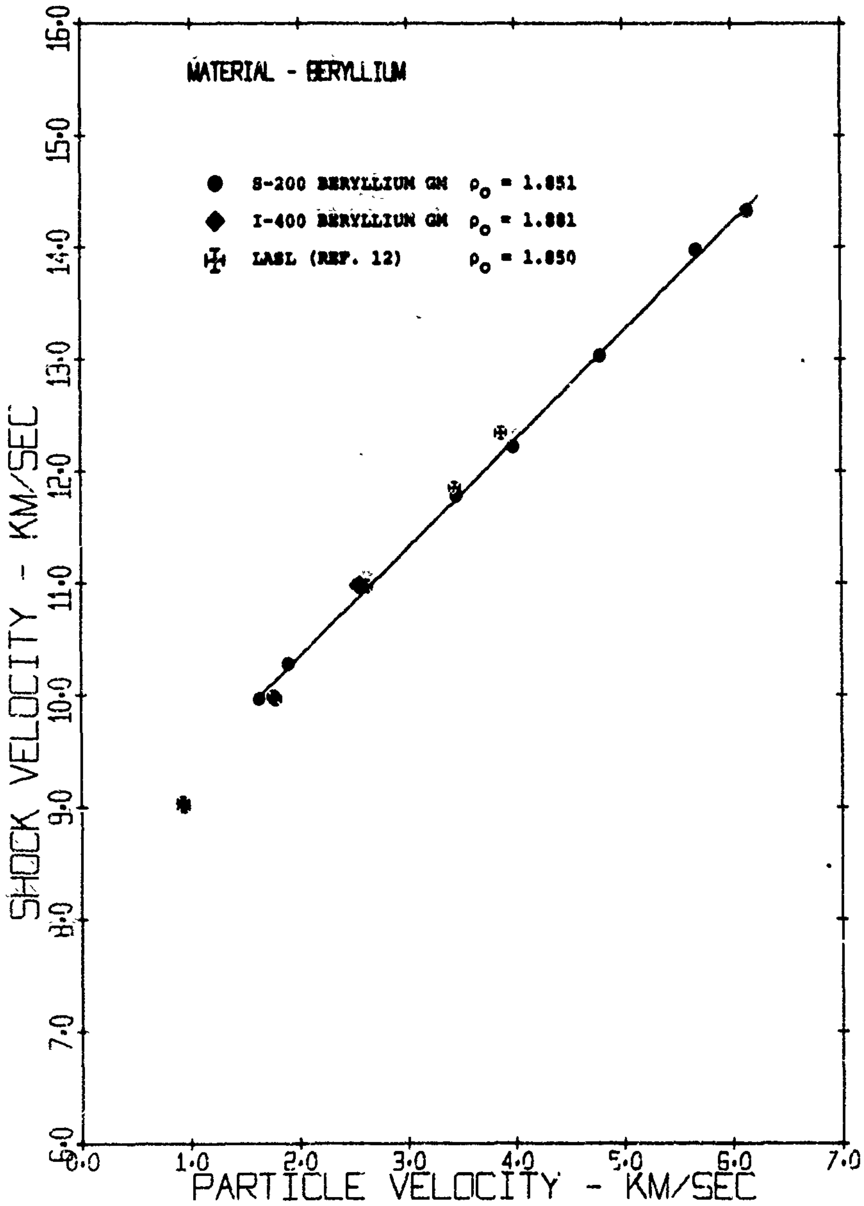

Figure 39 Shock Velocity vs Particle Velocity for Beryllium

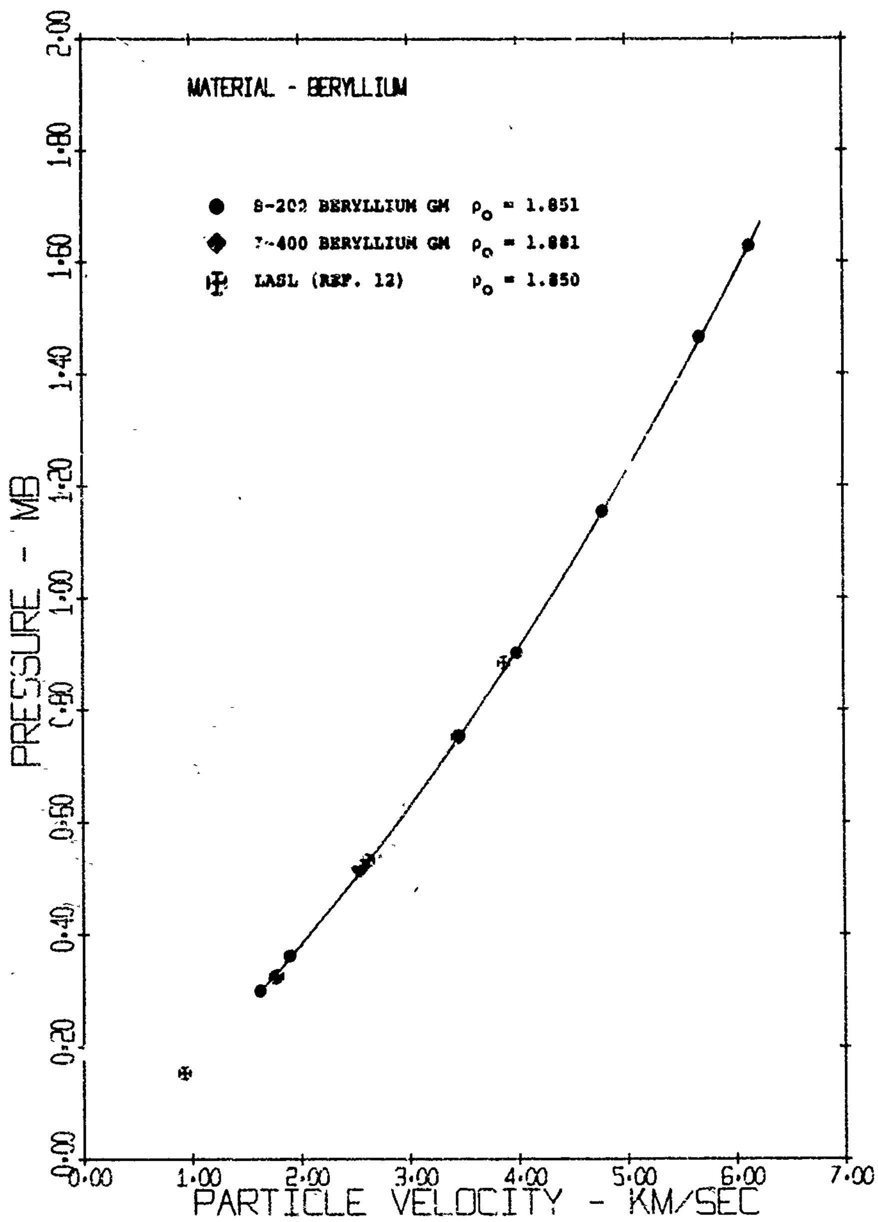

Figure 40 Pressure vs Particle Velocity for Beryllium

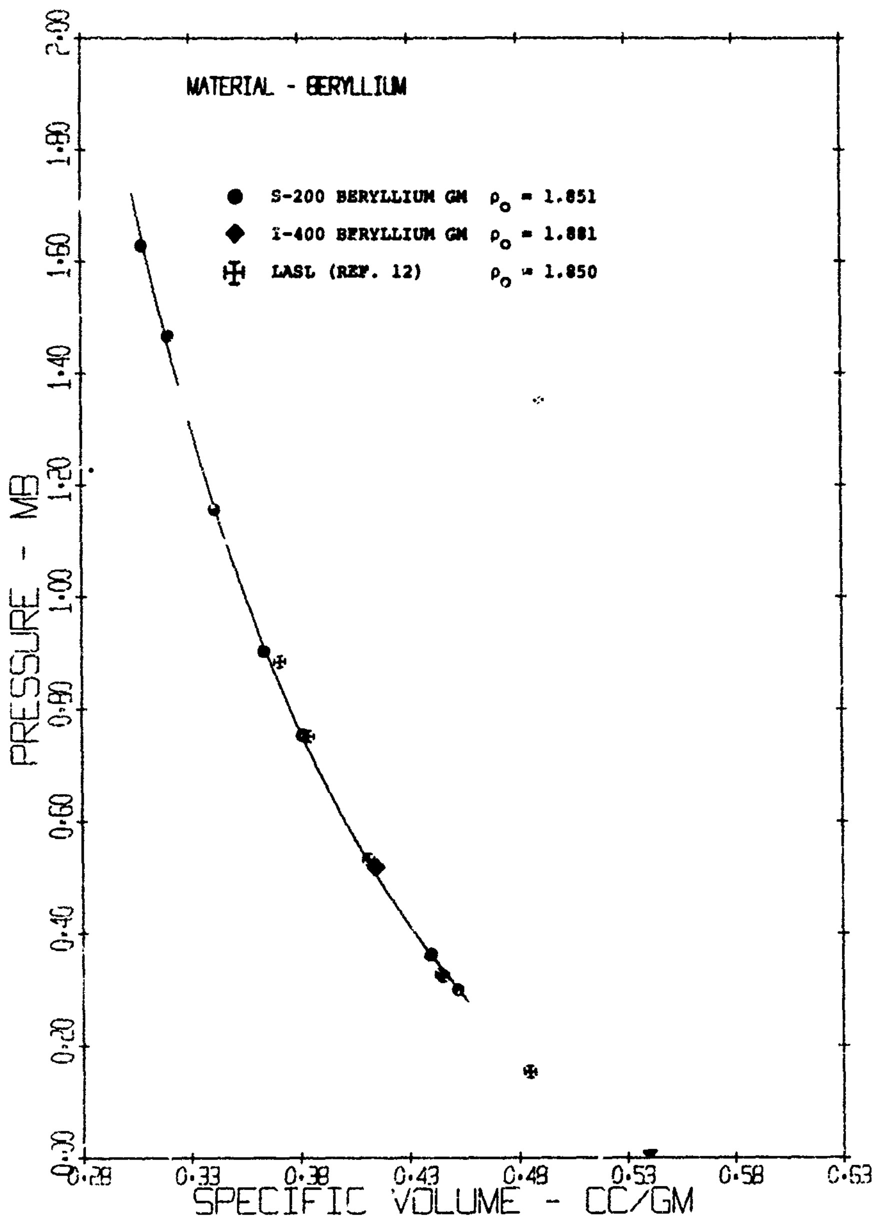

Figure 41 Pressure vs Specific Volume for Beryllium

The I-400 beryllium is slightly more dense (∿ 1.3%) than the S-200 beryllium due to a greater percentage of the heavier beryllium oxide compound. The data point is slightly above the fit of the S-200.

A comparison of the data with that of LASL[12] on a beryllium of similar BeO content shows a significant difference in the slopes of two linear fits, the slope LASL's data indicating a somewhat "stiffer" hugoniot than the present data ($U_s = 7.998 + 1.124\ u_p$). The reason for this difference is difficult to determine. The possibility of edge rarefactions affecting the measurements on the GM specimens was checked by firing several tests with specimens substantially thinner than the value dictated by the analysis in Section II. No significant differences in the measured values were noted.

AZ31B MAGNESIUM

Four hugoniot tests were performed on AZ31B magnesium tooling plate (ρ_o = 1.773 gm/cm^3) material. The nominal composition of the material is Mg 96.0%, Al 3.0%, and Zn 1.0%. The data shows more scatter than was found in tests with other metals. The hugoniot data are presented in Table 19 and in Figures 42, 43 and 44. The hugoniot is described by the linear equation:

$$U_s = 4.551 + 1.209\ u_p \text{ km/sec}$$

Root Mean Square Deviation of U_s = ± 0.083 km/sec for 4 data points.

The figures compare graphically the measured values with the AZ31B magnesium data of the LRL Compiler[21] and the data on 99.5% pure magnesium by LASL[12]. Linear fits to the other data are:

$$U_s = 4.516 + 1.256\ u_p \text{ km/sec (LASL, } \rho_o = 1.745 \text{ gm/cm}^3)$$

$$U_s = 4.648 + 1.198\ u_p \text{ km/sec (LRL Compiler, } \rho_o = 1.78 \text{ gm/cm}^3)$$

TABLE 19

HUGONIOT DATA FOR AZ31B MAGNESIUM

$V_o = 0.564\ cm^3/gm$
$\rho_o = 1.773\ gm/cm^3$

Shot	Impactor Material	Impact Velocity (km/sec)	Shock Velocity (km/sec)	Particle Velocity (km/sec)	Pressure (Mb)	Relative Volume	Volume (cm^3/gm)	Density (gm/cm^3)	Weighting Factor
S-79	Mg	3.539	6.731	1.769	0.211	.7372	.4158	2.405	3
S-80	Mg	5.911	8.020	2.956	0.420	.6314	.3561	2.808	3
S-89	Cu	6.631	10.884	4.959	0.957	.5444	.3070	3.257	1
S-91	FS	7.795	12.221	6.368	1.384	.4773	.2692	3.715	3

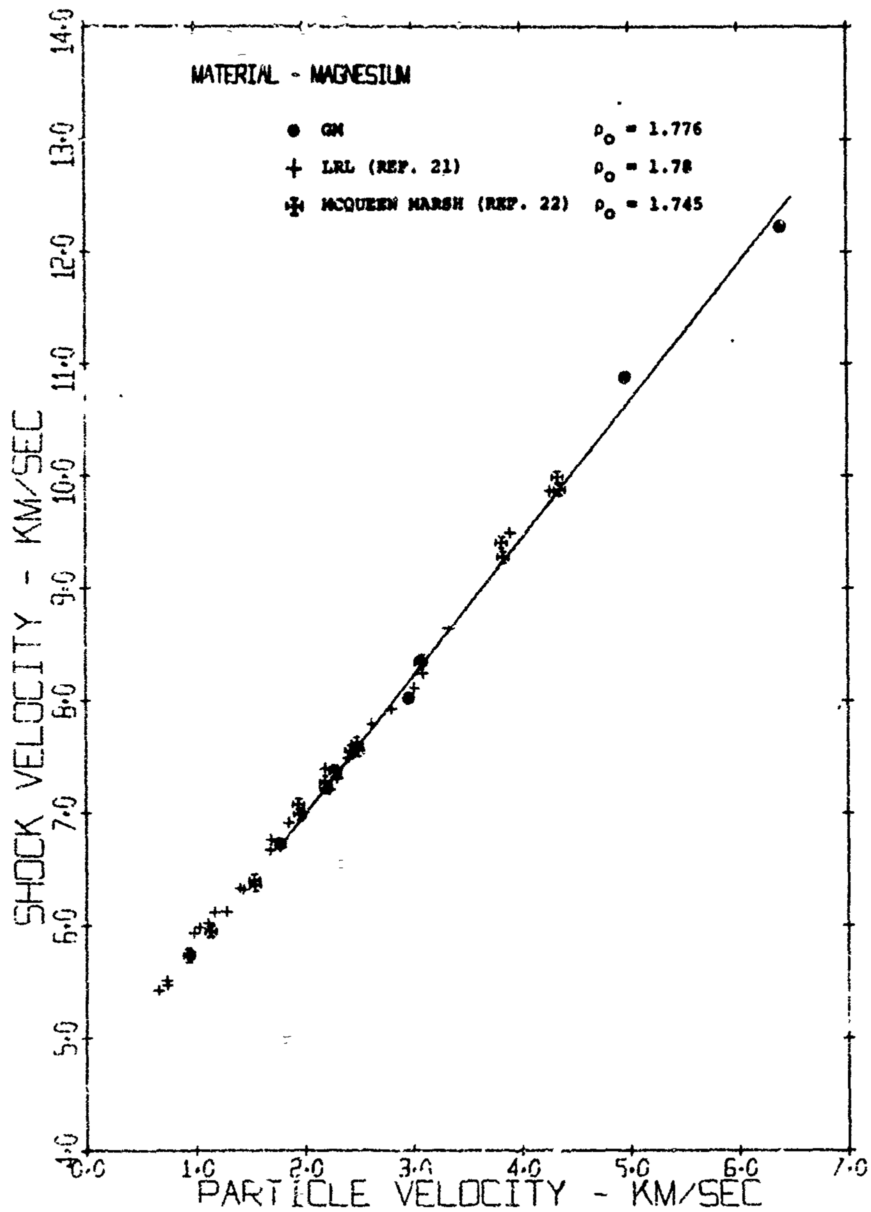

Figure 42 Shock Velocity vs Particle Velocity for Magnesium

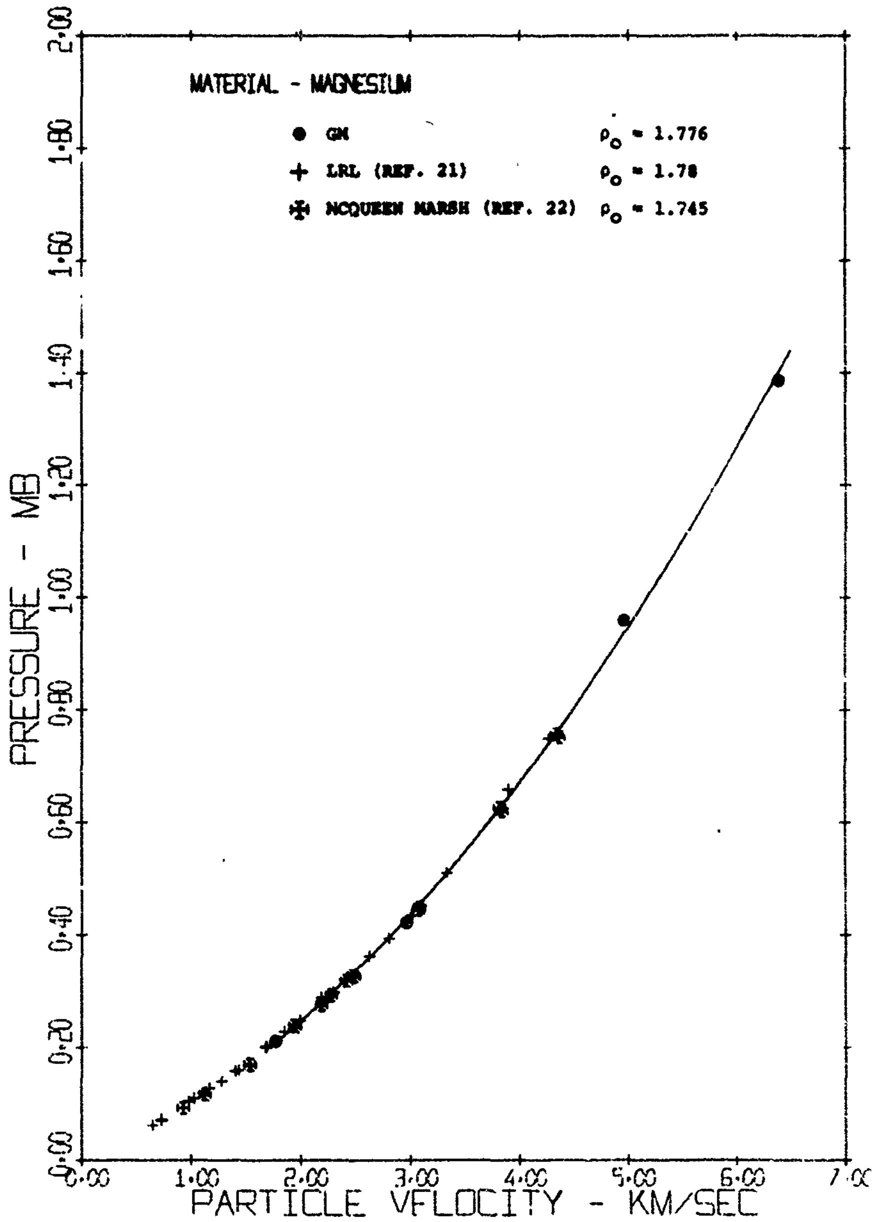

Figure 43 Pressure vs Particle Velocity for Magnesium

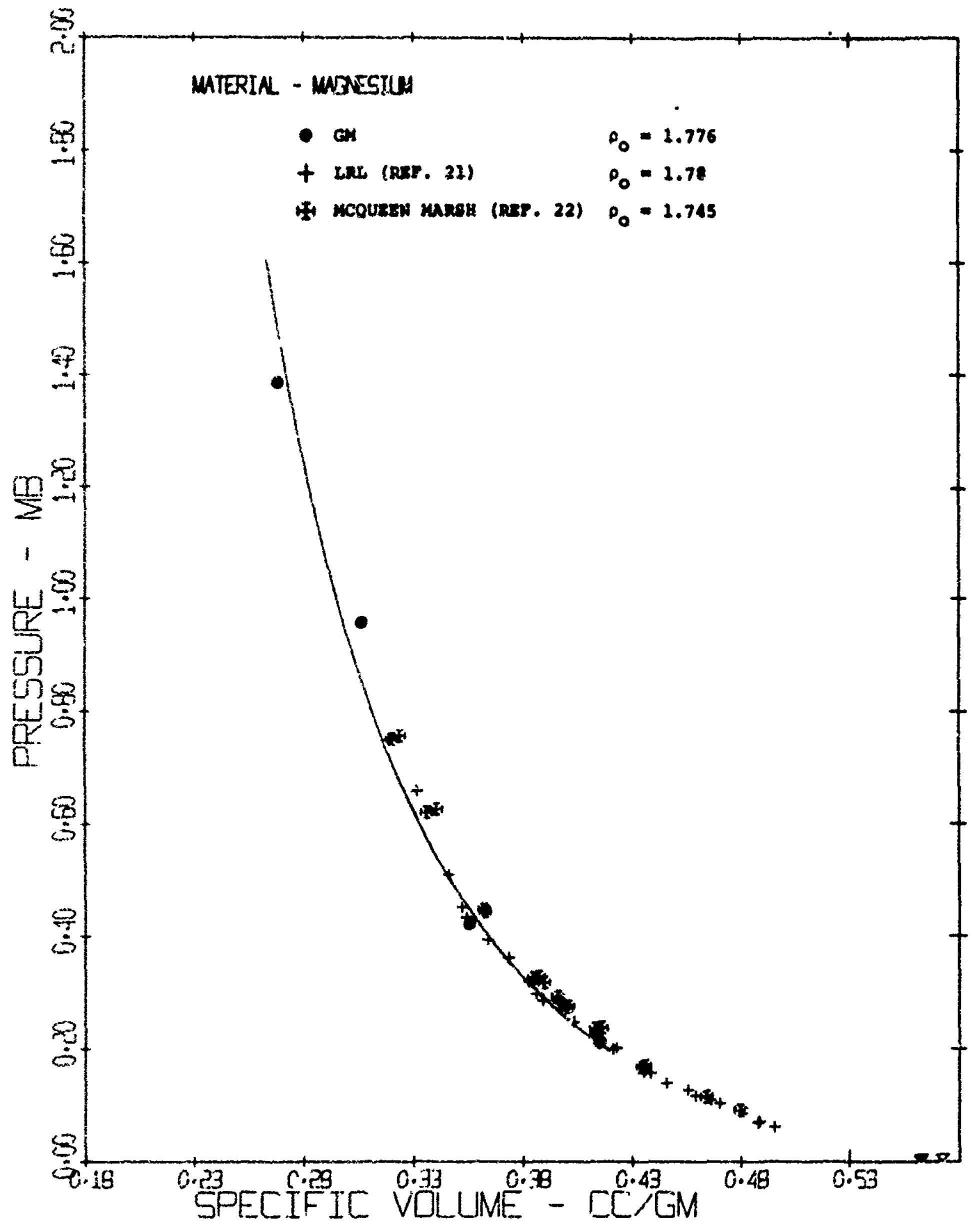

Figure 44 Pressure vs Specific Volume for Magnesium

PLEXIGLAS

The Plexiglas tested was identified as Rohm and Haas Type II UVA. Only two tests were performed, which served to provide a check on the extrapolation of the data of Hauver[23] taken above the phase transition at ∿ 0.2 megabars, (line A of Figure 45) into the higher pressure region investigated by Bakanova[23] (line B). The data are listed in Table 20. Fits to the above data are

$$U_s = 3.51 + 1.25\ u_p \text{ km/sec (Hauver) } (2.8 < u_p < 3.5)$$

$$U_s = 3.10 + 1.32\ u_p \text{ km/sec (Bakanova) } (3.0 < u_p < 8.0)$$

Figures 45, 46 and 47 display the present data as compared to that of Hauver and Bakanova with the line representing Bakanova's data between $3.0 < u_p < 8.0$ km/sec. The two data points determined in the present work are in good agreement with the data of Bakanova (difference in shock velocity less than 0.4%) and also are in agreement with the extrapolation of Hauver's data (difference in shock velocity of less than 2% at a pressure of 1.0 megabar).

TABLE 20

HUGONIOT DATA FOR PLEXIGLAS

$V_o = 0.8475\ cm^3/gm$

$\rho_o = 1.180\ gm/cm^3$

Shot	Impactor Material	Impact Velocity (km/sec)	Shock Velocity (km/sec)	Particle Velocity (km/sec)	Pressure (Mb)	Relative Volume	Volume (cm^3/gm)	Density (gm/cm^3)
S-96	Cu	6.907	10.482	5.592	0.692	.4666	.3954	2.529
S-97	FS	7.902	12.075	6.833	0.981	.4300	.3644	2.744

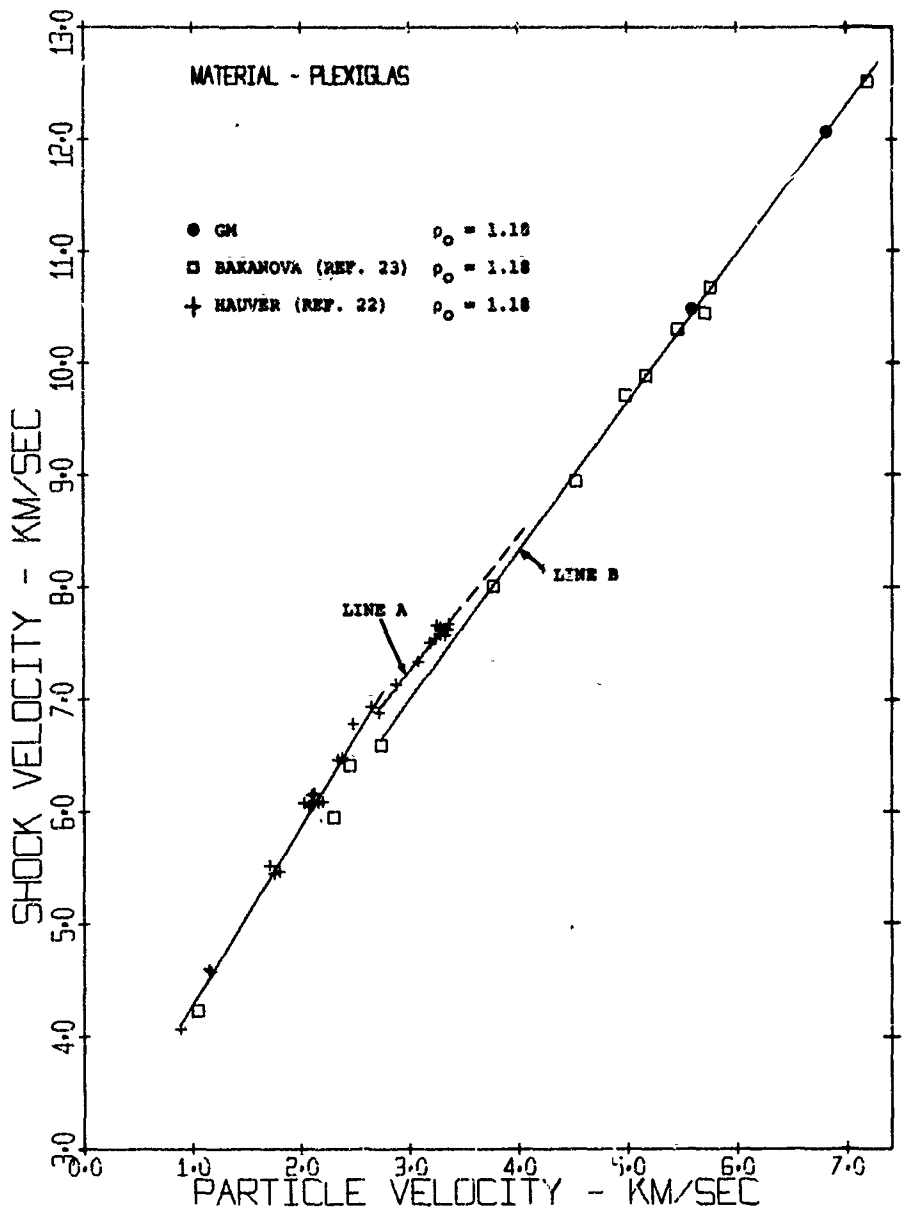

Figure 45 Shock Velocity vs Particle Velocity for Plexiglas

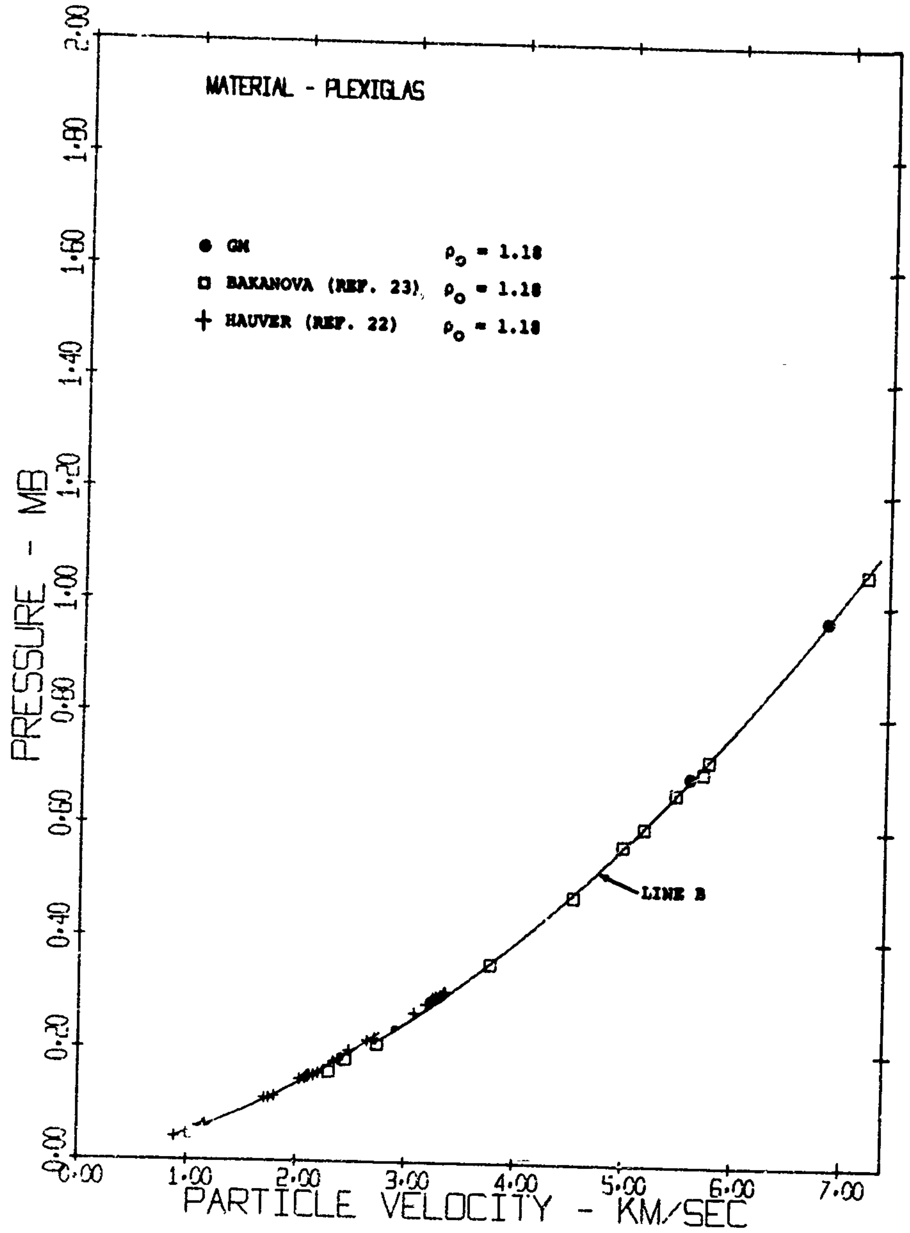

Figure 46   Pressure vs Particle Velocity for Plexiglas

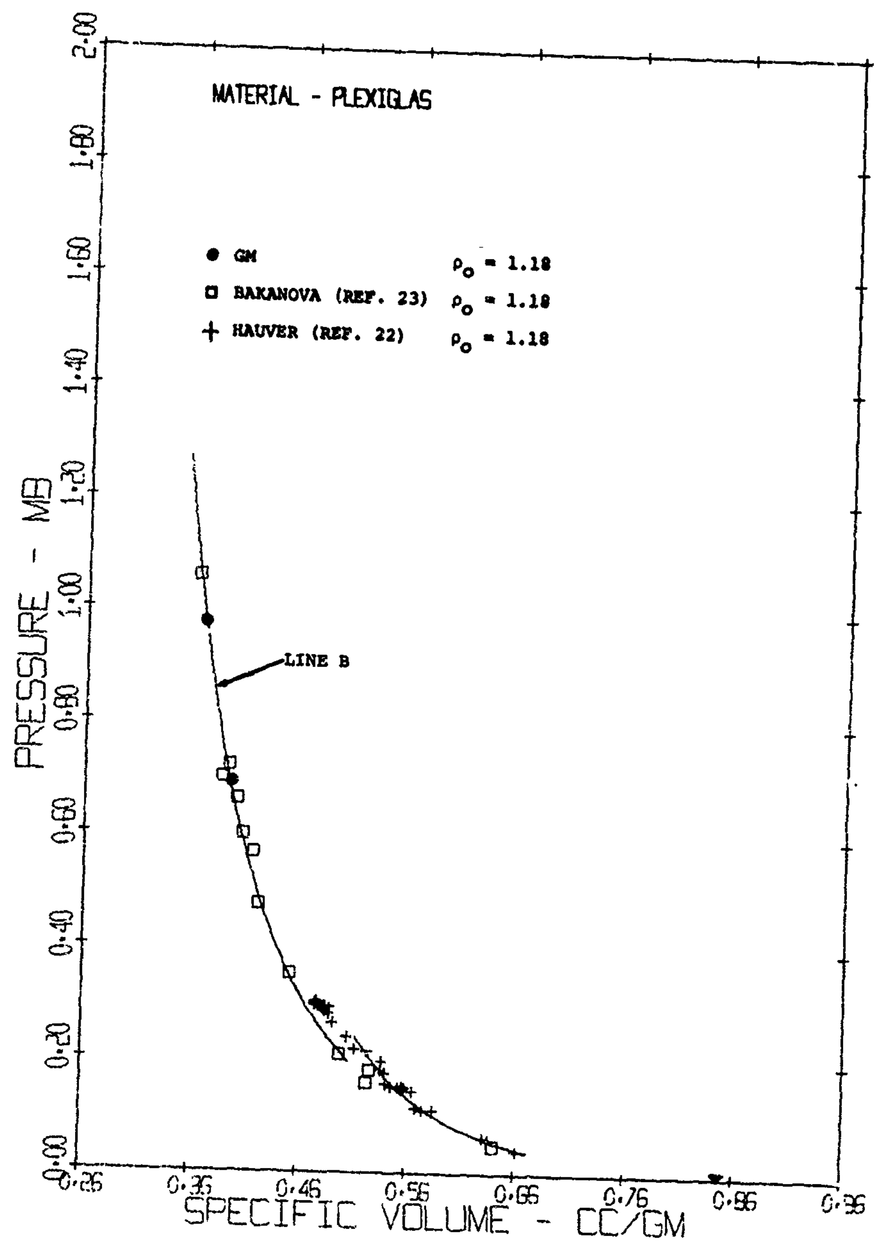

Figure 47 Pressure vs Specific Volume for Plexiglas

QUARTZ PHENOLIC

A single test was performed to locate a very high pressure point on the hugoniot of quartz phenolic. Lower pressure work was performed at this laboratory under Contract AF04-(694)-807 under directorship of the U.S. Air Force Ballistics Systems Division and is reported in Reference 25. All of the data are listed in Table 21 and are displayed in Figures 48, 49 and 50.

A phase change in clearly evident beginning at a pressure of ∿ 0.2 megabars. The data point obtained is on the higher pressure phase of the hugoniot.

The linear fit to the upper portion of the hugoniot is given by:

$$U_s = 1.949 + 1.364\ u_p \text{ km/sec}$$

Root Mean Square Deviation of U_s = ± 0.016 km/sec for 5 data points.

The initial density of the quartz phenolic is 1.80 gm/cm^3. The properties of the high pressure phase suggests that this may be related to the properties of quartz under high pressure, i.e., the high pressure polymorph-stishovite[7,26]. The tests were made with layup directions of the quartz cloth in the phenolic matrix both parallel and perpendicular to the shock front, but orientation effects on the wave velocity are apparently negligable at these pressures.

TABLE 21

HUGONIOT DATA FOR QUARTZ PHENOLIC

$V_o = 0.556\ cm^3/gm$

$\rho_o = 1.80\ gm/cm^3$

Shot	Impactor Material	Impact Velocity (km/sec)	Shock Velocity (km/sec)	Particle Velocity (km/sec)	Pressure (Mb)	Relative Volume	Volume (cm^3/gm)	Density (gm/cm^3)	Weighting Factor
PARALLEL **									
1159	Cu	1.619	4.479	1.341	.108	.7006	.3894	2.568	
1175	Cu	2.654	5.248	2.164	.204	.5875	.3267	3.061	
1157	Cu	3.088	5.343	2.522	.243	.5281	.2933	3.409	1
1173	Cu	4.798	7.160	3.793	.489	.4703	.2613	3.827	1
S-99	FS	7.985*	10.978	6.635 ±.13	1.311 ±.026	.3956 ±.0118	.2198	4.550	1
PERPENDICULAR**									
1174	Cu	1.412	4.357	1.172	.092	.7310	.4061	2.462	
1158	Cu	2.444	5.211	1.991	.187	.6179	.3433	2.913	
1171	Cu	2.475	5.234	2.015	.190	.6149	.3416	2.927	
1176	Cu	3.397	5.735	2.750	.284	.5205	.2892	3.458	1
1160	Cu	3.423	5.733	2.772	.286	.5165	.2869	3.486	
1172	Cu	4.718	7.032	3.738	.473	.4685	.2603	3.842	1

** Layup with respect to the plane of the shock front.

* Impact velocity determined from measured gun firing parameters.

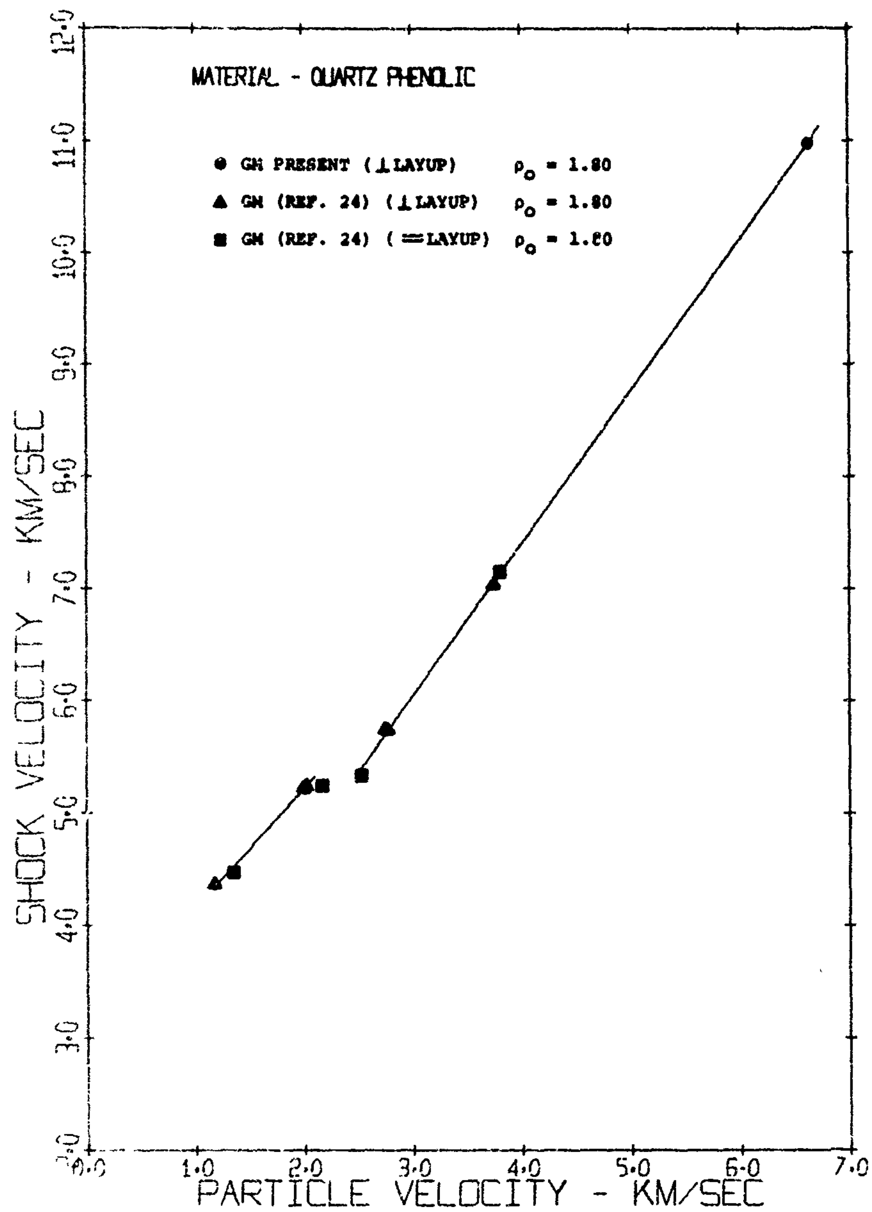

Figure 48 Shock Velocity vs Particle Velocity for Quartz Phenolic

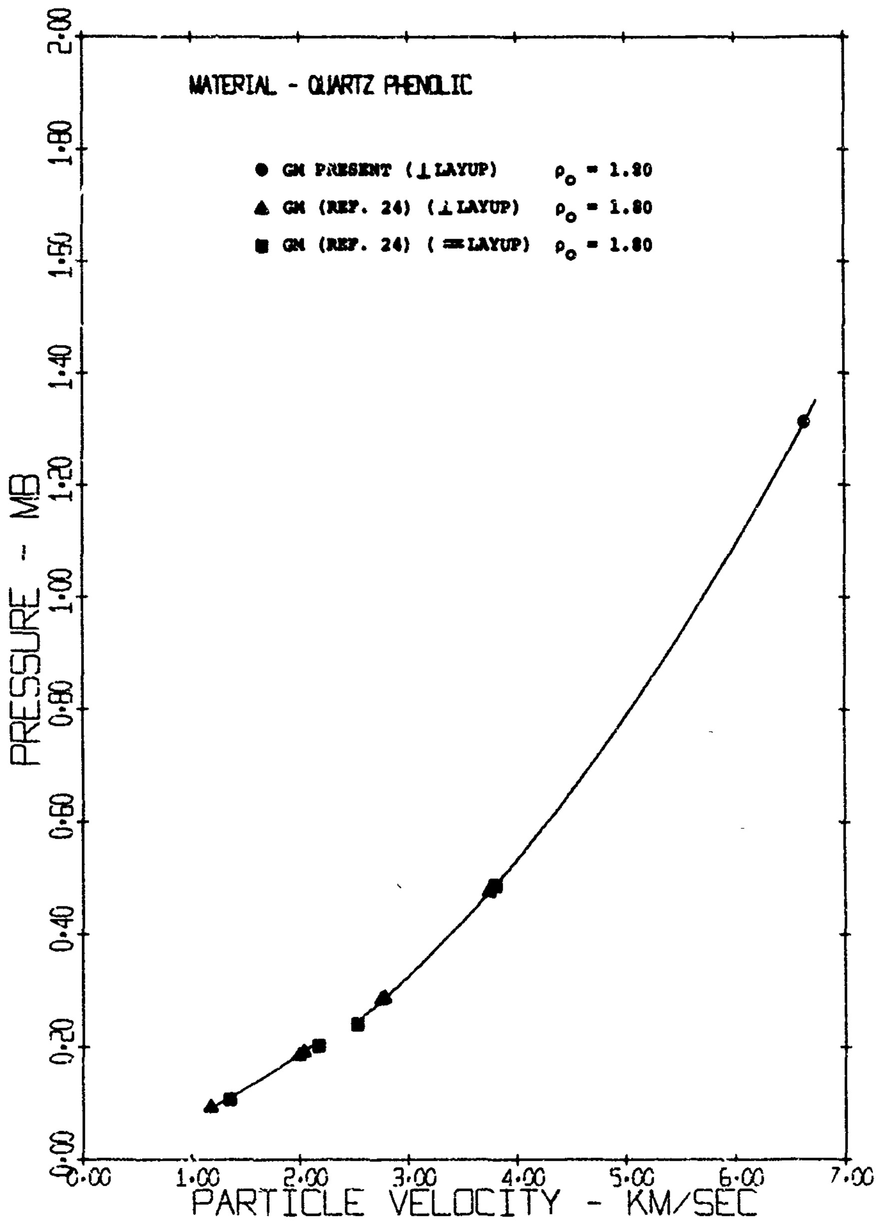

Figure 49 Pressure vs Particle Velocity for Quartz Phenolic

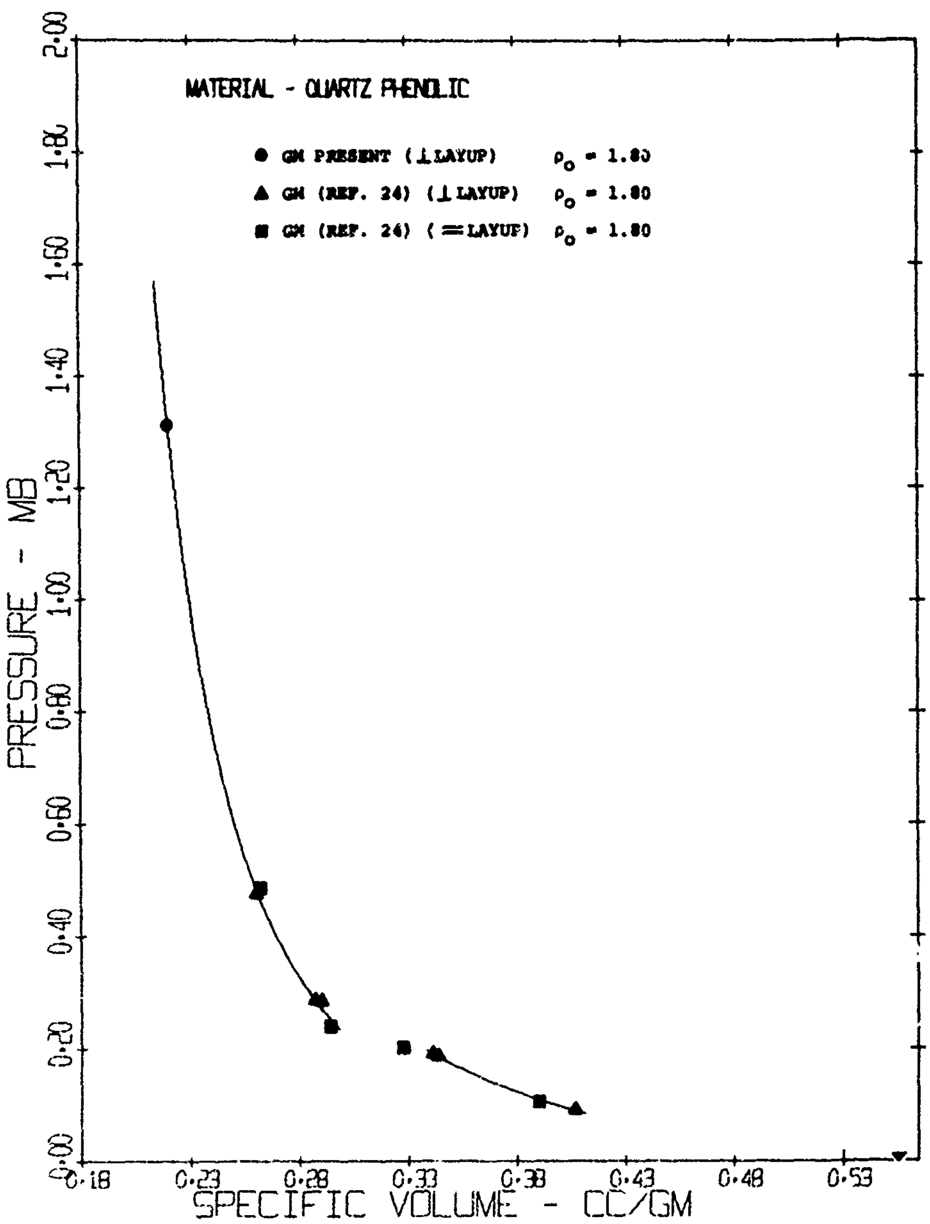

Figure 50 Pressure vs Specific Volume for Quartz Phenolic

SECTION V

SUMMARY

The research program has resulted in the relatively high precision determination of the high pressure hugoniot equations of state of eleven materials. The estimated error for shock velocity measurements with the experimental system was 0.2% to 0.6%. Estimated error in calculation particle velocity was 0.05% for like-like impact, but somewhat higher for dissimilar materials impact (see Appendix B).

Table 22 summarizes the results of the experimental program in terms of the constants of the linear hugoniot equation $U_s = C_o + Su_p$. Also included are the pressure ranges measured and the RMS deviations of the measurements. Figures 51 and 52 show the data points obtained, displayed in the P vs u_p plane.

Comparisons have been made of the data with that of other researchers. Space does not permit the inclusion of all data available for comparison and the data quoted is selected principally on the basis of pressure ranges studied and similarity of the materials in terms of density and composition.

The onset of melting in the shock front is evidenced by only very small changes in the measured parameters, shock velocity and particle velocity. Accordingly, very accurate data are required to substantiate theoretical predictions of the melting phenomenon. Although the linear fits to the high pressure data reported here are useful for calculating shock wave propagation, it is likely that several of the materials experience melting at the higher pressures, and the linear approximations become less accurate.

TABLE 22

HUGONIOT DATA FOR MATERIALS TESTED

Material	Density (gm/cc)	Particle Velocity Range (km/sec)	C_o (km/sec)	S	RMS Deviation from Linear Fit	No. of Shots Used For Fit	Comments
Fansteel-77	17.01 ±.10	0.4-3.9	4.008	1.262	0.021	17	All 17 tests 1% spread
OFHC Copper	8.930	1.7-4.7	3.964	1.463	0.009	12	
2024-T4 Aluminum	2.783	2.0-6.0	5.471	1.310	0.022	11	
Depleted Uranium	18.951	1.1-3.9	2.443	1.582	0.029	5	
Nickel	8.864	1.3-4.6	4.456	1.555	0.012	5	99.47% purity
Type 304 Stainless Steel	7.905	1.5-4.7	4.722	1.441	0.023	4	
Titanium	4.508	1.4-5.5	4.692	1.126	0.014	3	99.72% purity
I-400 Beryllium	1.881	2.5	---	---	---	1	Single test (excluded from least squares fit for S-200)
S-200 Beryllium	1.851	0.9-6.1	8.390	0.975	.017	7	
AZ 31B Magnesium	1.773	1.8-6.4	4.551	1.209	0.083	4	
Plexiglas	1.18	5.6-6.8	---	---	---	2	Rohm - Haas II UVA
Quartz Pehnolic	1.80 ±	2.5-6.6	---	1.364	0.016	5	High pressure phase (2nd wave)

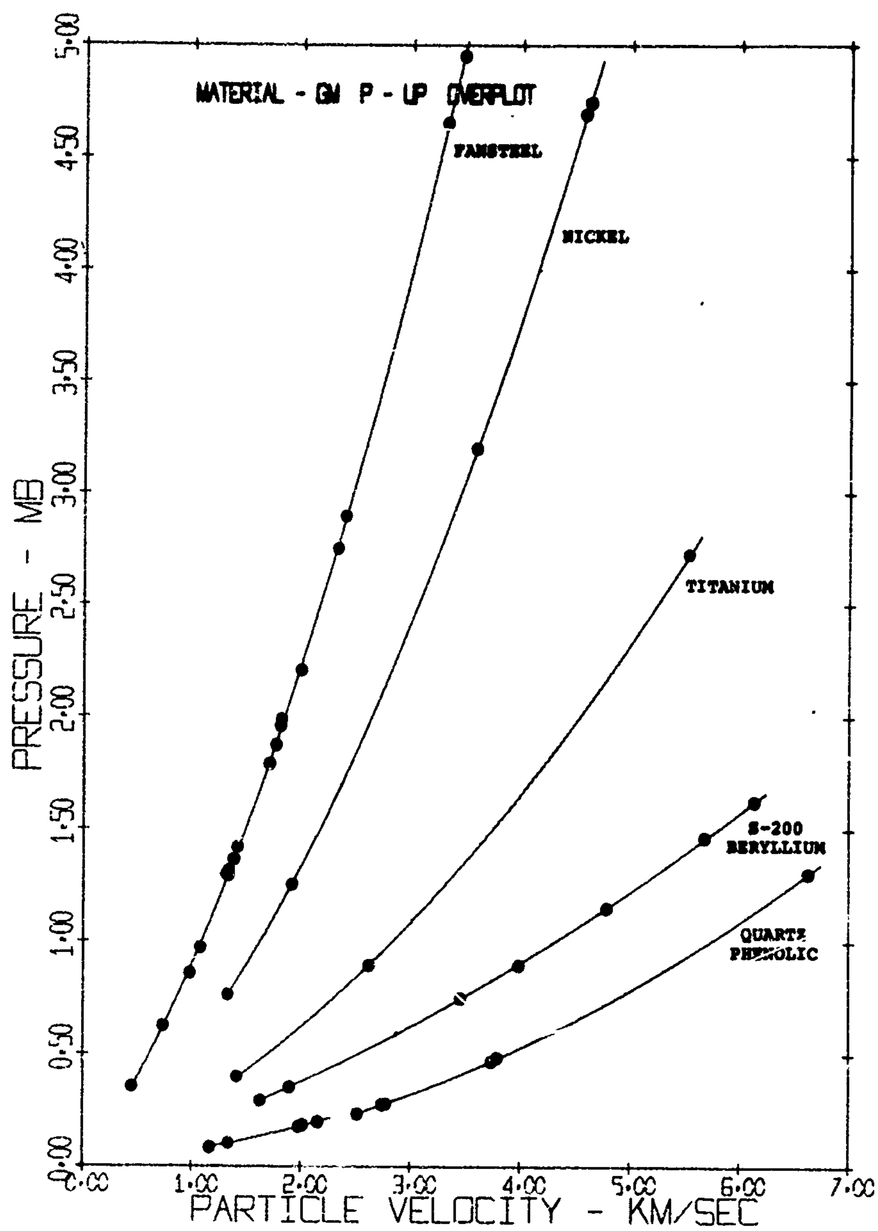

Figure 51   Compilation Of Hugoniots

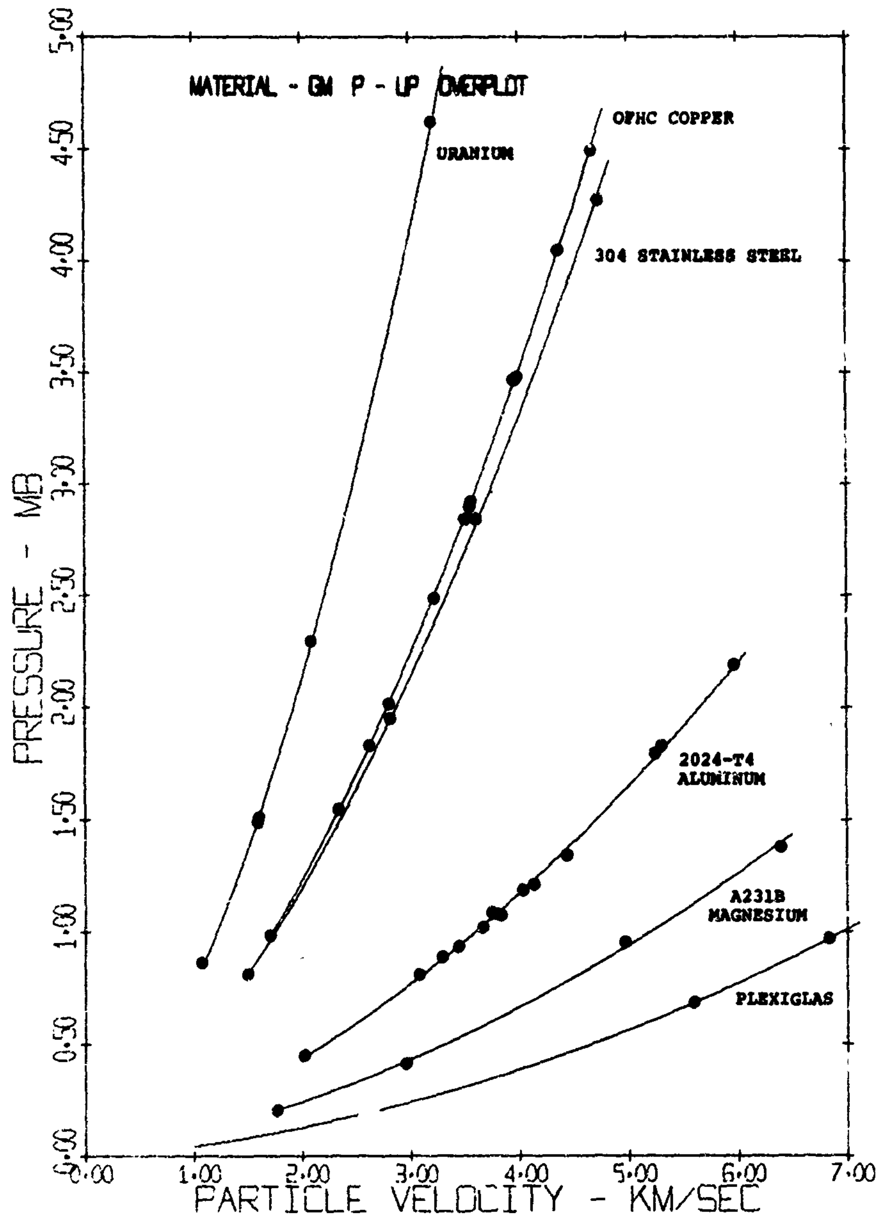

Figure 52 Compilation Of Hugoniots

CONCLUSIONS AND RECOMMENDATIONS

The research program has, by the attention to detail necessary to produce high precision measurements in multimegabar hugoniot determination, provided the opportunity to work out the difficulties and reduce the errors in a relatively new experimental system, the use of a light-gas gun for shock wave measurements. Although some problems still remain, the light-gas gun system is now better developed and more efficient than when the program began.

On the whole, good agreement was found with the data of other investigators. However, several interpretive problems are still unresolved. The behavior of the aluminum alloy 2024-T4 in the pressure range ∿ 1 megabar should be investigated further. The small differences in the slopes of aluminum and copper as measured by gun-launched impactor and by explosive techniques may be significant and need further investigation. The large differences in slopes of the beryllium and the nickel hugoniots when compared with other researchers are beyond the estimated experimental errors and need further systematic tests.

ACKNOWLEDGEMENTS

The authors gratefully acknowledge the invaluable assistance of a number of people; in particular, the light-gas gun crew, J. Paavola, J. M. Hessel, H. G. Reynolds, and their supervisor A. R. McMillan, and the talented abilities of J. W. Thomlinson and W. D. Fershman, who constructed the delicate target systems. R. Lingle and J. R. Havens supplied measurements of acoustic velocities and Dr. C. J. Maiden supplied helpful criticism.

Numerous helpful suggestions on material selection and data interpretation were provided by Dr. S. M. Taylor, the contract technical monitor, and by Mr. G. E. Hauver, both of the U.S. Army Ballistic Research Laboratories.

REFERENCES

1. Jones, A. H., Isbell, W. M. and Maiden, C. J., J.A.P., Vol. 37, p. 3493 (1966).

2. McQueen, R. G. and Marsh, S., J.A.P., Vol. 31, p. 1253 (1960).

3. Hart and Skidmore, I. C. (LRL Compendium) 1965.

4. Al'tshuler, L. V., Krupnikov, K. K. and Brazhnik, M. I., Soviet Phys. - JETP, Vol. 34, p. 614 (1958).

5. Walsh, J. M., Rice, M. H., McQueen, R. G. and Yarger, F. L., Phys. Rev., Vol. 108, p. 196 (1957).

6. Isbell, W. M., Shipman, F. H., and Jones, A. H., "Use of a Light-Gas Gun in Studying Material Behavior at Megabar Pressures", Symposium High Dynamic Pressure, Paris, France, September, 1967.

7. Jones, A. H., Isbell, W. M. and Shipman, F. H., "Material Properties Measurements for Selected Materials", Contract NAS2-3427 National Aeronautics and Space Administration, Ames Research Center, Moffett Field, California, April, 1968.

8. Lingle, R. and Jones, A. H., "Triggering System at the Muzzle of an Accelerating Light-Gas Gun", TR65-65, GM Defense Research Laboratories, Santa Barbara, California, September, 1965.

9. Al'tshuler, L. V., Kormer, S. B. and Brazhnik, M. I., Soviet Phys. - JETP, Vol. II, 766 (1960).

10. Curran, D. R., J.A.P., 34 (9), 2677 (1963).

11. McQueen, R. G., Marsh, S. P. and Carter, W. J., "The Determination of New Standards for Shock Wave Equation-of-State Work", Symposium High Dynamic Pressure, Paris, France, September, 1967.

12. McQueen, R. G., Marsh, S. P., Carter, W. J., Fritz, J. N. and Taylor, J. W., "High Velocity Impace Phanomenon", edited by E. V. Colen, Academic Press Inc., N. Y. (in press).

13. Al'tshuler, L. V., Kormer, S. B. and Bakanova, A. A., Soviet Phys. - JETP, Vol. 11, p. 573 (1960).

14. Kormer, S. B., Funtikov, A. I., Urlin, V. D. and Kolesnikova, A. N., Soviet Phys. - JETP, Vol. 15, p. 477 (1962).

15. Urlin, V. D., Soviet Phys. - JETP, Vol. 22, No. 2, p. 341.

16. March, S. P., Private communication with LRL.

17. Skidmore, I. C. and Morris, E., "Thermodynamics of Nuclear Materials", p. 173-216, Vienna, 1962.

18. Al'tshuler, L. V., Bakanova, A. A. and Trunin, R. F., Soviet Phys. - JETP, Vol. 16, p. 65 (1962).

19. Minor, E. E., Private communication, 1968.

20. Krupnikov, K. K., Bakanova, A. A., Brazhnik, M. I. and Trunin, R. F., Soviet Phys. - JETP, Vol. 8, p. 205 (1963).

21. Van Thiel, M., "Compendium of Shock Wave Data", UCRL-50108 (2 Vols.) ed., Lawrence Radiation Laboratory, University of California, Livermore, California, 1966.

22. McQueen, R. G. and Marsh, S. P, Report No. GMX-6-566, p. 51-62 (1964), Los Alamos Scientific Laboratory, GMX-6.

23. Hauver, G. E. and Melani, A., B.R.L. Report No. 1259 (1964), Ballistics Research Laboratory, Aberdeen Proving Grounds, Aberdeen, Maryland.

24. Bakanova, A. A., Dudoladov, I. P. and Trunin, R. F., Fizika, Tverdogo Tela, Vol. 7, p. 1616 (1965).

25. Isbell, W. M., Froula, N. H., Shipman, F. H., Fundamental Material Study, Vol. III, "Shock Wave Propagation and Equation of State Measurements of Quartz Phenolic", Technical Report TR67-07, Vol. III, February, 1967 prepared on Contract No. AF04-(694)-807 for Ballistic Systems Division Norton AFB, California 92409.

26. Wacklerle, J., J.A.P., Vol. 33, p. 922 (1962).

APPENDIXES

APPENDIX A

DATA ANALYSIS PROCEDURES FOR THE DETERMINATION OF HUGONIOT STATES FROM SHOCK WAVE DATA

INTRODUCTION

The following is a detailed description of the data analysis method employed for the determination of hugoniot state data derived from the experimental system described in the main body of this report. The first part of this appendix presents the equations and assumptions employed in the analysis and the second part describes a computer routine written to perform the calculations.

Experiment Analysis

Figure A-1 illustrates the system schematically with the following nomenclature:

v	= impact velocity	cm/μsec
b	= pin cap thickness	cm
g	= pin gap	cm
h	= target thickness	cm
x	= pin position on line 1-A	cm
Θ	= impactor tilt	radians
D	= shock velocity in target	cm/μsec

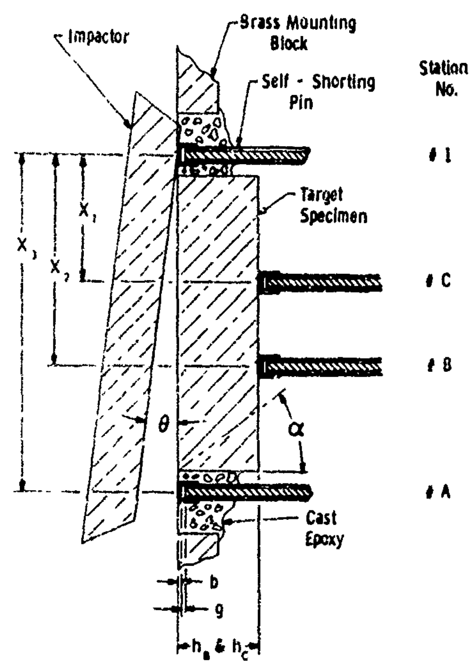

Figure A-1 Schematic of Equation of State Studies Target

Two cases of pin correction are necessary; the first involves the "start" pins 1 and A which are struck by the impactor directly. The second case involves the rear surface pins B and C, which receive the shock transmitted by the target material; and thus have closing velocities different from pins 1 and A.

The times to pin closure are given by:

$$t_1 = \frac{b_1}{U_{spin}} + \frac{g_1}{2\,u_{pin}} \tag{A-1}$$

$$t_A = \frac{X_3 \tan\theta}{v} + \frac{b_A}{U_{spin}} + \frac{g_A}{2\,u_{pin}} \tag{A-2}$$

$$t_B = \frac{(X_2 - h_B \tan\frac{D}{V}\,\Theta)\,\tan\Theta}{V} + \frac{h_B}{D}\sec(\frac{D}{V}\Theta) + \frac{b_B}{U_{spt}} + \frac{g_B}{2\,u_{pt}} \quad \text{(A-3)}$$

$$t_C = \frac{(X_3 - h_C \tan\frac{D}{V}\,\Theta)\,\tan\Theta}{V} + \frac{h_C}{D}\sec(\frac{D}{V}\Theta) + \frac{b_C}{U_{spt}} + \frac{g_C}{2\,u_{pt}} \quad \text{(A-4)}$$

where subscripts 1, A, B, C refer to pin locations, and

U_{spin} = pin cap shock velocity induced by impactor

u_{pin} = pin cap partical velocity induced by impactor

u_{spt} = pin cap shock velocity induced by target

u_{pt} = pin cap particle velocity induced by target

U_{spin} and u_{pin} are evaluated by the impedance match solution for the direct impact of the projectile material into the pin material. The particle velocity derived from this analysis is:

$$u_p = \frac{B - \sqrt{B^2 - 4AC}}{2A} \quad \text{(A-5)}$$

where $A = \rho_{op}S_p - \rho_{opin}S_{pin}$ (A-6)

$B = \rho_{op}C_{op} + \rho_{opin}C_{pin} + 2\rho_{op}C_{op}v$

$C = \rho_{op}v(C_{op} + S_p v)$

and $U_{spin} = C_{pin} + S_{pin}u_{pin}$ (A-7) the impactor hugoniot being given by:

$$U_{sp} = C_{op} + S_p u_p \tag{A-8}$$

For the pin gap velocity correction of the wave interaction between the specimen and the rear surface pins on the impedance match solution is employed again. Although the equations are similar to those already derived, the hugoniot state of the specimen must first be estimated and then determined by iteration.

The first approximation of the shock velocity is found by the following procedure: Subtracting Equation (A-6) from Equation (A-7) we obtain

$$\tan \Theta = \frac{v}{X_3} \left[(t_A - t_1) - \frac{b_A - b_1}{U_{spin}} - \frac{g_A - g_1}{2\, u_{pin}} \right] \qquad \text{A-9}$$

Neglecting several small corrections, the approximate shock velocity in the target at Station B is given by

$$D'_B = h_B \bigg/ \left[(t_B - t_1) - \frac{X_2}{v} \tan \Theta + \frac{b_1}{U_{spin}} + \frac{g_1}{2\, u_{pin}} \right] \tag{A-10}$$

The particle velocity, u', at this shock velocity is given by Equation (A-5), where:

$$\begin{aligned} A &= \rho_{op} S_p \\ B &= \rho_{op} C_{op} + \rho_{ot} D' + 2\rho_{op} S_p v \\ C &= \rho_{op} v (C_{op} + S_p v) \end{aligned} \tag{A-11}$$

The first approximation of the shock pressure is given by:

$$P' = \rho_{ot} D' u' \qquad \text{(A-12)}$$

The approximate shock and particle velocities thus obtained are used in the more exact solution for shock velocity given by Equation (A-13). The results may be iterated several times until the desired convergence is reached. With the convergence test set at 0.01% usually only two iterations are required.

$$U_{s_B} = h_B \sec \frac{D}{v}\Theta \Bigg/ \left[(t_B - t_1) - \frac{\tan\Theta\left[X_2 - h_B \tan\left(\frac{D}{v}\Theta\right)\right]}{v} + \frac{b_1}{U_{spin}} + \frac{g_B}{2\,u_{pin}} - \frac{b_B}{U_{spt}} - \frac{g_B}{2\,u_{pt}} \right] \qquad \text{(A-13)}$$

The particle velocity, u_p is calculated by Equation (A-5) with:

$$A = \rho_{op} S_p$$

$$B = \rho_{op} C_{op} + \rho_{ot} U_s + 2\rho_{op} S_p v \qquad \text{(A-14)}$$

$$C = \rho_{op} v (C_{op} + S_p v)$$

Pressure is calculated from

$$P = \rho_{ot} U_s u_p \qquad \text{(A-15)}$$

where it is assumed that $P_o = 0$

The procedure is then applied to analyze the data from pins 1, A and C, A, 1, and B, and A, 1 and C using the appropriate values of g, h, b, and X.

The procedure described above is a refinement upon the simplest form of average velocity determination (i.e. distance/time) where the time term is corrected for impactor tilt. The above refinement results in an average effect on U_s of $\sim$ 0.2% compared with the simplest form. The overall effect on a shot basis has been found for metals such as copper and Fansteel-77 to reduce data scatter about a linear form of the hugoniot in U_s-u_p.

Data Analysis Program - SHOVEL

The computer program described below is written in Mark I Fortran for use on the General Electric Timesharing Computer Service. This Fortran is very similar to Fortran IV used on many computers and provides some convenience for adapting to teletype I/O.

The program has two sections and one subroutine. The first portion of the program is merely an operator convenience to convert all input data into the required units and formats. The latter portion calculates the shock velocity at each station. The subroutine COMPUT is in the form of the quadratic solution that results in a meaningful value of u_p.

Definition of Terms

The terms presented below are in the following order:

1. Values required as input
2. Intermediate terms
3. Output values

1. INPUT TERMS

TERM	NAME	UNITS
Shot No.	SHOT	I
D	RUN	
Impactor Material	MATLP(2)	H
Target Material	MATLT(2)	H
Impactor C_o	CZERO	km/sec
Impactor S_p	SP	
Impactor ρ_o^p	RP	gm/cm^3
Target ρ_o	RT	gm/cm^3
Pin 1-B time	DTB	μsec
Pin 1-C	DTC	μsec
Pin 1 height	H1	in.
Pin A height	HA	in.
Pin B height	HB	in.
Pin C height	HC	in.
Pin 1 gap	G1	in.
Pin A gap	GA	in.
Pin B gap	GB	in.
Pin C gap	GC	in.
Pin 1-C Spacing	X1	in.
Pin 1-B Spacing	X2	in.
Pin 1-A Spacing	X3	in.
D	H2	
D	H3	
Polaroid target fiducial spacing	M2	cts.
Impactor to Window #1 Ref. Spacing	L1	cts.
Impactor to Window #2 Ref. Spacing	L2	cts.
X-ray Flash Time Interval	TSI1	μsec.
X-ray #1 to Pin C Time Interval	TSI2	μsec.
Front Surface Shim Thickness (If Used)	SHIM	in.
Tilt Time Interval	TILT	μsec.
Approximate Slope of Target Hugoniot (S=1.5 if zero)	S	
Pin Combination	COMBO	H
Computer Run No.	RUNS	I

I - Integer, D - Dummy, H - Holorith Field

2. COMPUTED TERMS

TERM	NAME	UNITS
X-ray 1 Scale Factor	F1	in/ct
X-ray 2 Scale Factor	F2	in/ct
Window Fiducial Spacing	D	in
Impact Velocity	W	ft/sec
Impact Velocity	W1	ft/sec
Impact Velocity	V	cm/μsec
D	USTAR	
Pin and ρ_o	RPIN	gm/cm^3
Pin Material Hugoniot Slope	SPIN	
Pin Material C_o	CØPIN	km/sec
Pin Cap Thickness	B1	in
Specific Volume (initial)	SVOLØ	cm^3/gm
Quadratic Solution Term	A	
Quadratic Solution Term	B	
Quadratic Solution Term	C	
Particle Velocity of Pin Cap	UPIN	cm/μsec
Shock Velocity of Pin Cap	USPIN	cm/μsec
Impactor Tilt	THETA	radians
First Approximation U_s (B Station)	USB1	cm/μsec
First Approximation u_p	UB1	cm/μsec
First Approximation P	PB1	Mb
First Approximation ρ_1	RT1	gm/cm^3
First Approximation Sound Velocity	C2	cm/μsec
Particle Velocity Induced by Target	UPT	cm/μsec
Shock Velocity Induced by Target	USPT	cm/μsec
Shock Wave Tilt in Target	THET1	radians

3. OUTPUT TERMS

B Shock Velocity	USB	km/sec
B Particle Velocity	UB	km/sec
B Pressure	PB	Mb
B Relative Volume	VOL	
Specific Volume	SVOL	cm^3/gm

The term labeling is essentially identical for the "C" station calculations with the output being:

C Shock Velocity	USC	km/sec
C Particle Velocity	UC	km/sec
C Pressure	PC	Mb
C Relative Volume	VOL1	
C Specific Volume	SVOL1	cm^3/gm

The "D" station calculation employs the C station approximate velocity and corrects for the time interval difference between B and C. The output terms are:

Shock Velocity	US	km/sec
Particle Velocity	U	km/sec
Pressure	P	Mb
Relative Volume	VOL2	
Specific Volume	SVOL2	cm^3/gm

Additional output terms:

D Station Calculation of Shock Tilt	THET3	Radians
Calculated Impactor Tilt Time Interval	TILT1	μsec
% Difference of (B-C)/C Shock Velocities	DIFF	%

The Mark II Time Sharing System allows chaining of programs and SHOVEL is continued as SHOVEN and an external file INFORM is used as the data source. Up to seven files may be linked and called in process.

SHOVEL

```
100  COMMON U,A,B,C
110 REAL DIMENSION MATLP(2), MATLT(2)
120 INTEGER SHOT,RUN,COMBO,RUNS
130C
140 200 READ(1,40)SHOT,RUN,MATLP(1),MATLP(2),MATLT(1),MATLT(2)
150 READ(1)CZERO,SP,RP,RT,DTB,DTC,H1,HA,HB,HC,G1,GA,GB,GC,X1,X2,X3,
160 +H2,H3,M2,L1,L2,TSI1,TSI2,SHIM,TILT,S
170C
180 40 FORMAT(5X,I5,I2,4A6)
190C
200 PRINT,"ENTER PIN COMBINATION (1 START = 1, A START = A) AND RUN NO."
210 INPUT 30, COMBO,RUNS
220C
230 30 FORMAT(2A1)
240C
250CMPTV COMPUTE TILT AND VELOCITY
252 PRINT 61,CZERO,SP,RT,RP,DTB,DTC,HB,HC,G1,GA,GB,GC,X1,X2,X3,
254 +TILT,S
256 61 FORMAT(////6F5.3,2F7.5,4F6.4//5F6.4///)
260C
270 IF(L1)46,48,46
280 46 F1=.4756E-03;F2=.4771E-03;D=11.9951
290 IF(L2)41,42,41
300 41 D1=(L1*F1+L2*F2+D)/12.0
310 VEL1=(D1/TSI1)*1.0E+06
320  42 D2=(L1*F1+D+M2*F2+.9537+SHIM)/12.0
330 VEL2=(D2/(TSI2-DTC))*1.0E+06
340 IF(L2)43,44,43
350 44 GO TO 45
360 43 W=VEL1;W1=VEL2
370 GO TO 49
380 45 W=VEL2;W1=0.0
390 GO TO 49
400  48 READ(1)W
410 W1=0.0
420C
430CTC CONVERT INPUT TO CGS
440C
450 49 V=(W/3.281)*1.0E+02
460 CZERO=CZERO*1.0E+05;USTAR=USTAR*1.0E+05
470 DTB=DTB*1.0E-06;DTC=DTC*1.0E-06;TILT=TILT*1.0E-06
480 H1=H1*2.54;HA=HA*2.54;HB=HB*2.54;;HC=HC*2.54
490 RPIN =8.41;SPIN=1.42;C0PIN=3.8E+05;B1=5.08E-03
500 G1=G1*2.54;GA=GA*2.54;GB=GB*2.54;GC=GC*2.54
510 X1=X1*2.54;X2=X2*2.54;X3=X3*2.54
520 THET3=0.0;SVOL0=1.0/RT;SVOL=0.0;SVOL1=0.0
530C
540CSV COMPUTE SHOCK VELOCITY
550C
560 IF (DTB)11,11,1000
```

SHOVEL CONTINUED

```
11 UB=0.0;PB=0.0;USB=0.0;VOL=0.0
GO TO 5
C
1000 B=RP*CZERO+RPIN*C0PIN+2*RP*SP*V
A=RP*SP-RPIN*SPIN;C=RP*V*(CZERO+SP*V)
CALL COMPUT
 UPIN=U;USPIN=C0PIN+SPIN*UPIN
THETA=(V/X3)*(TILT-(GA-G1)/(2*UPIN))
USB1=(HB-H1)/(DTB-X2*THETA/V)
1001 B=RP*CZERO+RT*USB1+2*RP*SP*V;A=RP*SP
C=RP*V*(CZERO+SP*V)
CALL COMPUT
UB1=U;PB1=RT*USB1*UB1
RT1=(RT*USB1)/(USB1-UB1)
C2=USB1*SQRT(.49+((USB1-UB1)/USB1)**2)
IF(S)50,50,51
50 S=1.5
51 B=RPIN*C0PIN+RT1*C2+2*RT1*S*UB1;A=S*RT1-SPIN*RPIN
C=S*RT1*UB1**2+RT1*C2*UB1+PB1
CALL COMPUT
UPT=U; USPT=C0PIN +SPIN*UPT
THET1=(USB1/V)*THETA
DELT1=DTB-THETA*(X2-(HB-H1)*THET1)/V
DELT1=DELT1+B1/USPIN+G1/(2*UPIN)-B1/USPT-GB/(2*UPT)
USB=(HB-H1)*SQRT(THET1**2+1)/DELT1
3 IF(.0001-(ABS((USB-USB1)/USB)))1002,1003,1003
1002 USB1=USB
GO TO 1001
1003 B=RP*CZERO+RT*USB+2*RP*SP*V;A=RP*SP;C=RP*V*(CZERO+SP*V)
CALL COMPUT
UB=U;PB=RT*USB*UB;VOL=1-UB/USB
SVOL0=1.0/RT;SVOL=VOL/RT
C
5 IF(DTC)6,6,7
6 USC=0.0;UC=0.0;PC=0.0;VOL1=0.0;TILT=TILT*1.0E+06;US=0.0;U=0.0
TILT1=0.0;USB=USB*1.0E-05;UB=UB*1.0E-05;PB=PB*1.0E-12
P=0.0;VOL2=0.0
SVOL1=0.0;SVOL2=0.0;DIFF=0.0
GO TO 2
C
7 B=RP*CZERO+RPIN*C0PIN+2*RP*SP*V
A=RP*SP-RPIN*SPIN;C=RP*V*(CZERO+SP*V)
CALL COMPUT
UPIN=U;USPIN=C0PIN+SPIN*UPIN
THETA=(V/X3)*(TILT-(GA-G1)/(2*UPIN))
USC1=(HC-H1)/(DTC-X1*THETA/V)
1004 B=RP*CZERO+RT*USC1+2*RP*SP*V;A=RP*SP
C=RP*V*(CZERO+SP*V)
CALL COMPUT
UC1=U;PC1=RT*USC1*UC1
```

SHOVEL CONTINUED

```
RT2=(RT*USC1)/(USC1-UC1)
C3=USC1*SQRT(.49+((USC1-UC1)/USC1)**2)
B=RPIN*C0PIN+RT2*C3+2*RT2*S*UC1;A=S*RT2-SPIN*RPIN
C=S*RT2*UC1**2+RT2*C3*UC1+PC1
CALL COMPUT
UPT1=U; USPT1=C0PIN+SPIN*UPT1
THET2=(USC1/V)*THETA
DELT2=DTC-THETA*(X1-(HC-H1)*THET2)/V
DELT2=DELT2+B1/USPIN+G1/(2*UPIN)-B1/USPT1-GC/(2*UPT1)
USC=(HC-H1)*SQRT(THET2**2+1)/DELT2
4 IF(.0001-(ABS((USC-USC1)/USC)))1005,1006,1006
1005 USC1=USC
GO TO 1004
1006 B=RP*CZERO+RT*USC+2*RP*SP*V;A=RP*SP;C=RP*V*(CZERO+SP*V)
CALL COMPUT
UC=U;PC=RT*USC*UC; VOL1=1-UC/USC
UB=UB*1.0E-5;USB=USB*1.0E-05;PB=PB*1.0E-12
UC=UC*1.0E-05;USC=USC*1.0E-05;PC=PC*1.0E-12
DELT=(DELT1-DELT2)*1.0E+06
TILT=TILT*1.0E+06
TILT1=(DTB-DTC)*X3/(X2-X1)*1.0E+06
DIFF=0.0;SVOL1=VOL1/RT
C
C
IF(DTB)70,70,21
70 TILT1=0.0;U=0.0;US=0.0;P=0.0;VOL2=0.0
GO TO 2
21 US1=(HC-H1)/DTC
B=RP*CZERO+RT*US1+2*RP*SP*V;A=RP*SP
C=RP*V*(CZERO+SP*V)
CALL COMPUT
U1=U;P1=RT*US1*U1
1007 RT3=(RT*US1)/(US1-U1)
C4=US1*SQRT(.49+((US1-U1)/US1)**2)
IF(S)22,22,23
22 S=1.5
23 B=RPIN*C0PIN+RT3*C4+2*RT3*S*U1;A=S*RT3-SPIN*RPIN
C=S*RT3*U1**2+RT3*C4*U1+P1
CALL COMPUT
UPT=U;USPT=C0PIN+SPIN*UPT
DTILT=DTB-(HB-H1)/US1+B1/USPIN+G1/(2*UPIN)-B1/USPT-GB/(2*UPT)
THET3=V*DTILT/X2
SHTIM=DTC-THET3*(X1-(HC-H1)*US1*THET3/V)/V+B1/USPIN+G1/(2*UPIN)
+-B1/USPT-GC/(2.*UPT)
 US=(HC-H1)*SQRT(1.0+(US1*THET3/V)**2)/SHTIM
B=RP*CZERO+RT*US+2*RP*SP*V;A=RP*SP
C=RP*V*(CZERO+SP*V)
CALL COMPUT
U=U;P=RT*US*U
IF(.0001-(ABS((US-US1)/US)))1008,1009,1009
```

SHOVEL CONTINUED

```
1008 US1=US;U1=U;P1=P
GO 101007
1009 VOL2=1-U/US;U=U*1.0E-05;US=US*1.0E-05;P=P*1.0E-12
SVOL1=VOL1/RT;SVOL2=VOL2/RT
DIFF=(ABS((USB-US)/USC))*100.0
$USE SHOVEN
```

SHOVEN

```
C  OUTPUT STATEMENTS FOR SHOVEL
C
2 PRINT 60,SHOT,RUNS,COMBO,MATLT(1),MATLT(2),MATLP(1),MATLP(2),
+RT,RP,SVOL0,W,THET3,V,TILT,W1,TILT1,DIFF,
+USB,UB,PB,VOL,SVOL,USC,UC,PC,VOL1,SVOL1,US,U,P,VOL2,SVOL2
C
C  OUTPUT FORMAT
C
60 FORMAT(////////10X,9HSHOT NO. ,I5,10X,8HRUN NO. ,A1//
+10X,17HPIN COMBINATION: ,A1,1X,7H- START,//
+5X,14HTARGET MATL.- ,2A6,
+4X,13HPROJ. MATL.- ,2A6//8X,9HDENSITY- ,F6.3,1X,5HGM/CC,8X,
+9HDENSITY- ,F6.3,1X,5HGM/CC//8X,8HVOLUME- ,F6.4,1X,5HCC/GM,
+/////5X,18HPROJECTILE VEL. = ,E12.5,
+1X,6HFT/SEC,4X,13HSHOCK TILT = ,F9.6//23X,E12.5,1X,6HCM/SEC,
+4X,13HTILT MEAS. = ,F9.6//23X,E12.5,1X,6HFT/SEC,4X,
+13HTILT CALC. = ,F9.6///5X,21HSHOCK VEL. SCATTER = ,F7.3,1X,1H%,
+//////2X,4HSTA.4X,10HSHOCK VEL.4X,10HPART. VEL. 7X,8HPRESSURE
+4X,4HV/V05X,6HVOLUME//10X,6HKM/SEC,8X,6HKM/SEC,11X,8HMEGABARS,
+13X,5HCC/GM////
+2X,1HB,6X,F8.4,6X,F8.4,8X,F10.6,1X,F9.5,1X,F8.5//
+2X,1HC,6X,F8.4,6X,F8.4,8X,F10.6,1X,F9.5,1X,F8.5//
+2X,1HD,6X,F8.4,6X,F8.4,8X,F10.6,1X,F9.5,1X,F8.5//////)
GO TO 200
END
SUBROUTINE COMPUT
COMMON U,A,B,C
U=(B-SQRT(B**2-4*A*C))/(2*A)
RETURN
END
$FILE INFORM
```

APPENDIX B

ANALYSIS OF SYSTEMATIC MEASUREMENT ERRORS

An analysis of systematic errors in the experimental system was performed.* Each of the 22 parameters involved in the calculation of a hugoniot equation of state point from information obtained using the light gas gun system was considered and an estimated error was calculated. These errors were combined mathematically to yield an average systematic error for the hugoniot parameters calculated; pressure, particle velocity, shock velocity, and volume. Errors in measurement of impact velocity were also calculated.

Two cases were considered: (1) dissimilar impact, in which the hugoniot point is calculated from the impact velocity, the shock wave velocity, and the measured hugoniot for the impactor and (2) symmetric impact, in which only the impact velocity and the shock wave velocity are necessary for the calculation.

Since the error analysis is dependent on the shock impedances of the specimen and the impactor as well as on the pressure attained, a complete error analysis could be performed for each data point. This formidable task was avoided by calculating errors involved in an "average" data point, and briefly examining the errors at the limits of the system. As the variance in errors at the limits do not substantially change the values for the average case, only the average case is reported.

The parameters operated upon involved a measurement made on copper with a Fansteel-77 impactor or a copper impactor launched at 6km/sec. The method is a statistical procedure called the analysis of variance.

* The authors are indebted to Mr. W. L. Rearick of Systems Analysis, Manufacturing Development, for his assistance in the formulation of the system error analysis procedure.

By definition the standard error of the variable, x, is given by:

$$\sigma_{SE} = \sqrt{\Sigma_1^n \sigma^2_{xi}/n} \qquad (a)$$

where σ_{xi} is the deviation of the ith term from some f(x).

When σ_x, σ_1, σ_2, σ_n are mutually dependent, the variance of x is then:

$$\sigma_x^2 = \sigma_{x1}^2 + \sigma_{x2}^2 + \ldots + \sigma_{xn}^2 \qquad (b)$$

with σ_n^2 denoting the nth element component of x.

In the present case, a σ (or standard deviation) is determined for the system components of all the mutually dependent variables, listed in Table 1-B.

The variances of mutually independent variables may be determined using the rules presented below. By definition the mean, μ_x, of a variable, x, is given by:

$$\mu_x = (x_1 + x_2 + \ldots x_n)/n \qquad (c)$$

where $x_1, x_2, \ldots, x_n$ are element components of a statistical distribution.

If the variance of x and y are small compared their means, i.e., $\sigma_x^2 << \mu_x$, and independent, the following rules may be employed to determine the variances of the sums, products and quotients of variables x and y:

TABLE 1-B

SYSTEMATIC ERROR PARAMETERS

PARAMETER	TERM	CASE	μ MEAN	σ^2 VARIANCE 10^{-6}	σ DEVIATION 10^{-3}	UNITS
IMPACT VELOCITY	v					
Impact Position		1&2	30.0	308.58		cm/μsec
Film resolution		1&2		25	5	cm
Image contrast		1&2		25	5	cm
Motion blur		1&2		4	2	cm
Film shrinkage		1&2		0.04	0.2	cm
X-ray misalign.		1&2		100	10	cm
Fiducial ref.		1&2		0.25	0.5	cm
Time Interval	z	1	37.98	202	14	
Time Interval	z	2	100.0	202	14	
Signal risetime				1	1	
Digital error				100	10	
SHOCK VELOCITY						
Target Thickness	h_n	1	0.39	0.01	0.1	cm
Target Thickness	h_n	2	0.58	0.01	0.1	cm
Pin Spacing	x_n	1	0.56	25	5	cm
Pin Spacing	x_n	2	1.21	25	5	cm
Pin Gap	g_n	1&2	0.005	0.04	0.2	cm
Pin Cap	b_n	1&2	0.005	0.04	0.2	cm
Time Interval	ΔT_n	1	0.36	1.02	1	μsec
Time Interval	ΔT_n	2	0.90	1.02	1	μsec
Signal risetime		1&2	0.01	0.1	0.3	μsec
Digital error		1&2	1	1	1	μsec

TABLE 1-B

SYSTEMATIC ERROR PARAMETERS (CONTINUED)

PARAMETER	TERM	CASE	μ MEAN	σ^2 VARIANCE 10^{-6}	σ DEVIATION 10^{-3}	UNITS
SHOCK VELOCITY (Continued)						
Impact Tilt	$\tan\theta$	1&2				
Pin baseline	x_3	1	1.12	4	2	cm
Pin baseline	x_3	2	1.92	4	2	cm
Tilt interval	ΔT_t	1&2	0.030	2.25	1.5	μsec
Pin gap diff.	Δg	1&2	0.005	0.16	0.4	cm
Gap close vel.	U_{pin}	1	0.46	100	10	cm/μsec
Gap close vel.	U_{pin}	2	0.15	100	10	cm/μsec
DENSITY						
Impactor Density	ρ_{op}	1&2	17.01	100	10	gm/cc
Target Density	ρ_{ot}	1&2	8.93	9	3	gm/cc
IMPACTOR HUGONIOT						
Slope	C_{op}	1	1.262	34.63	5.88	cm/μsec
Intercept	S_p	1	0.4008	0.864	0.923	

Addition: $$\sigma^2_{x\pm y} = \sigma_x^{\ 2} + \sigma_y^{\ 2} \qquad \text{(d)}$$

Multiplication: $$\sigma_{xy}^{\ 2} = \sigma_x^{\ 2}\sigma_y^{\ 2}+\sigma_x^{\ 2}\mu_y^{\ 2}+\sigma_y^{\ 2}\mu_x^{\ 2} \qquad \text{(e)}$$

Division: $$\sigma_{x/y}^{\ 2} = \frac{\sigma_x^{\ 2}\mu_y^{\ 2}+\sigma_y^{\ 2}\mu_x^{\ 2}}{\mu_y^{\ 4}} \qquad \text{(f)}$$

where in (f), $\mu_y >> 0$

The present analysis was carried out using the tabulated values of μ and σ of Table 1-B. The variance of each term of equations 1 through 4 was determined and then combined to yield the resultant variance for each operation.

Impact Velocity: $$v = y/z \qquad (1)$$

Impactor Tilt: $$\tan\theta = \frac{v}{x_3}\left(\Delta t_t \frac{\Delta g}{2-u_{pin}}\right) \qquad (2)$$

Shock Velocity: $$U_{s_n} = h_n \sec\left(\frac{D^1}{v}\right)/[(T_1-T_n) -$$

$$\frac{x_n-h_n\tan\theta\tan\left(\frac{D^1}{v}\theta\right)}{v} + \frac{b}{U_{spin}} + \frac{g_1}{2\cdot u_{pin}} - \qquad (3)$$

$$\frac{b}{U_{spt}} - \frac{g_n}{2\cdot upt}]$$

Symmetrical Condition Particle Velocity: $$u_p = 1/2v \qquad (4)$$

To determine the variance resulting from the impedance mismatch solution for the particle velocity, it is necessary to know the variances of the terms of the hugoniot equation of the standard. Since the hugoniot equation is itself a statistical inference, the following approach was used:

$$\mu_{up} = \Sigma_1^n \frac{u_{pi}}{n} \qquad (g)$$

where n is the number of data employed in the least squares analysis. The variance is then given by:

$$\sigma_{up}{}^2 = \Sigma_1^n \left(u_{pi}-\mu_{up}\right)^2 \qquad (h)$$

For an equation in the form:

$$U_s = C_o + S_{up} \qquad (i)$$

the variances of the zeroth and first order terms using equation (a) are given by:

$$\sigma_{C_{op}}{}^2 = \frac{\sigma_{se}{}^2}{n} \qquad (j)$$

$$\sigma_{s_p}{}^2 = \frac{\sigma_{se}{}^2}{\sigma_{up}{}^2} \qquad (k)$$

The analysis of variance is then applied to equation 5a through 5c.

Impedance mismatch particle velocity:

$$u_p = \frac{B-\sqrt{B^2-4AC}}{2A} \qquad (5)$$

$$A = \rho_{op} \cdot S_p \tag{5a}$$

$$B = \rho_{op}C_{op}+\rho_{ot}U_s+2\cdot\rho_{op}\cdot S_p\cdot v \tag{5b}$$

$$C = \rho_{op}C_{op}v+\rho_{op}S_p v^2 \tag{5c}$$

To determine the variance of the square root operation, the binomial expansion is used; i.e.

$$\sigma^2 \sqrt{\mu^2 + \sigma^2} = \frac{\sigma^2}{2\mu} \tag{1}$$

The variances are then determined for the remaining hugoniot relations.

Shock Pressure: $$P = \rho_{ot}U_s u_p \tag{6}$$

Shock Specific Volume: $$V = \frac{1-\frac{u_p}{U_s}}{\rho_{ot}} \tag{7}$$

Table 2-B presents a summary of the systematic error analysis. The percent error column shows the marked difference in the accuracy with which measurements can be performed on symmetric (Case 2) versus dissimilar material (Case 1) experiments. The larger errors involved in the dissimilar material tests (Case 1) concern the errors in the hugoniot of the impactor material. For tests using impactor materials with precisely measured hugoniots these errors will be correspondingly smaller.

TABLE 2-B

SUMMARY OF SYSTEMATIC ERRORS

PARAMETER	CASE	MEAN	VARIANCE 10^{-6}	DEVIATION 10^{-3}	% ERROR
Impact Velocity	1	0.79 cm/µsec	0.301	0.549	0.07
	2	0.30 cm/µsec	0.033	0.181	0.06
Shock Velocity	1	1.12 cm/µsec	43.67	6.608	0.59
	2	0.65 cm/µsec	18.04	4.247	0.65
Particle Velocity	1	0.46 cm/µsec	90.03	9.488	2.01
	2	0.15 cm/µsec	0.008	0.091	0.06
Pressure	1	4.59 Mb	9354.0	0.097	2.02
	2	0.87 Mb	8.064	0.003	0.33
Specific Volume	1	0.07 cm/gm	0.932	0.965	1.46
	2	0.06 cm/gm	0.007	0.085	C.10

UNCLASSIFIED
Security Classification

DOCUMENT CONTROL DATA - R & D

(Security classification of title, body of abstract and indexing annotation must be entered when the overall report is classified)

1. ORIGINATING ACTIVITY *(Corporate author)* Manufacturing Development General Motors Corporation GM Technical Center, Warren, Michigan 48090	2a. REPORT SECURITY CLASSIFICATION UNCLASSIFIED 2b. GROUP

3. REPORT TITLE

HUGONIOT EQUATION OF STATE MEASUREMENTS FOR ELEVEN MATERIALS TO FIVE MEGABARS

4. DESCRIPTIVE NOTES *(Type of report and inclusive dates)*
Final Report 1966, June - 1968, December

5. AUTHOR(S) *(First name, middle initial, last name)*

Isbell, W. M., Shipman, F. H., Jones, A. H.

6. REPORT DATE	7a. TOTAL NO. OF PAGES	7b. NO. OF REFS
1968 December	125	26

8a. CONTRACT OR GRANT NO. DA-18-001-AMC-1126(X) b. PROJECT NO. DASA Subtask No. 15.025 c.	9a. ORIGINATOR'S REPORT NUMBER(S) MSL-68-13 9b. OTHER REPORT NO(S) *(Any other numbers that may be assigned this report)*

10.

This document has been approved for public release and sale; its distribution is unlimited.

11. SUPPLEMENTARY NOTES Aberdeen Proving Grounds, Maryland 21005.	12. SPONSORING MILITARY ACTIVITY Department of the Army U.S. Army Ballistics Research Laboratories Aberdeen Proving Ground, Maryland 21005

13. ABSTRACT

An experimental technique is utilized in which a light-gas gun is used to launch flat impactor plates to high velocities (∿ 8 km/sec) at specimens suspended at the muzzle of the gun. Impact-induced shock waves at pressures to ∿ 5 megabars are recorded and are used to determine the shock state in the specimen. The ability to launch unshocked, stress-free flat plates over a wide and continuous velocity range, coupled with the ability to launch impactor plates of the same material as the target, results in hugoniot measurements of relatively high precision. Measurements were made on Fansteel-77 (a tungsten alloy), aluminum (2024-T4), copper (OFHC, 99.99%), nickel (99.95%), stainless steel (type 304), titanium (99.99%), magnesium (AZ31B), beryllium (S-200 and I-400), uranium (depleted), plexiglas, and quartz phenolic. The results are compared with those of other researchers.

Deviation from linear shock velocity - particle velocity was found in aluminum beginning at ∿ 1.0 megabars, probably attributable to melting in the shock front.

DD FORM 1 NOV 65 1473 REPLACES DD FORM 1473, 1 JAN 64, WHICH IS OBSOLETE FOR ARMY USE.

UNCLASSIFIED
Security Classification

14. KEY WORDS	LINK A		LINK B		LINK C	
	ROLE	WT	ROLE	WT	ROLE	WT
Hugoniot Equation of State						
Shock Wave Propagation						
Megabar Dynamic Pressure Measurements						